Inorganic-Organic Hybrid Networks Constructed from Different Metal Ions and Ligands

Liangming Hu

Thesis submitted to the faculty of the Virginia Polytechnic Institute and State University in partial fulfillment of the requirements for the degree of

Doctor of Philosophy

In

Chemistry

Dr. Brian E. Hanson

Dr. Richard D. Gandour

Dr. Joseph S. Merola

Dr. Karen J. Brewer

Dr. Carla Slebodnick

Dr. Ross J. Angel

Date April 15th, 2009

Blacksburg, Virginia

Keywords: hybrid networks, transition metal ions, ligands, templates, hydrothermal synthesis, X-ray diffraction

Inorganic-Organic Hybrid Networks Constructed from Different Metal Ions and Ligands

Liangming Hu

ABSTRACT

Hybrid inorganic-organic networks have been studied in both chemistry and materials science due to properties, (e.g. porosity, magnetic and electronic behaviors) that may lead to applications in catalysis, gas absorption and storage. It is important to understand the different structural topologies shown by hybrid networks to help develop practical applications for these materials. The research is focused on the design and synthesis of well-defined hybrid network structures that have potential to contain molecular size cavities that can be used for catalysis and gas storage.

In the field of organic-inorganic hybrid networks, the goals are to design and synthesize 1D, 2D and 3D networks with cavities, and to characterize them by X-ray, TGA and surface area measurements. Twenty-six networks have been successfully made with interesting structure topologies. These hybrid network structures are classified into three series based on their ligands. Series **I** contains ten hybrid networks constructed from the flexible ligand, 4, 4'-trimethylenedipyridine (TMDP), Zn^{2+} ions, and H_3PO_3, and with aromatic alcohols as templates to direct the formation of various hybrid network structures. Series **II** consists of five structures constructed from the relatively rigid ligand, 4, 4'-bisimidazolelybipyridine (BIB) with metal ions (Cu^{2+}, Ni^{2+}) and the conjugated bases of H_3PO_3 and H_3PO_4. The BIB ligand is not commercially available so is produced and characterized by NMR, mass spectrometry and TGA. Rigid network structures were expected to construct with pores of molecular dimensions with the BIB ligand. To date, the BIB ligand has not yield the desired porous network, however, these 3D hybrid networks have interesting topologies, one of which is an interdigitated network that is the precursor for 3D

interpenetrated networks. Series **III** contains five hybrid structures constructed from various organic ligands, such as tartaric acid, picolinic acid and 1, 2, 4-triazole. In addition to the hybrid networks, six hydrogen bonded networks were prepared. Graph-Analysis is applied to study these hydrogen bonded network structures. The π….π interaction is also discussed within the hydrogen bonded networks.

ACKNOWLEDGMENTS

The completion of this thesis is by no means my personal effort alone. I am indebted to a number of individuals for their guidance and help throughout the arduous process of completing Ph. D work. First and foremost I thank Dr. Brian E. Hanson, my advisor, mentor and friend. He provided the opportunity, the environment, and the encouragement for me to grow. His guidance and support created an excitement for me within this field, and I thank him for pointing the way towards a new and bright direction for my life. It has been an honor and privilege to work under his direction. I wish I could put words in the best way to express my gratitude to him.

I thank my committee members, Drs. Ross J. Angel, Carla Slebodnick, Richard D. Gandour, Karen J. Brewer, and Joseph S. Merola, for their guidance in the development and completion of this study and to my professional development.

I thank Dr. Gordon T. Yee and Dr. Paul. A. Deck and other people in the inorganic division of the chemistry department at Virginia Tech for their help. I appreciate that my friend Dr. Elinor C. Spencer has been helping me in my research and dissertation. I thank my friends, Raymond H. Myers, Sharon L. Myers, Chao Yang, Xingguo Chen, Hirofumi Motegi and Theresa A. Detrie for their friendship and help. These wonderful people made my days at Blacksburg a truly memorable one.

I thank my mother. Without her love and support, it would not be possible for me to pursue my dream. I deeply thank my husband, Nan. He is always providing inspiration that keep me going.

This list is probably incomplete and certainly insufficient to express my true thanks. I will remember all these people who have been helping me with my Ph. D degree in my lifetime. Thanks to all of you having faith on me and we will achieve our dreams together.

Table of Contents

List of Figures

List of Schemes

List of Tables

Chapter 1

Introduction to Hybrid Networks

1.1 Background to hybrid networks

Hybrid inorganic-organic networks are an important class of materials that have been studied intensively over recent decades due to their porosity, and their magnetic and electronic properties. These properties lead to potential applications in catalysis, gas absorption and storage, and sensors. It is important to understand what hybrid materials are and how to synthesize and characterize them so that they may be developed for practical applications. Common alternate terms are for hybrid materials include "coordination polymers", "metal organic frameworks/networks" and "hybrid networks". Searching these terms in SciFinder[1], shows a dramatic increase in publications using these terms during the last ten years (Figure 1.1). Hybrid inorganic-organic materials are a class of metal coordination compounds. "Inorganic-organic hybrid materials" are defined as compounds that contain both organic and inorganic moieties that are integral parts of a network with bonding connectivity in at least one dimension throughout the entire material. The coordination compounds with infinite one-, two-, three-dimensional network structures with backbones constructed by metal ions and ligands are called "coordination polymers".[2] Metal organic frameworks (MOFs)[3] can be defined as extended array of metal ions or complexes that are linked by mutifuntional bridging organic ligands. MOFs are specially defined as strong bonding (such as covalent bonding) three dimensional networks with geometrically well-defined structure.[3] "Hybrid inorganic-organic networks" are crystalline materials in which both inorganic and organic units are covalent, ionic, or hydrogen bonded inside the structures. Hybrid networks can be 1D, 2D and 3D coordination polymers or MOFs. At present, most of hybrid networks are based on M-X-M, in which M = transition metal ions, X

= atoms O, N, Cl. Scheme 1.1 shows all these terms are related to network solids. In this thesis, I will focuse on synthesis and structure of hybrid networks and briefly discussion of hydrogen-bonded networks.

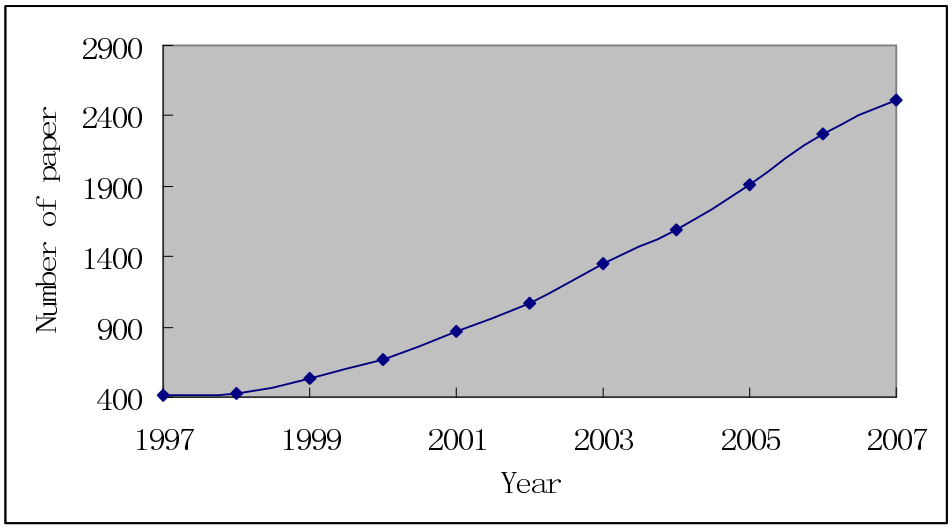

Figure 1.1: The number of papers published during the period 1997-2007 that feature the term “hybrid networks” , “metal organic frameworks/networks”, and “coordination polymers” were published from 1997-2007. (Source: SciFinder Scholar 2007)

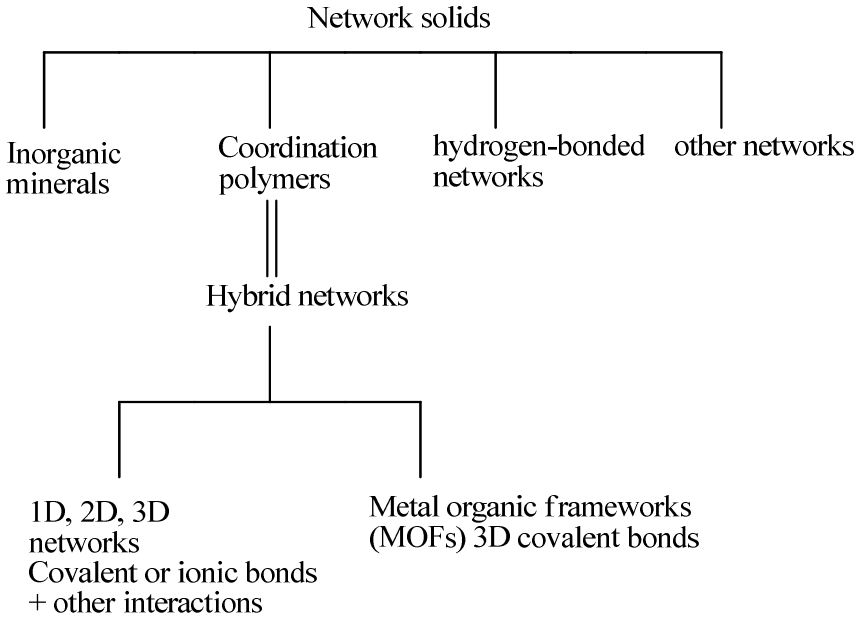

Scheme 1.1: Relative terms are used in network solids.[2, 3]

The history of "hybrid network" started in early 20th. Werner extensively investigated coordination compounds in the early 20th century, and was awarded the Nobel Prize in chemistry for his pioneering work in 1913.[4] Coordination compounds with infinite structures are called hybrid network, a term which appeared in the early 1960's. In 1964, hybrid networks were reviewed by Bailar.[5] Since 1970's, more hybrid networks have been discovered and studied by chemists. The term, "organic-inorganic hybrid materials" appeared in the early 1990's. Hoskins and Robson introduced this term in their papers in 1990's (Scheme 1.1).[6-11] In 1989, Hoskins reported the 3D network structure, $Cu[C(C_6H_4CN)_4]BF_4 \bullet xC_6H_5NO_2$, in which rod-like connecting units that may form an array of cavities.[12] In 1990, Hoskins published an infinite framework $Cd(CN)_2 \bullet 2/3H_2O \bullet tBuOH$, in which CdCNCd rods from linear channels; the distance between Cd-Cd is 5.55-5.60Å.[6] The science of controlling the formation and structure of hybrid networks with potentially useful applications, by using well-defined chemical building blocks has attracted the attention of many research groups, such as Yaghi's group[13-16], Ferey's group[17], and Lin's group[18]. Yaghi and his co-workers have contributed to the following examples to the hybrid materials field: (I) reticular synthesis from building blocks(more detail is on the following chapter); (II) change chemical functionality without changing the underlying framework topology; (III) design porous framework structures; (IV) discussion about interpenetration and interweaving topologies.[19] Several hundred MOF structures have been published by Yaghi's group.[13-16, 20-22] MOF-5, $Zn_4O(C_8H_4O_4)_3$ is one of the MOF structures published by Yaghi et al., which contains cavities diameter 18.5Å.[23] Since then, more and more groups have focused on the synthesis and characterization of novel hybrid networks. Ferey et al. reviewed the utilization of fluorine for the preparation of crystalline porous metal-organic frameworks.[17] Lin et al. reviewed homochiral porous metal organic frameworks which is related to future applications in many fields, such as organic chemistry, physics chemistry, and analytical chemistry.[18]

Numerous hybrid networks contain 1D chain, 2D sheets and 3D networks. For example, Maji et al. published a hybrid network, Cu_2[bis(3-aminopropyl)methyl amine]$_2Ni(CN)_4(ClO_4)_2 \bullet 2.5H_2O$ that consists of 1D chains elongated along the

crystallographic b axis.[24] Chen *et al.* reported a 2D hybrid network, [Tb_2(4-hydroxy-pyridyl-2,6-dicarboxylate)$_3$(H_2O)$_4$] •2H_2O.[25] In this hybrid network structure, there are two crystallographically independt Tb^{3+} anions and six ligands that from a square unit that assemble into a 2D sheet.[25] Another 3D hybrid netowrk, Ba(4,4'-azodibenzoic acid)$_n$ was reported by Chen *et al*. In this structure Ba(II) carboxylate units assemble into 2D sheet, which are linked by organic units to form a 3D network.[26]

1.2 Properties and applications

1.2.1 Gas storage

Generating electricity from hydrogen and oxygen using fuel cells for use as a power source for transportation vehicles can reduce CO_2 emissions and air pollution, which are worldwide issues. For this to be possible, an effective storage method for these gases is required. The United States Department of Energy has set a number of short-term capacity goal for hydrogen storage materials: 6.0 wt% and 45 gL^{-1} in the range of 1-10 atm and 25-120°C by the year of 2010.[27] Any storage material should be of minimal weight and volume, since the space in the vehicle is limited.

In the past decade, hybrid materials have become a promising candidate for hydrogen storage due to their high porosity, molecular size, and well-defined structure topology. Typically, hybrid materials have 3D structures with molecular sized pores and channels. These molecular sized pores and channels are often filled with guest species, such as, solvent molecules. The removal of the guest molecules usually causes the hybrid network to collapse which is a problem for many applications. Retaining the integrity of hybrid network structures after removal of guest species is still a challenge in this area of research.

In 2003, Yaghi et al. reported the first measurement of hydrogen absorption on a metal organic framework (MOF): the hybrid material $Zn_4O(bdc)$ (bdc = 1,4-benzenedicarboxylate) (Figure 1.2) has 4.5 wt% H_2 at 77K and pressures less than 1 atm, and 1.0 wt% H_2 at room temperature and 20 bar.[21] However, later studies showed that this value is incorrect, and the storage capacity is approximately 0.42~1.3 wt% at 77K.[28] But the idea was impressive: porous hybrid materials can be used as hydrogen storage materials. Since 2003, more and more unique hybrid materials have been reported as possible gas storage media. The surface area and pore volume are the important factors for the amount of gas absorption possible. In general, it is believed that larger pore sizes in hybrid networks means there is a greater possibility of gas absorption. Ferey et al. reported a hybrid network, $Cr_3F(H_2O)_2O[C_6H_3(CO_2)_2]_3$ (MIL-101) (Figure 1.3A), that shows significant capacity at 77K: 6.1 wt% under 8 MPa.[29] The "MIL" hybrid materials contain water and free carboxylate acids as guests. The removal of guest molecules create voids with the accessible diameter of 29 Å in MIL-101.[29] In 2006, Yaghi et al. reported a series of isoreticular (isoreticular: the same topology in different networks.[21]) metal organic frameworks (IRMOFs) that have extremely high surface area which can be used in H_2 uptake.[30, 31] The IRMOF-20, $Zn_4O(C_8H_2O_4S_2)_3$ was constructed by thieno(3,2-b)thiophene-2,5-dicarboxylic acid with Zn(II). The crystal structure of IRMOF-20 has pores with a diameter approximately 14.0 Å (Figure 1.3B).[31] The porosity measurement showed H_2 adsorption data for IRMOF-20 is 13.5 mg/g at 1atm and 77K.[31]

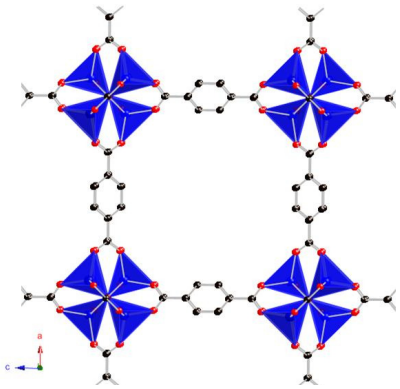

Figure 1.2: The crystal structure of $Zn_4O(bdc)$ (bdc = 1,4-benzenedicarboxylat). (Blue = zinc; black = carbon; red = oxygen.)[21, 23]

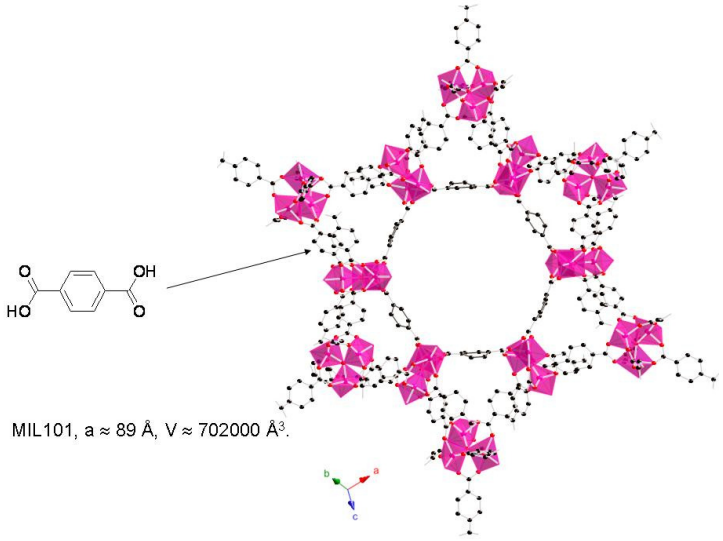

Figure 1.3A: The porous hybrid networks $Cr_3F(H_2O)_2O[C_6H_3(CO_2)_2]_3$ (MIL-101). (purple = chromium, black = carbon, red = oxygen.)[29]

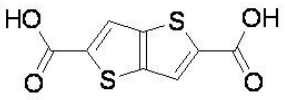

thieno(3,2-b)thiophene-2,5-dicarboxylic acid

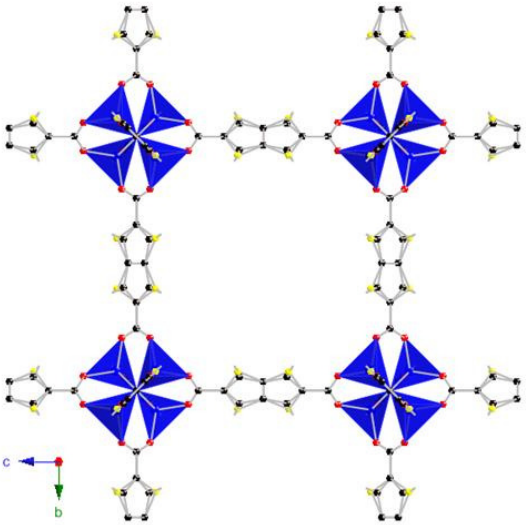

Figure 1.3B: The crystal structure of IRMOF-20, Zn4O(C8H2O4S2)3. (blue = zinc, black = carbon, red = oxygen, yellow = sulfur.)[31]

Some studies have reported that smaller pores actually have higher gas absorption ability.[32, 33] Lin et al. reported that two hybrid networks with very large cavities of approximately 19 x 19 x 19 $Å^3$ form interpenetrated structures.[33] The idealize pore size is approximately 4.5-5.0 Å, which allows the dihydrogen molecules to interact with the network structure.[33] Even though it is difficult to determinate these gas absorption values, it should be considered in the future.

Other important factors that may influence gas absorption are thermal activation and metal-based hydrogen binding sites. The removal of solvent or guest molecules via thermal activation is important for the gas absorption because some of guest molecules might block the access of gas. Chen et al. reported the removal of axial ligands from dicopper paddlewheel hybrid frameworks, so the copper binding sites are exposed.[34]

1.2.2 Chiral properties

Ideally, the chiral functionalities of hybrid networks should generate heterogeneous asymmetric catalysts for the synthesis of enantiomerically pure compounds. Further, chiral hybrid frameworks may perform enantioselective separations of racemic mixtures via 'filtration' through its chiral pores or channels. Successful design of homochial porous hybrid networks will expand the utility of zeolitic materials into chirotechnology.[18]

Three approaches have been used in the construction of homochial hybrid networks. The first approach is to build chiral networks from achiral building blocks. In principle, any hybrid materials can be crystallized in a chiral space group as long as all building blocks arrange in a particular way. However, these hybrids tend to self-assemble in both enantiomorphic forms, resulting in racemic mixtures. An example of a chiral framework obtained form achiral building blocks has been reported by Ezuhara and his coworkers.[35] The reported helical hybrid framework (space group is $P2_1$),

Cd[5-(anthracen-10-yl)pyrimidine]$(NO_3)_2(H_2O)$(EtOH), was obtained from 5-(anthracen-10-yl)pyrimidine and $Cd(NO_3)_2 \bullet 4H_2O$ (Figure 1.4).[35] The water-nitrate hydrogen-bond interactions formed screw axis 2_1. Solid-state circular dichroism (CD) indicated that the crystals are homochiral. The application of this homochiral framework to enatioselective catalysis or separation science has not been studied in their paper.

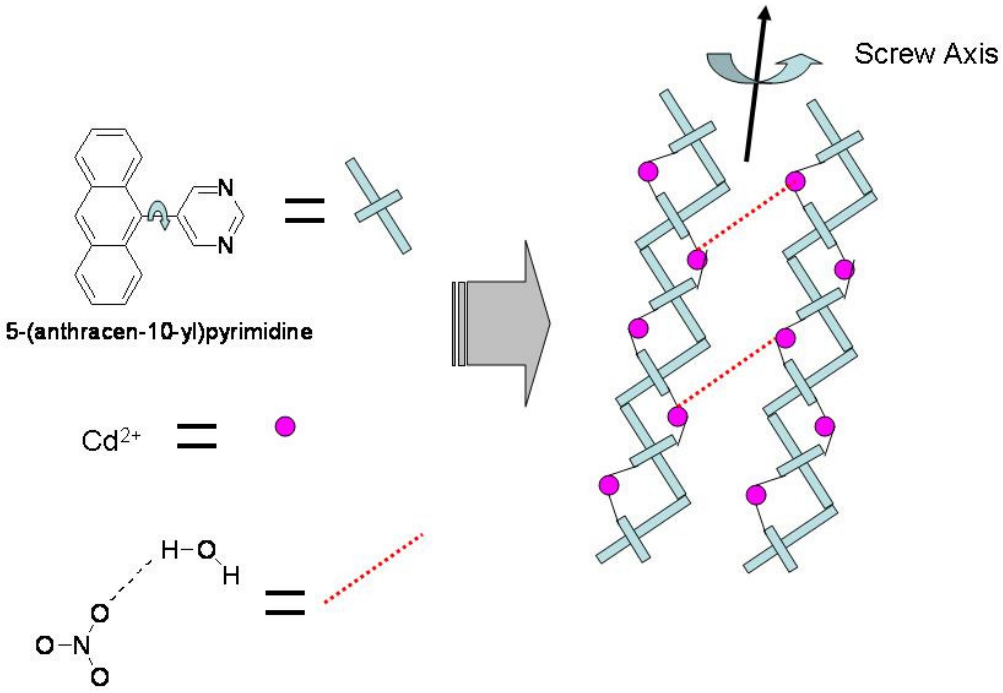

Figure 1.4: A view of the homochiral hybrid network Cd[5-(9-anthracenyl)pyrimidine]$(NO_3)_2(H_2O)$(EtOH) formed by hydrogen-bonding interactions between water and nitrate groups.[35]

The second approach is to crystallize hybrids from chiral templates. However, even if chiral building blocks are used, it is possible that a racemic mixture will result. Tosseinsky et al. reported the use of enantiomerically pure 1,2-propanediol as a template to construct the homochiral porous hybrid network Ni_3(1,3,5-bricarboxylate acid)-$_2$(pyridine)$_6$(1,2-propanediol)$_3$ (Space group is $I4_132$.).[36] In this crystal, 1,2-propanediol acts as a chiral template that causes chirality in the network creating chiral pores along a axis (Figure 1.5).[36] The solvent molecules can be carefully removed from this structure to form

empty chiral pores, and vacant coordination sites around the metal ions.[36] A related compound, Ni_3(1,3,5-tricarboxylate)$_2$(3-picoline)$_6$ (1,2-propanediol)$_3$•[9(1,2-propanediol)•11H_2O] has shown enantioselective adsorption of 1,1′-bi-2-naphthol with a capacity of 7.3 wt% and enantiomeric excess of 8.3%.[36]

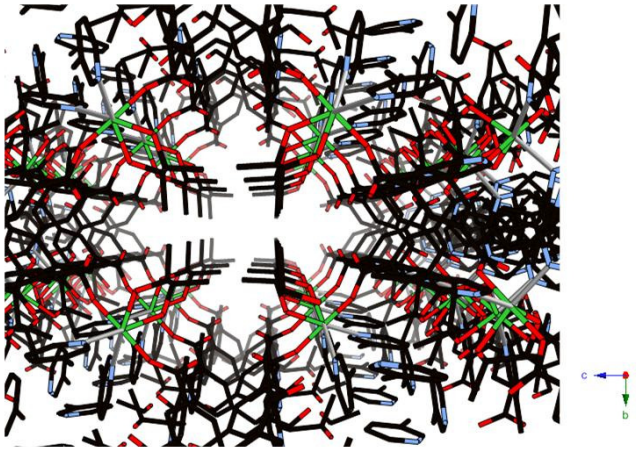

Figure 1.5: A view of the homochiral network, Ni_3(1,3,5-tricarboxylate)-$_2$(pyridine)$_6$(1,2-propanediol)$_3$ showing the helical motifs along a axis.[36] (green = nickel, black = carbon, light blue = nitrogen, red = oxygen.)

The third approach is to generate homochiral hybrids with chiral ligands. Chiral ligands can be included in the hybrid network structure, which can then catalyze organic transformations by metal ion in asymmetric way. Kim et al. reported the first example of the use of a homochiral framework as an asymmetric catalysis. The hybrid framework [Zn_3(μ_3-O)(L)$_6$]•2H_3O•12H_2O (L = (4S,5S)--2,2dimethyl--5--(pyridine--4--ylcarbamoyl)--1,3--dioxolane--4--carboxylic acid, see Scheme 1.2A, crystal structure is in Figure 1.6) has a layer structure with large 1D chiral channels parallel to the crystallographic c axis, the cross section of which is approximately an equilateral triangle with side length ~13.4Å.[37] The pyridnium groups of the ligand are located within the open channels.[37] The acetate of 1-phenyl-2-propanol was synthesized within the network's channels, and was produced with an enantiomeric excess of about 8% in favor of the S-enantiomer (Scheme 1.2B).[37]

L

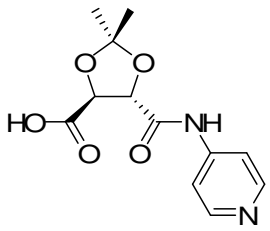

(4*S*,5*S*)-2,2-dimethyl-5-(pyridin-4-ylcarbamoyl)-1,3-dioxolane-4-carboxylic acid

Scheme 1.2A: Chiral ligand L.[37]

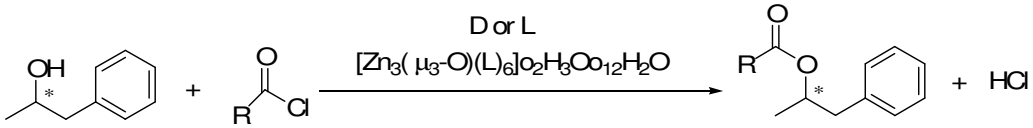

racemic mixture 8% enantiomeric excess of S or R

Scheme 1.2B: The synthesis of ester with a homochiral framework $[Zn_3(\mu3\text{-}O)(L)_6]\bullet2H_3O\bullet12H_2O$.[37]

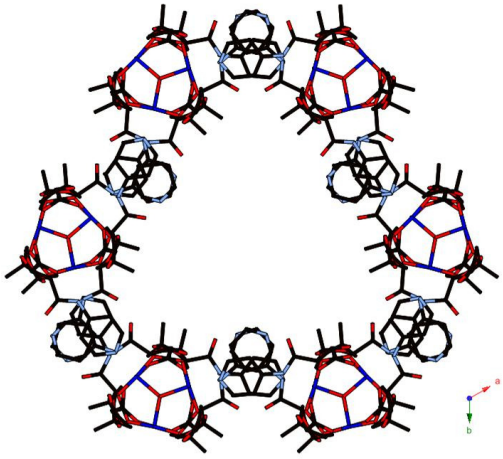

Figure 1.6: The hexagonal framework of chiral $[Zn_3(\mu_3\text{-}O)(L)_6]\bullet2H_3O\bullet12H_2O$. (Blue = zinc, black = carbon, light blue = nitrogen, red = oxygen.)[37]

There has been significant progress in the synthesis of homochiral hybrid networks over the past few years. Even though research in this field is still at an early stage, chiral porous hybrid materials have already shown catalytic activity and enantioselectivity for several organic transformations.[37] It is hopeful that hybrid materials will be developed further

for use in chirotechnology applications in the future.

1.2.3 Ion exchange

The ion exchange properties of hybrid materials could lead to their potential application in water/solvent purification systems. Black et al. reported a hybrid network, Ag(4,4′-bipyridine)•(NO_3)(Figure 1.7),[15] that when placed in aqueous solutions containing anions such as PF_6^-, MoO_4^-, BF_4^- or SO_4^{2-}, underwent anion exchange between NO_3^- and solution anions.[15] They observed that PF_6^- ion exchange is completed after 6 hours in water [A slightly excess of $NaPF_6$ was added to a suspension of crystalline Ag(4,4′-bipyridine)•(NO_3)].[15] The ion exchange product remained crystalline structure. The ion exchange process could be reversed by placing the ion exchanged crystals in a KNO_3 solution.[15]

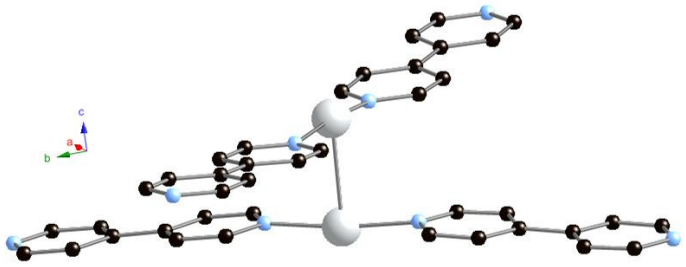

Figure 1.7: The 3D framework of Ag(4,4′-bipyridine)•(NO_3). (For clarity, NO_3^- is omitting. Silver = silver, black = carbon, light blue = nitrogen.)[15]

1.2.4 Luminescence and nonlinear optical properties

Hybrid materials can show luminescent properties, which means that they may be useful as selective sensor materials. Brandys et al. reported a 1D hybrid chain

$[Au_2(trans\text{-}Ph_2P(CH_2)_4PPh_2)_3]\bullet 2(CF_3CO_2)\bullet 2(CH_4O)$ (Figure 1.8),[38] for which luminescence was observed.[38] But this hybrid network is not porous.[38]

Lin et al. reported diamondoid networks bis(isonicotinato)Zn and bis(4-pyridylacry)Cd$\bullet H_2O$, which show nonlinear optical behavior.[39] They found that the zinc/cadmium network displayed a second order nonlinear optical response three times that of potassium dideuterophosphate.[39]

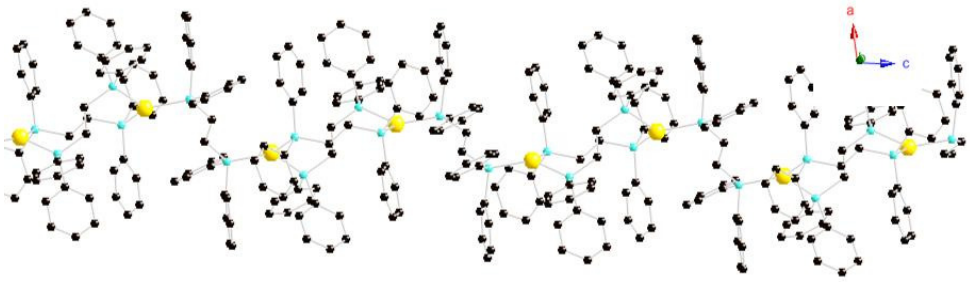

Figure 1.8: A view of 1D hybrid chain structure of $[Au_2(trans\text{-}Ph_2P(CH_2)_4PPh_2)_3]\bullet 2(CF_3CO_2)\bullet 2(CH_4O)$. (For clarity, CF_3CO_2 and CH_4O are omitting. Gold = gold, black = carbon, light blue = phosphous.)[38]

1.3 Synthetic methods

1.3.1 Reticular synthesis

It is challenging to investigate methods to synthesize crystalline hybrid network materials because of the lack of control over the topology of hybrids produced from the traditional synthesis. The starting materials do not maintain their structure integrities, which

makes it difficult to predict the topology of the hybrid network structure that will form. Yaghi et al. introduced the concept of "reticular synthesis" to this field.[21] Reticular synthesis is about the predicable design and synthesis of extended 3D hybrid networks. The idea is to use building blocks with well-defined geometry in the synthesis, and these building blocks maintain their structural integrity during the network formation. Reticular synthesis is different from retrosynthesis and supramolecular synthesis. When considering the retrosynthesis of organic compounds, it is not necessary for the starting materials to retain their structural integrity. Whereas the networks that are prepared by supramolecular synthesis may be constructed using weaker bonds such as hydrogen bonds; in reticular synthesis, the network is connected in all three dimensions by covalent bonds.

Although we cannot predict with 100% accuracy the topology of a hybrid network from a synthesis procedure, reticular synthesis does provide some way of controlling the possible products of a synthesis method.

1.3.2 Solvothermal synthesis

The particles in a crystal are vibrating about their fix positions. As the temperature rises, the particles vibrate more. When the particles have enough kinetic energy to break free of their positions, the crystal is destroyed (melting). If the solid and liquid phases remain contact, then a dynamic equilibrium can be established in which the melting rate equals the freezing rate. However, it is much easier to destroy a crystal than to grow a crystal, because the entropy decrease due to the ordering of molecules within the system is overcompensated by the thermal randomization of the surroundings due to release of the heat of fusion. So the growth of a crystal is under kinetic control, rather than thermodynamic control.[40]

Hybrid networks are often prepared by solvothermal synthesis. Solvothermal synthesis is a technique for crystallizing substances from high-temperature solutions at high vapor pressures. There are a wide variety of factors that need to be considered when planning a

solvothermal synthesis, including concentration of starting materials, stoichiometry, pH value, solubility, reaction temperature, and reaction time. Hydrothermal synthesis is the special case when the solvent is water. In many cases, a solvent mixture is used to affect the crystallization. The reaction temperature depends on the chemical properties of the starting materials, for example, the melting, boiling, and decomposition temperatures. The choice of reaction temperature and solvent determinates the kind of reaction container that can be used for the reaction. With water as the solvent, if low temperatures (less than 100℃) are required, vials can be used for the reaction. For temperatures greater than 100℃, but less than 140℃, sealed glass tubes can be used. For temperatures above 140℃, but less then 250℃, stainless steel bombs are used. Stainless steel bombs allow higher working pressures, up to 1800 psi, and the volume of the bombs is ~23mL.[41] Vials, glass tubes, and stainless steel bombs are used a lot in the synthesis of hybrid networks.

1.3.3 Other synthetic techniques

Other less frequently used techniques in hybrid network synthesis include slow evaporation, vapor diffusion, and solvent diffusion, etc.[42]

Slow evaporation. If the compounds are not sensitive to ambient condition, slow evaporation is one of the simplest way to grow crystals. A saturated or nearly saturated solution is covered and palced in a vibration free container for crystal growth.

Vapor diffusion. The first solution S1 is placed in the test tube or vials, and the second solution S2 is placed in a closed beaker. The test tube with S1 is placed in beaker. Then beaker is sealed. Slow diffusion of one solution into another solution form crystals.

Solvent diffusion. This method is about layering technique. The first solute in a test tube is with solution (S1), and second solute in another test tube is with different solution (S2). The density of S2 and S1 should be different. If the density of S2 is less than S1, S2 can be

added slowly into S1 and form discrete layers. Crystal can form at between two layers.

1.4 Introduction of chelating ligand and bridging ligand

A ligand can be an organic molecule or ion that is capable of binding to metal ions through one or more sites. Chelating ligands bind to a single metal ion by more than one site. Chelating ligands commonly form discrete molecular complexes instead of networks, for example, oxalate, 2, 2'-bipyridine and 1,10-phenanthroline are chelating ligands (Scheme 1.3). Metal complexes of chelating ligands are prototypical coordination compounds.[43] Bridging ligands also contain more than one coordination site; however, the geometry of the donor atom prevents the ligand from forming more than one connection to a single metal ion. The use of bridging ligands is associated to the formation of networks. Examples of bridging ligands used in this study are 4, 4'-bipyridine, terephthalic acid, and 4-(2-(4-hydroxyphenyl)ethynyl)phenol (Scheme 1.4). Bridging ligands with a variety of functional groups are common in network construction. The rigidity and size of the ligand backbone can influence the topology of the network. For example, larger ligands may lead to the formation of large cavities in the network.

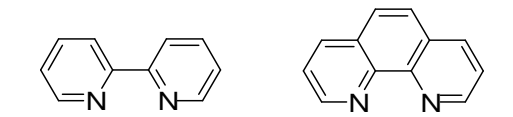

2-(pyridin-2-yl)pyridine 1,10-phenanthroline

Scheme 1.3: Examples of some chelating ligands.

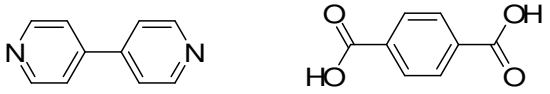

4,4'-dipyridine terephthalic acid

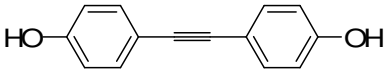

4-(2-(4-hydroxyphenyl)ethynyl)phenol

Scheme 1.4: Examples of some bridging ligands.

1.5. Transition metal ions

Transition metals are elements that have a partially filled *d* shell in one or more of their commonly occurring oxidation states. Most transition metals have several readily accessible oxidation states. They are often colored, and many of their compounds are paramagnetic. Many transition metal ions can form complexes or networks when allowed to react with a wide of variety of ligands. Transition metal ion based hybrids may show magnetic behavior and in principle, the metal may be accessible to substrate in a catalytic reaction.

Coordination number 2

Transition metal ions such as Cu^+, Ag^+, Au^+, and Hg^+, each have a ground-state d^{10} electron configuration. When these transition metal ions form complexes, they tend to have linear geometry. For example, Liu et al. reported a Ag^+ coordination complex constructed with 1,3,5-tris(imidazol-1-ylmethyl)-2,4,6-trimethylbenzene, in which the Ag^+ ions were linked by ligands to form cages (Figure 1.9).[44] In these cages, the N-Ag-N angle is linear for all three of the Ag^+ ions.[44]

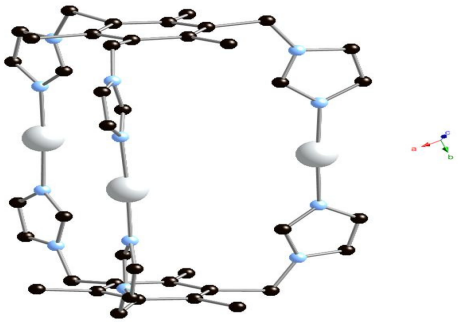

Figure 1.9: Ag^+ cages in a complex $[Ag_3(titmb)_2](PF_6)_3$. [titmb = 1,3,5-Tris(imidazole-1-ylmethyl) -2,4,6-trimethylbenzene]. (For clarity, PF_6 molecules are omitting. Silver = silver, black = carbon, light blue = nitrogen.)[44]

Coordination number 3

Only a few transition metal ions have coordination number 3. Most complexes that have the empirical formula ML_3 (M = metal ion, L = ligand) actually are octahedral. For example, $CrCl_3$ has a layer lattice in which each Cr atom is coordinated to 6 Cl atoms. In hybrid network construction, three-coordinated transition metal ions are not commonly used.

Coordination number 4

This is one of the most common coordination numbers uses in hybrid network construction. Four coordinate ions are typically, tetrahedral or square planar. For example, Zn^{2+}, Co^{2+}, Fe^{2+}, and Mn^{2+} ions tend to show tetrahedral geometry. When the metal ions have d^8 configuration, square planar geometry is often preferred. For example, Ni^{2+} has tetrahedral geometry in $NiCl_4^{2-}$ but shows square planar geometry in $Ni(CN)_4^{2-}$. Hybrid networks containing metal ions that show tetrahedral or square planar geometry tend to form 2D or 3D structures. Choi et al. reported the H_2 absorption capacity in the Co(1,4-benzenedipyrazolate) framework (Figure 1.10).[45] In this structure each Co^{2+} is tetrahedrally coordinated to N atoms from four different 1,4-benzenedi(4′-pyrazolyl) ligands.[45] Castillo et al. reported a complex crystal, $Cu(C_{15}H_{14}NO_2)_2$, in which the Cu(II) ions are four-coordinated and have a slightly distorted square planar geometry (Figure 1.11).[46]

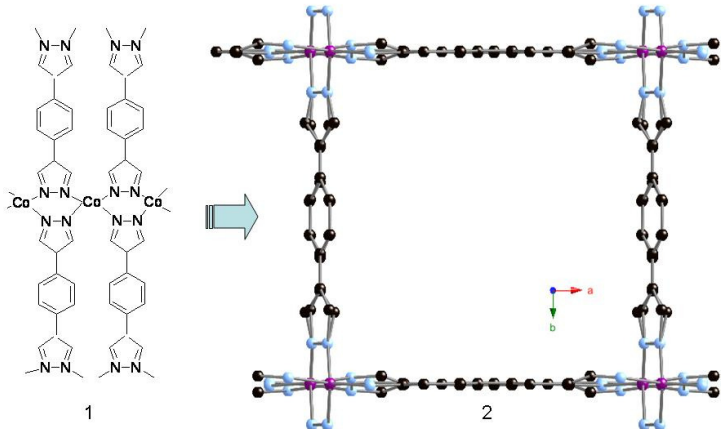

Figure 1.10: (1) Schematic picture shows the Co^{2+} coordination geometry. (2) Structure of a portion of the metal organic framework in Co(BDP)•2DEF•H_2O (H_2BDP = 1,4-benzenedi(4′-pyrazolyl), DEF = N, N-diethylformamide, purple = cobalt, black = carbon, light blue = nitrogen.)[45]

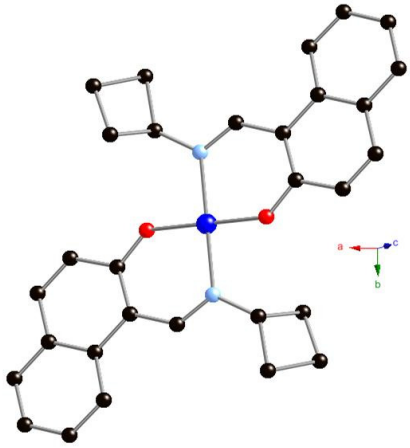

Figure 1.11: Molecular structure of crystal of $Cu(C_{15}H_{14}NO_2)_2$.[46]

Coordination number 5

Metal ions that are five-coordinated can have trigonal bipyramidal or square pyramidal geometry. Both coordination geometries are known in network structures. For example, Angulo-Cornejo et al. reported some interesting Cu(II) complexes.[47] One of these complexes,

$C_{28}H_{18}CuN_4O_2S_2$•DMF (DMF = Dimethylformamide) contains five-coordinate Cu(II).[47] In this complex crystal structure, Cu(II) ion was coordinated by two deprotonated ligands with N, O-coordination and a DMF molecule (Figure 1.12).[47] The Cu(II) is a trigonal bipyramidal geometry.[47] Two nitrogen atoms are in axial , and two oxygen and DMF are in equatorial positions.[47] Another metal complex, $C_{12}H_{12}CuN_4O_5$•$3H_2O$ was reported by Dong et al.[48] In this complex, the coordination environment of Cu(II) ion is a slightly distorted square pyramidal (Figure 1.13).[48] One water molecule is on axial position, and two nitrogen atoms and two oxygen atoms are on equatorial positions.[48]

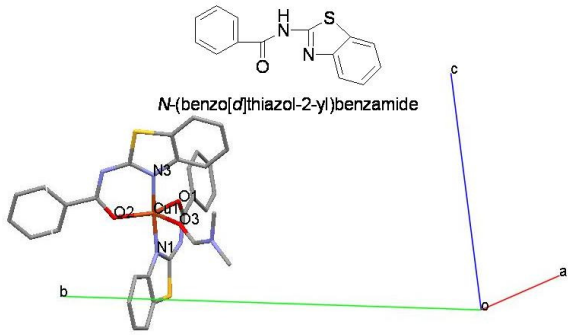

Figure 1.12: Ligand and metal complex $C_{28}H_{18}CuN_4O_2S_2$•DMF. (copper = copper, red = oxygen, gray = carbon, light blue = nitrogen, yellow = sulfur.)[47]

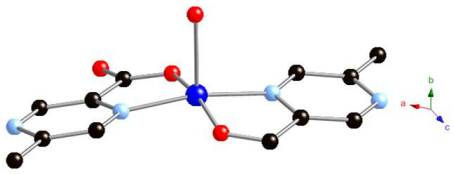

Figure 1.13: Square pyramidal geometry of Cu(II) in complex $C_{12}H_{12}CuN_4O_5$•$3H_2O$. (blue = copper, light blue = nitrogen, black = carbon, red = oxygen.)[48]

Coordination number 6

Coordination number 6 is very important in complexes and networks. Typically, six coordinate metal ions show octahedral, or distorted octahedral geometry. For example, Co^{2+} and Ni^{2+} ions with octahedral geometries are common in metal organic frameworks. Clausen

et al. reported a network, $Co_3(C_8H_4O_4)_4(C_4H_{12}N)_2(C_5H_{11}NO)_3$, in which one of the Co^{2+} ions (Co(2) in Figure 1.14) is situated on an inversion center (space group *C2/c*) and displays octahedral geometry, and all six coordination sites are used in network construction (Figure 1.14).[49] Yao et al. reported a new network, [Ni_2(benzimidazole-5,6-dicarboxylic acid)$_2(H_2O)_4]\cdot 3H_2O$, in which all the NI(II) ions are six coordinate with the same distorted octahedral geometry environment, although two of the six coordination sites is typically not used for network construction. (Figure 1.15).[50]

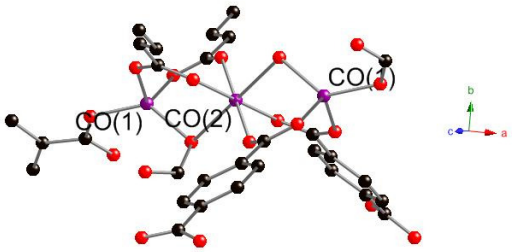

Figure 1.14: Octahedral geometry of Co(II) in network. (purple = cobalt, black = carbon, red = oxygen.)[49]

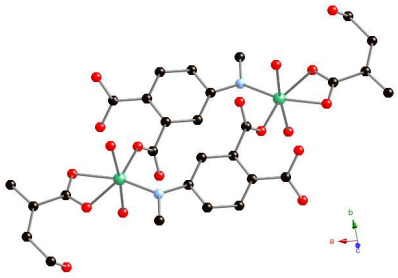

Figure 1.15: The coordination environment of Ni(II) atom in network [Ni_2(benzimidazole-5,6-dicarboxylic acid)$_2(H_2O)_4]\cdot 3H_2O$. (green = nickel, black = carbon, light blue = nitrogen, red = oxygen.)[50]

Coordination number 7

Coordination number 7 is relatively uncommon in complexes and networks. In the few available examples, one or more of the seven coordination sites are typically not used for

network construction. Liu et al. have reported an example of this coordination mode; a two dimensional network, Cd_3(naphthylmethylimidazole)$_2$(terephthalate)$_3$(DMF)$_2$•0.5H_2O, containing seven-coordinated Cd(II) ions (Figure 1.16).[51] In this crystal structure, only 6 coordination sites on Cd(II) are used in the network formation.

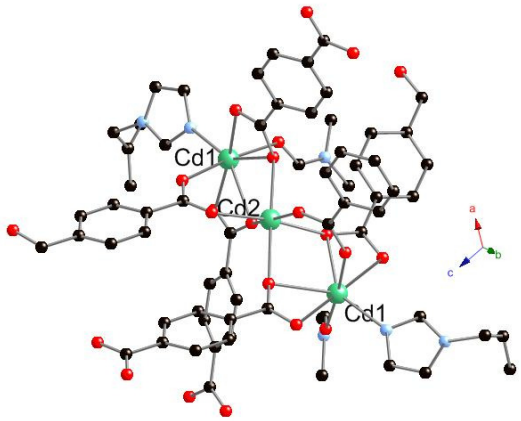

Figure 1.16: Seven-coordinated Cd(II) in network Cd_3(naphthylmethylimidazole)$_2$(terephthalate)$_3$(DMF)$_2$•0.5H_2O. (green = cadmium, black = carbon, light blue = nitrogen, red = oxygen.)[51]

Higher coordination numbers

Metal ions with coordination number 8 can be found in some coordination complexes, such as $Na_3Mo(CN)_8$•4H_2O and $[N(n\text{-}C_4H_9)_4]_3Mo(CN)_8$.[52] Metals with coordination number 9, show tricapped trigonal prismatic geometry e.g. $Nd(H_2O)_9^{3+}$ and ReH_9^{2-}. Metal ions with coordination number 10, 11 or 12 are occasionally found in metal complexes containing lanthanide and actinide ions. There use in network synthesis has not been explored.

1.6 Templates

Templates are relatively small organic molecules that can connect to network structure via weak intermolecular bonds, such as hydrogen bonds and π…π interactions. Templates

play an important role in the construction of hybrid materials due to their ability to direct network formation (sometimes, they are called structure-directing agents). Usually, the size, the charge, and the functional groups of templates molecules have an obvious influence on the structure topologies of the hybrid networks in which they are incorporated. For example, ClO_4^-, BF_4^-, PF_6^-, and NO_3^- have been used as templates in a variety of network constructions[53-55]. Li et al. reported a ClO_4^- templated 3D open framework, $[Ln_2(1,2\text{-bdc})_2(H_2O)_2\ Cu(inic)_2](ClO_4)$.[55] In this case, $NaClO_4$ was purposely introduced into the reaction mixture because ClO_4^- is a useful and effective template.[55] Chiral templates may direct homochiral hybrid network formation. For example, R-binaphthol co-crystallized with TMDP to form a chiral, hydrogen-bonded organic network; the formation of this network appears to be directed by the template molecules. In another example, Chen et al. reported a homochiral material (EMIm)$[Co_2(D\text{-cam})_2(ac)]$ (D-H_2cam = D-camphoric acid; ac = acetate; EMIm = 1-ethyl-3-methylimidazolium) that was templated by small organic molecules.[54] In their crystal synthesis, D-camphoric acid acted as both the solvent and the template.[54] Another example is provided by Gómez-Hortigüela et al. who investigated the potential catalytic consequences of using an enantiomerically pure chiral template, *S*-(−)-1-benzyl-2-pyrrolidinemethanol, in the synthesis of hybrid frameworks.[53]

1.7 Characterization

1.7.1 X-ray single crystal and powder diffraction

X-ray crystallography is the most powerful and unambiguous method for the determination of the structure of crystalline materials. Max von Laue discovered X-ray diffraction in 1912.[56] Photographic plates were used to record early diffraction experiments. The development of modern high speed computers, automated diffractometers, and powerful structure solution program makes X-ray diffraction become a standard technique for crystal determination.

The electrons in the crystal scatter X-rays to produce the diffraction pattern. The frequency of X-ray is high, the diffraction time scale is short and the motion of atoms is stable. Also, the thermal motion or vibration of atoms will affect the diffraction patterns. The structure determination depends on the positions of atoms. Intensity of diffracted beams is determined by atom position within the unit cell.

X-rays are generated by a high-vacuum X-ray tube. A beam of electrons is directed towards a target of high purity metal, e.g. copper and molybdenum, known as the anode. The electron beam is generated from a cathode source. X-rays are produced in two ways. The electrons approach and enter the metal target and generate radiation which is electromagnetic radiation with a range of wavelengths. Another method is used in diffraction experiments. The X-ray generation is the electron beam ionizes the metal target, ejecting electrons form the K-shell. Electrons from a higher energy orbital, L-shell, relax in the lower energy K-shell and emit two wavelength X-rays ($K_{\alpha 1}$ = 0.70926 Å and $K_{\alpha 2}$ = 0.713543 Å for Mo targets).

The trade-off-optimal size of single crystal used in X-ray diffraction experiment is $2/\mu$, but smaller than X-ray beam (collimator size).The single crystal is mounted on a nylon loop and centered on the goniometer. When single crystals are observed under the microscope by using plane-polarised light, they will be seen to “extinguish” when rotated.

X-ray diffraction data collection is processed automatically using the diffractional software in diffractometers. The software is supplied by instrument manufacture (Oxford Diffraction) for use with their diffractometers.

1.7.2 Thermal analysis

Thermal analysis[57] includes a series of techniques in which change in mass of a material are measured as a function of temperature. Current fields of applications provide

information on composition, product reliability, stability, chemical reactions and dynamic properties. Thermal analysis has been used to determine the physical and chemical properties of polymer, crystalline materials, geological materials. Thermal analysis plays an important role in both quantitative a qualitative analyses. Qualitative study of thermal behavior can indentify and characterize materials. Quantitative results come from changes in weight and enthalpy as the sample is heated.

Thermogravimetric analysis (TGA) is one of the many thermal analysis techniques. TGA provides a quantitative measurement of weight change vs temperature. Typically, TGA is used to investigate the thermal stability and compositional analysis of materials. TGA can record directly the weight change as a function of temperature or time for transitions that involve dehydration or decomposition. Over a range of temperature, TGA curves show the characterization of a compound or material based on the different results of physical transition and chemical reactions. The weigh change can be related to the molecular structure. For example, the volatile weakly coordinated will come off first. The TGA data can investigate the thermodynamics and kinetics of the reactions and transitions that can be the thermal application of the materials. Typically, the temperature range of TGA is from room temperature to 1200°C in nitrogen gas or air, and linear heating rates form 5 to 10°C. In the TGA analysis, the weight of a sample is record continuously as the temperature is increased. A sample is placed in a dish that is sitting in a furnace on a quartz beam which is attached to the automatic recording balance. Any change in the weight of the sample causes the deflection of the beam which is sensed by photodiodes. When the beam is restored to the original position, the balance detects the current which is send from the photodiodes. The current is proportional to the change of weight of the sample.

1.7.3 Other characterizations

X-ray single crystal diffraction and TGA are the most useful analysis techniques for characterization of hybrid materials. Other characterizations, such as IR, NMR and magnetic

susceptibility measurement are also used in our research.

Chapter 2

Series I: Hybrid networks containing the flexible ligand

4, 4′-trimethylenedipyridine (TMDP)

2.1 Introduction to series I

Templated zinc phosphites exhibit a variety of three-dimensional architectures that reflect the versatility of ZnPO systems.[58-69] Typically, the pseudotetrahedral $(HPO_3)^{2-}$ anion is three-connected, and the Zn^{2+} cation is four-connected in these framework structures. Fully connected (3,4) nets built from HPO_3^{2-} and Zn^{2+} have the stoichiometry $3Zn^{2+}$:$4(HPO_3)^{2-}$ and a net anionic charge that requires extra framework cations as counterions.[70] Hybrid frameworks form when one or more zinc coordination sites are occupied by a ligand other than $(HPO_3)^{2-}$, and the resulting structures are typically neutral with a composition of 1 mol L (organic compound):1 mol of Zn^{2+}:1 mol of $(HPO_3)^{2-}$.[58-65, 67, 68, 70, 71] The role of L, either as a template or a ligand, is likely to be dictated by temperature, pH, and ligand basicity. At low pH, a nitrogen base may be more likely to adopt the role of a template and direct the formation of a three-dimensional structure, while at higher pH, the nitrogen base may act as a ligand to form a hybrid structure. The simple equilibrium represented in Equation 2.1 is clearly important in determining the role of the ligand in the synthesis of hybrid structures.

$$Zn^{2+} + LH^{+} \rightleftharpoons ZnL^{2+} + H^{+}$$

Equation 2.1: Equilibrium in the synthesis.

2.2 Flexible bridging ligand 4, 4'-trimethylenedipyridine (TMDP)

Ligand flexibility is important in generating materials with a dynamic response upon adsorption of small molecules.[2, 72] Flexible ligands tend to adopt a variety of conformations when they are used in network construction. Typically, coordination sites of flexible ligands are appended via a flexible link. Examples of flexible ligands that have been used in network construction are N,N'-di(4-pyridyl)adipoamide[73], bis(2-pyrimidinylthio)methane[74], and 3,3'-thiodipropionic[22] (Figure 2.1).

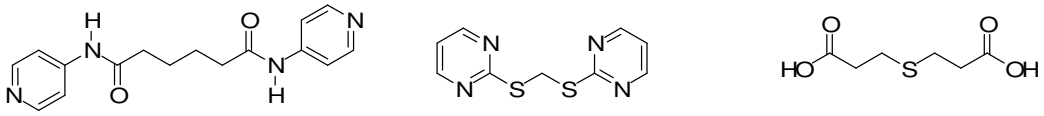

N, N'-di(4-pyridyl)adipoamide bis(2-pyrimidinylthio)methane 3,3'-thiodipropionic acid

Figure 2.1: Some examples of flexible ligands.

The ligand 4, 4'-trimethylene-dipyridine (TMDP) (Scheme 2.1) has been used widely in the synthesis of both organic[75-83] and hybrid inorganic-organic[84-91] framework structures. One of the advantages of TMDP is its flexibility, which allows it to connect to a variety of organic and inorganic units in network structures.[80] The potential energy surfaces for conformations of 1,3-disubstituded propanes, such as 1,3-diphenylpropane[92] and TMDP, is relatively flat and it is apparent that the energy cost of conformational change in TMDP during the generation of network structures is more than offset by other factors, e.g. low concentration of starting materials in the crystallization process. There is a balance between materials' solubility and crystallization. Typically, staring materials are moderately soluble in solvent. If the concentration of starting materials is too low, materials will remain soluble in solvent and no crystals form. On the other hand, it is important to avoid solvents that give supersaturated solutions to yield small, poorly quality crystals.

Conformational energy calculations for diprotonated TMDP in water were done with the CACHE molecular modeling program with PM5 parameters.[93] Calculations were performed with protonated TMDP to simulate the form of the ligand under acidic reaction conditions. Additionally, inclusion of the proton on the nitrogen lone pair simulates the coordination of the pyridine ligand to a metal cation. Local minima were searched for the idealized starting points: *c*, *g*, *a*, *c*; *c*, g^-, *a*, *c*; *c*, *a*, *a*, *c*; *c*, *g*, *g*, *c*; and *c*, g^-, *g*, *c*; where *c* (*clinal*) represents a dihedral of 90 ± 15°, *g* (*gauche*) represents a dihedral of 60 ± 15° (g^-, −60 ± 15°), *a* (*anti*) represents a dihedral of 180 ± 15°, and *s* (*syn*) represents a dihedral of 0 ± 15°. Energies are reported in kcal mol^{-1} relative to the most stable conformation found, *c*, g^-, *a*, *c*, as defined in the following paragraph. For comparison, we repeated the TMDP conformational calculations using 3-diphenylpropane; these were in good agreement with the literature values (i.e. the calculated most stable conformation had dihedral angles within 5° of the reported values).[92] The energies for the crystallographically observed conformations were calculated by fixing the dihedral angles to values obtained from the single crystal X-ray data. The dihedral angles were locked, and the energy optimized with PM5 parameters with protonated TMDP in water.

The dihedral angles ϕ_1, ϕ_1', ϕ_2, and ϕ_2' in TMDP are defined in Scheme 2.1. In defining the dihedral angles ϕ_1 and ϕ_1', we arbitrarily chose one of the two "*ortho*" carbon atoms; the two choices give dihedral angles that differ by 180°. The sign of the dihedral angle refers to the direction of rotation; a negative value indicates a clockwise rotation. The dihedral angles ϕ_1 and ϕ_1' are always defined in a positive sense. The dihedral angles ϕ_2 and ϕ_2' are defined as *gauche* (*g*) if the angles are near 60° and minus *gauche* (g^-) if the angles are near −60°. Table 2.1 lists six conformations that give local minima in the potential energy surface of TMDP. Pictures of these conformations are given in Figure 2.2. The highest energy of these is calculated to lie 1.5 kcal mol^{-1} above the most stable *c*, g^-, *a*, *c* conformation. Rotation about ϕ_1' in the *c*, g^-, *a*, *c* conformation is calculated to have an activation barrier of 0.5 kcal mol^{-1};

rotation about ϕ_2' in the *c*, g^-, *a*, *c* conformation is calculated to have an activation barrier of 3 kcal mol^-.

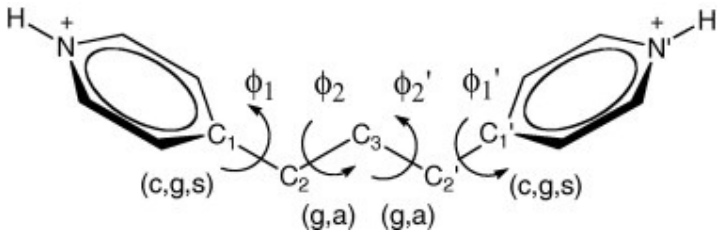

Scheme 2.1: TMDP ligand with dihedral angles ϕ_1, ϕ_1', ϕ_2, and ϕ_2'.

Table 2.1: Calculated and observed conformations for 1,3-di(4-pyridyl)propane.

	Configuration	ϕ_1	ϕ_2	ϕ_2'	ϕ_1'	**ΔE (kcal mol^{-1})**
Calculated						
I	*c*, −*g*, *a*, *c*	78	−68	178	76	0
II	*g*, *g*, *a*, *g*	65	64	178	67	0.1
III	*c*, *a*, *a*, *g*	75	179	179	64	0.1
IV	*g*, −*g*, −*g*, *g*	59	−65	−67	72	0.3
V	*g*, *g*, *g*, *g*	53	59	60	53	0.4
VI	*g*, −*g*, *g*, *g*	56	−82	69	68	1.5
Observed						
7	*g*, *a*, *a*, *g*	73	−178	176	85	0.3
8	*c*, *g*, *a*, *a*	87	67	176	7	1.5

	Configuration	ϕ_1	ϕ_2	ϕ_2'	ϕ_1'	ΔE (kcal mol^{-1})
9	*s*, *a*, *a*, *g*	0	179	178	22	2.0
10	*g*, *g*, *a*, *g*	63	67	173	24	1.1

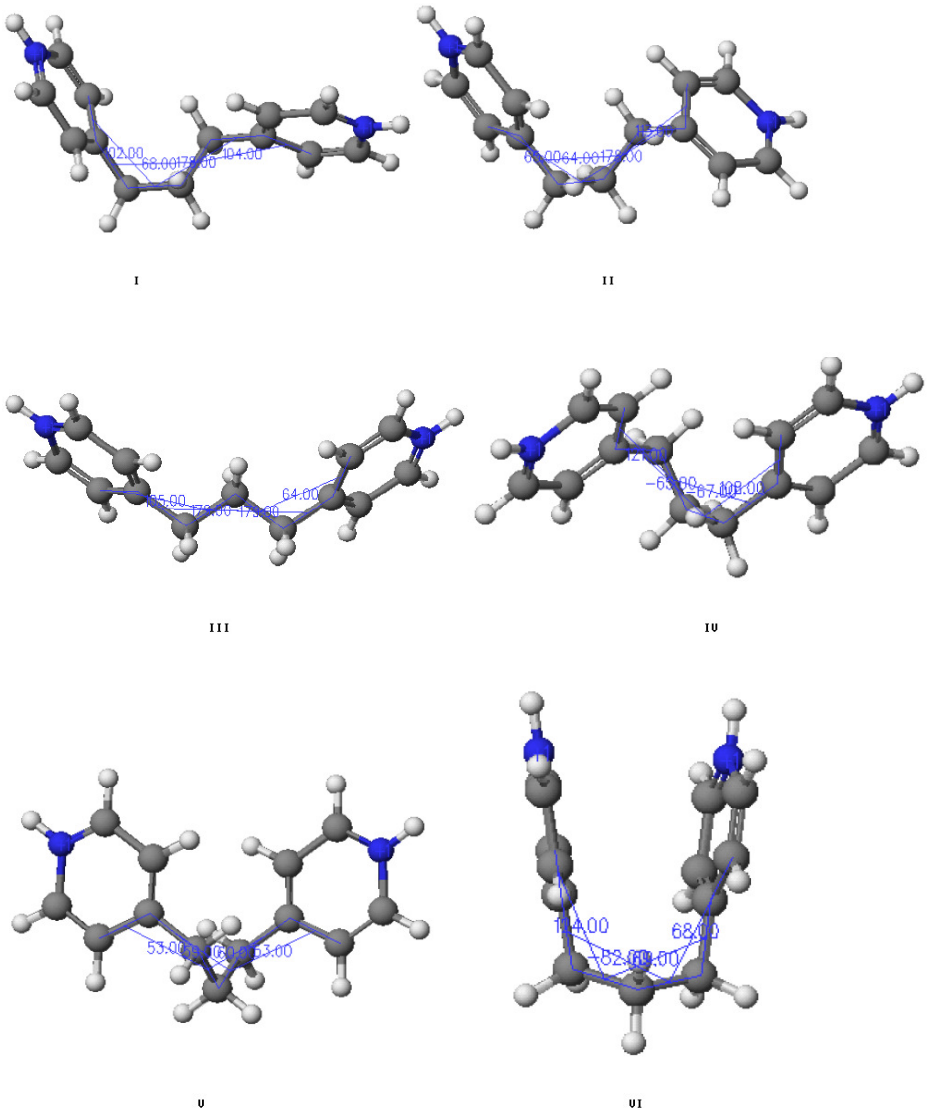

Figure 2.2: The calculated stable conformations for TMDP.

Although TMDP is extremely flexible it is impossible for the C_1–N and C_1'–N′ vectors to be collinear. The pyridine rings rotate to be nearly π stacked and eclipsed, a local space minimum is found for this situation in the *c*, g^-, *g*, *c* conformation; this conformation lies 1.5 kcal mol^{-1} above the *c*, g^-, *a*, *c* conformation.

Additionally, the observed conformations of TMDP in the network solids reported herein are given in Table 2.1. For comparison, the crystallographically observed conformations were "protonated" and the energies were calculated in water as was done for TMDP alone. The energies reported for the crystallographically observed conformations are relative to the most stable conformation, *c*, g^-, *a*, *c*, found by calculation.

The relative energy cost to access the conformations of TMDP that are observed crystallographically (see table 2.1) is calculated to be ≤2.0 kcal mol^{-1} for the examples reported here. This is indicative of the flexibility of the ligand, and is expected to be compensated for by the formation of zinc–oxygen and zinc–nitrogen bonds. Further, it is very likely that there is a favorable entropic component to the formation of crystals associated with the desolvation of ions and polar components of the reaction mixture in the aqueous reaction environment.

In most of the observed structures the dihedral angles, ϕ_2 and ϕ_2', as defined above, are both *anti*. These two angles are responsible for the relative direction of the nitrogen lone pairs. Deviations from the idealized (*anti*, *anti*; *gauche*, *gauche*; or *gauche*, *anti*) ϕ_2 and ϕ_2'angles come at a cost of a few kcal mol^{-1} in energy. The angles ϕ_2 and ϕ_2', however, only deviate seven degrees or less from their ideal *gauche* and *anti* values in the observed structures.

2.3 Metal ion Zn(II) in hybrid network series I

The Zn^{2+} ion has a d^{10} configuration and is typically four or six coordinate. Five-coordination is known but not common. Lower coordination number, such as two- or three-coordination requires bulky ligands. For example, Margraf et al. reported the complex $Zn[N(SiMe_3)_2]_2$, in which the Zn(II) atom is coordinated to two N atoms (Figure 2.3).[94] Hannant et al. reported three-coordinated Zn cations in complex $[ZnMe(DAD)]^+$[DAD = $(MeC{=}NC_6H_3Pr^i_2\text{-}2,6)_2$] (Figure 2.4)[95]. Evans and Lin reported a 2D coordination hybrid network $(Zn_4\text{-benzeato})_8$•{3-[2-(4-pyridyl)ethenyl]benzoic acid}•H_2O that contains four-coordinate Zn(II) ions (Figure 2.5).[96] A five-connected Zn(II) example is reported in a complex [1,5-bis(2-pyridylmethy)-1,5-diazacyclooctane]Zn(s-C_6H_4-p-CH_3)BPh_4(Figure 2.6).[97] The Zn(II) ion has octahedral geometry in the network Zn[1,3,5-tris(imidazole-1-ylmethyl)-2,4,6-trimethylbenzene]$_2(CLO_4)_2$ (Figure 2.7).[98]

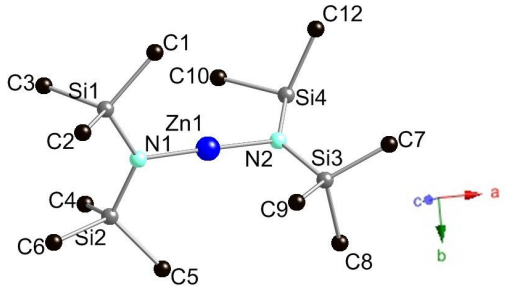

Figure 2.3: Zn(II) is two-coordinated in complex $Zn[N(SiMe_3)_2]_2$. [94]

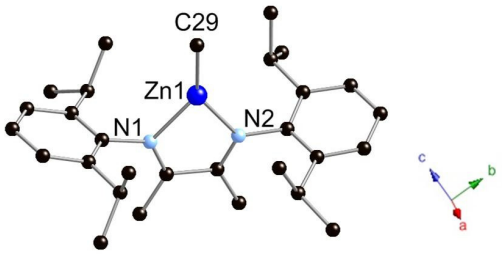

Figure 2.4: Three-coordinated Zn(II) in a complex $[ZnMe(DAD)]^+$[DAD = $(MeC{=}NC_6H_3Pr^i_2\text{-}2,6)_2$].[95]

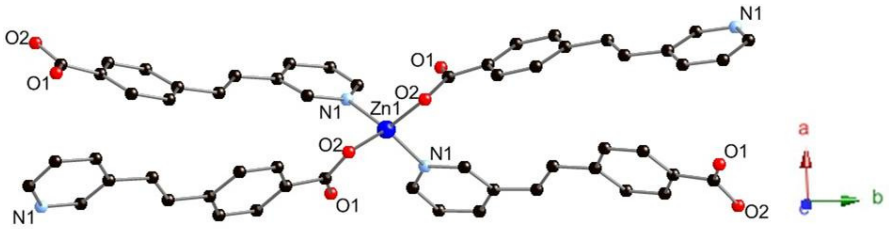

Figure 2.5: Zn(II) is four-coordinated in a 2D network structure {Zn_4-benzeato}$_8$•{3-[2-(4-pyridyl)ethenyl]benzoic acid}•H_2O.[96]

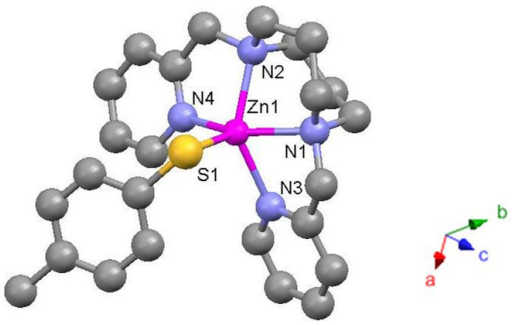

Figure 2.6: Five coordinated Zn(II) ion in [1,5-bis(2-pyridylmethy)-1,5-diazacyclooctane]Zn(4-methylphenylthiolato)BPh_4.[97]

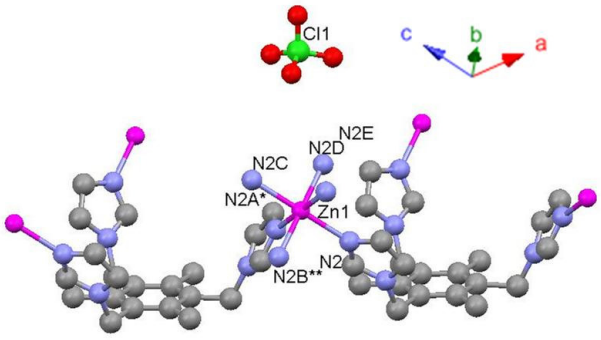

Figure 2.7: Six-coordinated Zn(II) in a network Zn[1,3,5-tris(imidazole-1-ylmethyl)-2,4,6-trimethylbenzene]$_2$(CLO_4)$_2$.[98]

In the hybrid network series **I** reported in this dissertation, Zn(II) is used as metal node, for which tetrahedral geometry is commonly exhibited by the Zn^{2+} ions.[85]

2.4 Other building blocks: Organic/Inorganic acids

It is known that metal ions in hybrid networks carry positive charge while bridging ligands can be neutral, negatively charged or positive charged. If the metal organic network has a positive charge, the conjugated base of organic/inorganic acids may incorporate into the network structure to balance the network charge. The other anions can act as building blocks and participate in network construction via hydrogen bonds or covalent or ionic bonds. The anions in networks can be classified as covalently bonded, ionic bonded, or hydrogen bonded. Covalently bonded organic/inorganic acids are building blocks that are part of a network structure. It is possible for there to be more than one anion species in a hybrid network, for example, carboxylate[99-102] (organic acid) and phosphate[103-105] (inorganic acid) have been reported together in a variety of network structures. Anions such as RCO_2^- and $H_2PO_3^-$ can be hydrogen bonded in networks. In these cases, anions do not directly participate in the construction of networks, instead they act to balance the charges. For example, Li et al. reported Ag[2,4,6-tris(4-pyridyl)-1,3,5-triaine]$(NO_3)_2$•$4H_2O$, which contains hydrogen bonded NO_3^- to balance network charge.[106] Clearly anions, no matter how they are connected in the network, play an important role in the network formation.

2.5 Templates in hybrid networks series I

In hybrid network series **I**, we used aromatic alcohols as templates for the network construction. The aromatic alcohols act as a hydrogen bond donors to the organic ligand TMDP in the crystal structures. In total, eight aromatic alcohols were used in the synthesis of these networks. These eight templates molecules are phenol, catechol, hydroquinone,

resorcinol, pyrogallol, 4-nitropheol, 4-bromophenol, and 4-flurophenol. They are shown in Scheme 2.2.

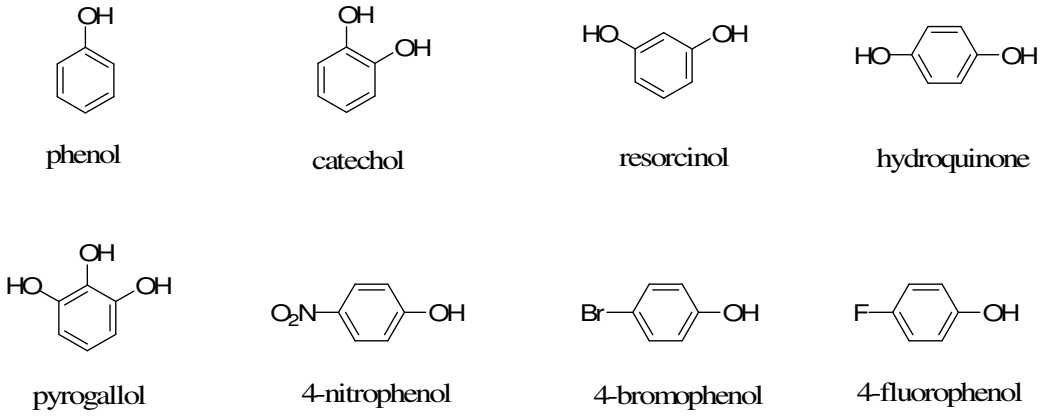

Scheme 2.2: Aromatic alcohol templates used in the construction of Series **I** networks.

2.6 Motifs in hybrid network series I

In a recent example from the literature, the piperidinium ion, $(C_5H_{12}N)^+$, templates zinc phosphite to give a framework structure of composition $(C_5H_{12}N)_2Zn_3(HPO_3)_4$.[9] The framework contains helical chains (ZnO_4 and HPO_3 groups), 4 rings (2 Zn^{2+} ions and 2 HPO_3^{2-} groups), and 16 rings (8 Zn^{2+} ions and 8 HPO_3^{2-} groups). The 16-rings are formed from $Zn(HPO_3)_2^{2-}$ chains and perpendicular $Zn(HPO_3)$ stair steps (Scheme 2.3). Both the anionic chain[107] and the stair step are common motifs in ZnPO structural chemistry. The resulting 16-ring channels are filled with piperidinium ions.

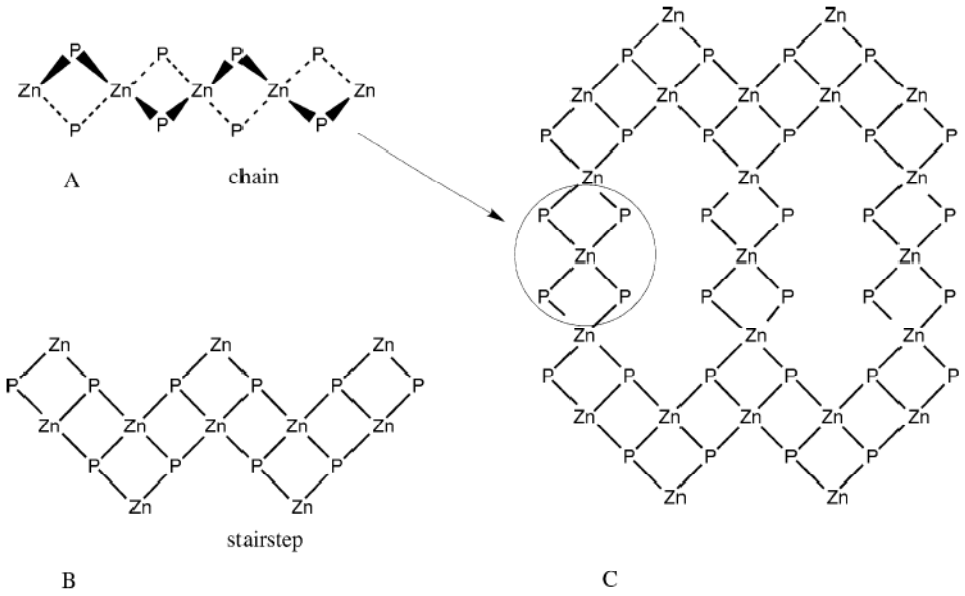

Scheme 2.3: (A and B) Schematic representation of the perpendicular chain motifs in $(NC_5H_{12})_2Zn_3(HPO_3)_4$[9] and (C) combination of chains to give 16-Rings.

Dong et al. reported that piperazinium also templates zinc phosphite to give a framework of composition $(C_4H_{12}N_2)_{0.5}Zn_3(HPO_3)_4 \cdot H_3O$.[59] This structure is built from similar $Zn(HPO_3)_2^{2-}$ chains that pillar neutral $Zn(HPO_3)$ sheets that have the 4.8^2 topology,[108] another common structural motif in these materials. The pillars are connected to nearest-neighbor zinc atoms within adjacent layers to form 12-ring (6 Zn^{2+} ions and 6 HPO_3^{2-} groups) channels.[66] Alternatively, piperazine can template a related composition, $(C_4H_{12}N_2)Zn_3(HPO_3)_4$,[65] in which $Zn(HPO_3)_2^{2-}$ chains are present. Another example is in zinc phosphite is templated in the presence of propylamine, neutral sheets of the 4.8^2 topology form. These are also pillared by $Zn(HPO_3)_2^{2-}$ chains to give 12-ring channels,[66] which are filled with propylammonium cations.

Imidazole ligands typically bind to zinc in the formation of hybrid structures although examples are known in which the imidazole group acts as both ligand and template (Scheme 2.4).[109-111]Ligands, such as 2,2'-bipyridine (Scheme 2.5A), commonly coordinate to give

molecular structures or hybrids.[112-114] Bridging dipyridine ligands, such as 4,4'-bipyridine (Scheme 2.5B), have recently been used to construct a variety of hybrid solids including pillared layered structures.[69] The use of dipyridines that have structural flexibility, such as 4,4'-trimethylenedipyridine (Scheme 2.5C), leads to a variety of metal-organic framework structures.[115, 116]

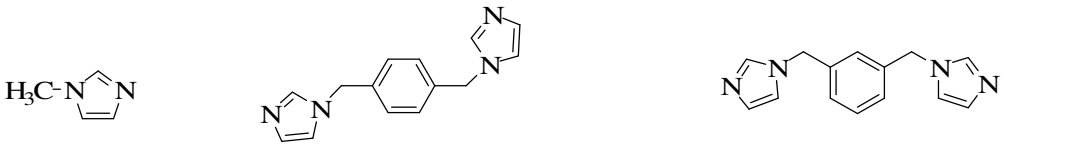

1-methylimidazole 1, 4-bis(imidazol-1-ylmethyl)bezene 1, 3-bis(imidazol-1-ylmethyl)bezene

Scheme 2.4: Examples of imidazole ligands.

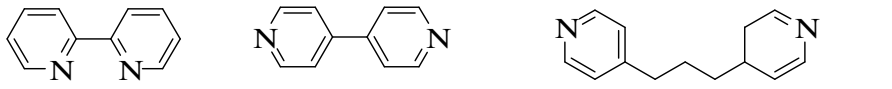

2, 2'-bipyridine A

4, 4'-bipyridine B

4, 4'-trimethylenedipyridine C

Scheme 2.5: 2,2′-bipyridine, 4,4′-bipyridine, and 4,4′-trimethylenedipyridine.

Here 4,4'-trimethylenedipyridine (TMDP) was reported to reacts with zinc phosphite at high temperature with diprotonated TMDP as a template, to form a pillared framework structure with a new 16-ring topology. In contrast, at low temperature or at higher pH, hybrid structures are formed in which the ligand binds directly to zinc. Significantly, neutral guest molecules, water, phenol, and catechol, may be incorporated into the framework depending on the reaction conditions used during the synthesis.

2.7 Experimental section for hybrid network series I

All commercially available chemicals are reagent grade and were used as received without further purification. Elemental analyses of C, H and N were performed by Galbraith Laboratories, Inc. Thermogravimetric measurements were performed on a TGA Q500 thermal analyzer under flowing N_2 with a heating rate of 10 °C min^{-1}. TGA traces for the hybrid materials presented herein are included in the Appendix A.

(4,4'-$(C_5H_4N)_2(CH_2)_3$)$Zn_3(HPO_3)_4$, 1.

Zinc acetate dihydrate (220 mg, 1.0 mmol), phosphorous acid (164 mg, 2.0 mmol), 4,4'-$(C_5H_4N)_2(CH_2)_3$ (300 mg, 1.5 mmol), and 6 mL of water were added to a heavy-walled glass tube that was then sealed under vacuum. The tube was placed in an oven for 10 days at 130 °C. The sample contained crystals of **1** and a microcrystalline solid that were collected by filtration. The bulk sample did not give satisfactory results from elemental analysis. A comparison of the calculated powder diffraction pattern and the experimental powder pattern (Appendix B) show that the most of the material is an unidentified phase. The TGA of a manually separated crystalline sample of **1** shows a 2.2% weight loss by 200 °C, up to 400 °C an additional 6.2% weight loss is observed, and from 430 to 500 °C the sample loses 25% giving a total weight loss of 35%. The material is a glassy black solid after being heated to 500 °C. The templating ligand corresponds to 27% of the mass of the sample. Selected IR bands: 3443(b), 3041(w), 3015(w), 2945(w), 2865 cm^{-1}(w).

(4,4'-$(C_5H_4N)_2(CH_2)_3$)$Zn_2(HPO_3)_2 \cdot 2.5H_2O$, 2.

Zinc acetate dihydrate (220 mg, 1.0 mmol), phosphorous acid (164 mg, 2.0 mmol), 4,4'-$(C_5H_4N)_2(CH_2)_3$ (300 mg, 1.5 mmol), and 6 mL of water were added to a heavy-walled

glass tube sealed under vacuum. The tube was left at room temperature for 2 weeks during which time crystals of **2** formed. The crystals were collected by filtration. Yield 240 mg, 90% based on zinc acetate. Selected IR bands: 3094(w), 3061(w), 2966(w), 2608 cm^{-1}(b). Anal. Calcd for (4,4'-$(C_5H_4N)_2(CH_2)_3$)$Zn_2(HPO_3)_2$: C, 31.90%; H 3.30%; N 5.53%; found (for a dried sample): C 31.14%; H 3.55%; N 5.52%. The TGA of a fresh sample of **2** shows a weight loss of 8.2% from 25 to 150 °C; the calculated value for loss of water is 8.4%. Further heating results in an additional loss of 19.1% by 350 °C.

(4,4'-$(C_5H_4N)_2(CH_2)_3$)$Zn_2(HPO_3)_2 \cdot 3H_2O$, 3.

Zinc acetate dihydrate (220 mg, 1.0 mmol), phosphorous acid (164 mg, 2.0 mmol), 4,4'-$(C_5H_4N)_2(CH_2)_3$ (300 mg, 1.5 mmol), NaOH (60 mg, 1.5 mmol), and 6 mL of water were added to a heavy-walled glass tube that was then sealed under vacuum. The tube was left at room temperature for 1 week during which time crystals of **3** formed. Yield 230 mg, yield 85% based on zinc acetate. Selected IR bands: 3333(b), 2972(w), 2865 cm^{-1}(w). Anal. Calcd for (4,4'-$(C_5H_4N)_2(CH_2)_3$)$Zn_2(HPO_3)_2$: C, 31.90%; H 3.30%; N 5.53%; found (for a dried sample): C 31.52%; H 3.42%; N 5.56%. TGA of a freshly prepared sample of **3** shows a 10.3% mass loss in the 25 to 100 °C temperature range (calcd w% for three water molecules = 9.9%). The material is stable until 420 °C. At 500 °C, it loses a total of 38% of its mass to yield a glassy black solid.

(4,4'-$(C_5H_4N)_2(CH_2)_3$)$Zn_2(HPO_3)_2 \cdot$phenol, 4.

Zinc acetate dihydrate (220 mg, 1.0 mmol), phosphorous acid (164 mg, 2.0 mmol), 4,4'-$(C_5H_4N)_2(CH_2)_3$ (300 mg, 1.5 mmol), NaOH (80 mg, 1.5 mmol), phenol (188 mg, 2 mmol), and 6 mL of water were added to a heavy-walled glass tube that was then sealed under vacuum. The tube was left at room temperature for 1 week during which time crystals of **4** formed. Selected IR bands for the crystals: 3295(b), 3060(w), 3045(w), 3018(w),

2990(w), 2929(w), 2861(w), 2706(w), 2608 cm^{-1}(w). The bulk sample did not give satisfactory results for elemental analysis; however, a comparison of the calculated powder diffraction pattern and the experimental powder pattern for the material (Appendix B) shows that the bulk of the isolated solid is compound **4**. TGA of a crystalline sample shows a continuous mass loss over the 25 to 500 °C temperature range, until only 50% of the mass remains.

(4,4'-$(C_5H_4N)_2(CH_2)_3)_2Zn_2(HPO_3)_2$·(catechol)$_2$, 5.

Zinc acetate dihydrate (220 mg, 1.0 mmol), phosphorous acid (164 mg, 2.0 mmol), 4,4'-$(C_5H_4N)_2(CH_2)_3$ (297 mg, 1.5 mmol), catechol (220, 2 mmol), and 6 mL of water were added to a heavy-walled glass tube that was then sealed under vacuum. The tube was left at room temperature for 1 week during which time crystals of **5** formed. Selected IR bands from a crystalline sample: 3490(m), 3205(b), 3095(w), 3062(m), 2950(m), 2932(m), 2862(m), 2695 cm^{-1}(m). The bulk sample did not give satisfactory results for elemental analysis. A comparison of the calculated powder diffraction pattern and the experimental powder pattern (Appendix B) show that the bulk of the material is an unidentified phase. The TGA of a crystalline sample of **5** show a continuous mass loss over the25 to 500 °C temperature range, until only 45% of the mass remains.

(4,4'-$(C_5H_4N)_2(CH_2)_3)Zn_2(HPO_3)_2(H_2O)$, 6.

Zinc acetate dihydrate (219.5 mg, 1.0 mmol), phosphorous acid (164.0 mg, 2.0 mmol), 4,4'-$(C_5H_4N)_2(CH_2)_3$ (297 mg, 1.5 mmol), NaOH (80 mg, 2.0 mmol), alanine (180 mg, 2.0 mmol), and 6 mL of water were added to a heavy-walled glass tube that was then sealed under vacuum. The tube was left at room temperature for 1 week during which time crystals of **6** formed. Yield 235 mg, 96% based on zinc acetate. Selected IR bands: 3660(b), 3443(b), 3042(w), 2988(w), 2946(w), 2901 cm^{-1}(w). Anal. Calcd for

(4,4'-$(C_5H_4N)_2(CH_2)_3)Zn_2(HPO_3)_2(H_2O)$: C, 30.80%; H 3.55%; N 5.52%; found: C 31.33%; H 3.47%; N 5.63%. In the TGA, a 2.6% weight loss is observed up to 200 °C. This roughly corresponds to loss of coordinated water, 3.6%. From 250 to 350 °C, an additional 9.0% weight loss is observed from 430 to 500 °C, the sample loses additional mass until only 63% of the mass remains.

(4,4'-$(C_5H_4N)_2(CH_2)_3)Zn_2(HPO_3)_2\cdot(C_6H_6O_2)$, 7.

Zinc acetate dihydrate (220 mg, 1.0 mmol), phosphorous acid (164 mg, 2.0 mmol), 4,4′-$(C_5H_4N)_2(CH_2)_3$ (300 mg, 1.5 mmol), resorcinol (220 mg, 2 mmol) and 6 mL water were added to a heavy walled glass tube that was then sealed under vacuum. The tube was left at room temperature for one week during which time crystals of **7** formed. Yield: 264 mg, yield 88.1% based on zinc acetate. Anal. Calc. for $C_{19}H_{22}N_2O_8P_2Zn_2$: C, 38.1; H, 3.70; N, 4.68. Found: C, 37.0; H, 3.86; N, 4.53%.

(4,4'-$(C_5H_4N)_2(CH_2)_3)Zn_2(HPO_3)_2\cdot 2(C_6H_5NO_3)$, 8.

Zinc acetate dihydrate (220 mg, 1.0 mmol), phosphorous acid (164 mg, 2.0 mmol), 4,4′-$(C_5H_4N)_2(CH_2)_3$ (300 mg, 1.5 mmol), 4-nitrophenol (278.2 mg, 2 mmol) and 6 mL water were added to a heavy walled glass tube that was then sealed under vacuum. The tube was left at room temperature for one week during which time crystals of **8** formed. Yield: 325 mg, yield: 84.9% based on zinc acetate. *Anal*. Calc. for $C_{25}H_{26}N_2O_{12}P_2Zn_2$: C, 39.1; H, 3.42; N, 7.30. Found: C, 39.1; H, 3.32; N, 7.20%.

(4,4'-$(C_5H_4N)_2(CH_2)_3)_2Zn_4(HPO_3)_4 \cdot 2(C_6H_6O_2)$, 9.

Zinc acetate dihydrate (220 mg, 1.0 mmol), phosphorous acid (164 mg, 2.0 mmol), 4,4′-$(C_5H_4N)_2(CH_2)_3$ (300 mg, 1.5 mmol), hydroquinone (220 mg, 2 mmol) and 6 mL water were added to a heavy walled glass tube that was then sealed under vacuum. The tube was left at 0 °C for one week during which time crystals of **9** formed. Yield: 225 mg, yield: 75.1% based on zinc acetate. *Anal*. Calc. for $C_{19}H_{22}N_2O_8P_2Zn_2$: C, 38.1; H, 3.70; N, 4.68. Found: C, 39.6; H, 4.01; N, 4.20%.

(4,4'-$(C_5H_4N)_2(CH_2)_3)Zn(HPO_3) \cdot 2(C_6H_5BrO)$, 10.

Zinc acetate dihydrate (220 mg, 1.0 mmol), phosphorous acid (164 mg, 2.0 mmol), 4,4′-$(C_5H_4N)_2(CH_2)_3$ (300 mg, 1.5 mmol), 4-bromophenol (345.8 mg, 2 mmol) and 6 mL water were added to a heavy walled glass tube that was then sealed under vacuum. The tube was left at room temperature for one week during which time crystals of **10** formed. Yield: 416 mg, yield: 60.4% based on zinc acetate. *Anal*. Calc. for: C, 43.5; H, 3.65; N, 4.06. Found: C, 43.4; H, 3.56; N, 4.11%.

Crystallographic Analyses

Low-temperature (100 K) single-crystal X-ray diffraction measurements for complexes **1**-**10** were collected on an Oxford Diffraction Xcalibur diffractometer equipped with a Sapphire 3 CCD detector.. Crystals were mounted on a nylon CryoLoop (Hampton Research) with Krytox Oil (DuPont). The data collection routine, unit cell refinement, and data processing were carried out with the program CrysAlis.[117-119] The structures were solved by SHELXTL-NT and refined by full-matrix least-squares[117-119]. The final refinements involved

an anisotropic model for all non-hydrogen atoms. A summary of all crystallographic data is given in Table 2.2.

Table 2.2: Crystal data and structure refinement parameters for **1-10**.

	1	**2**
Empirical formula	$C_{6.5}H_9NO_6P_2Zn_{1.5}$	$C_{26}H_{42}N_4O_{17}P_4Zn_4$
F_w	358.15	1068.0
T/K	100	100
Space group	P*ccn*	C*2/c*
a/Å	10.1034(7)	23.860(4)
b/Å	25.1550(16)	5.1324
c/Å	9.1040(6)	32.021(5)
α/degree	90	90
β/degree	90	97.364(12)
γ/degree	90	90
V/Å^3	2313.8(3)	3888.9(10)
Z	8	4
μ/mm^{-1}	3.425	2.678
R1[a][I>2σ(I)]	0.0322	0.0513
*w*R2[b][I>2σ(I)]	0.1150	0.0905

	3	**4**
Empirical formula	$C_{13}H_{22}N_2O_9P_2Zn_2$	$C_{19}H_{22}N_2O_7P_2Zn_2$
F_w	543.01	583.07
T/K	100	100
Space group	P*ccn*	P*nma*
a/Å	9.6220(14)	9.9947(3)
b/Å	24.389(4)	23.8866(9)

c/Å	8.4590(11)	9.5533(11)
α/degree	90	90
β/degree	90	90
γ/degree	90	90
V/Å^3	1985.1(5)	2280.7(3)
Z	4	4
μ/mm^{-1}	2.627	2.287
R1[a][I>2σ(I)]	0.0310	0.0329
*w*R2[b][I>2σ(I)]	0.0708	0.0667

	5	**6**
Empirical formula	$C_{38}H_{42}N_4O_{10}P_2Zn_2$	$C_{13}H_{18}N_2O_7P_2Zn_2$
F_w	907.4	506.97
T/K	100	100
Space group	P*na2$_1$*	C*2/c*
a/Å	18.0264(5)	16.6901(10)
b/Å	12.4289(3)	14.9412(9)
c/Å	17.6357(11)	16.0256(10)
α/degree	90	90
β/degree	90	117.730(6)
γ/degree	90	90
V/Å^3	3951.3(2)	3537.3(4)
Z	4	8
μ/mm^{-1}	1.357	2.933
R1[a][I>2σ(I)]	0.0345	0.0225
*w*R2[b][I>2σ(I)]	0.0690	0.0584

	7	**8**
Empirical formula	$C_{19}H_{22}N_2O_8P_2Zn_2$	$C_{25}H_{26}N_4O_{12}P_2Zn_2$

F_w	599.07	767.18
T/K	100	100
Space group	$P2_12_12_1$	$P2_1/n$
a/Å	9.6299(2)	10.3340(9)
b/Å	9.76980(10)	28.4469(16)
c/Å	24.5639(4)	11.7505(11)
α/degree	90	90
β/degree	90	90
γ/degree	90	90
V/Å^3	2311.03	3068.16
Z	4	4
μ/mm^{-1}	2.262	1.736
R1[a][I>2σ(I)]	0.0249	0.0296
wR2[b][I>2σ(I)]	0.0428	0.0596

	9	**10**
Empirical formula	$C_{38}H_{44}N_4O_{16}P_4Zn_4$	$C_{25}H_{25}Br_2N_2O_5PZn$
F_w	324.37	689.63
T/K	100	100
Space group	$P2_1/c$	$P2_1/c$
a/Å	22.9229(14)	12.2340(13)
b/Å	9.9797(6)	12.3314(10)
c/Å	9.7714(6)	18.4265(17)
α/degree	90	90
β/degree	91.535(5)	107.461(10)
γ/degree	90	90
V/Å^3	2234.54	2651.77
Z	2	4
μ/mm^{-1}	0.089	4.039

R1[a][I>2σ(I)]	0.0382	0.0356
*w*R2[b][I>2σ(I)]	0.0879	0.0822

[a]R1 = Σ ||F_o| - |F_c||/Σ|F_o|. [b]*w*R2 = {Σ[$w(F_o^2 - F_c^2)^2$]/Σ[$w(F_o^2)^2$]}$^{1/2}$,

where $w = 1/[\sigma^2(F_o)^2 + (aP)^2 + bP]$, $P = [(F_o)^2 + 2(F_c)^2]/3$.

2.8 Crystal structures of hybrid network series **I**

2.8.1 Crystal structure (4,4'-$(C_5H_4N)_2(CH_2)_3)Zn_3(HPO_3)_4$, **1**.

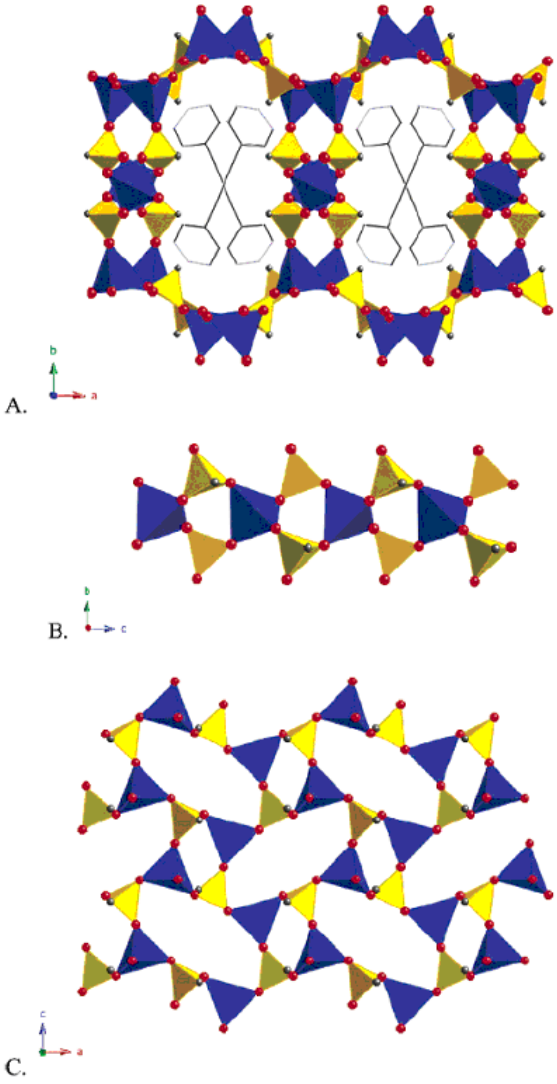

Figure 2.8: Schematic representations of the structure of **1**. Zinc, blue tetrahedra; phosphorus, yellow tetrahedra. Oxygen atoms are represented as red spheres, and the protonated TMDP ligands are drawn in stick form. (A) Packing diagram view down the 16-ring channels filled with protonated TMDP molecules. (B) View of the $[Zn(HPO_3)_2]^{2-}$ chain that serves as the pillar in **1**. (C) Projection of the 4.8^2 sheet onto the *ac* plane.

The framework of **1** is shown in Figure 2.8. The structure consists of puckered $4.8^{2\,116}$ sheets (Figures 2.1c and 2.1b, respectively). Each zinc atom in the 4.8^2 layer serves as an anchor point for a pillar connecting it to the next layer. Within each eight-membered ring, alternating zinc atoms support pillars on the same side of the 4.8^2 layer. The pillars consist of $Zn(HPO_3)_2^{2-}$ chains. The resulting structure has channels that run parallel to the crystallographic *c*-axis and a net framework composition of $Zn_3(HPO_3)_4^{2-}$. The TMDP ligand is diprotonated and fills the channels (Figure 2.8A). The dipyridinium ions are hydrogen bonded to oxygen atoms of the framework that are 13.8 Å apart (hydrogen-bond parameters for structures **1**-**10** are given in Table 2.2) The phosphite hydrogen atoms are directed toward the inside of the channels and define a rectangle of dimension 6.8 Å × 10.1 Å. Thus, the templates occupy cavities within the channels that are larger than the channel opening.

2.8.2. Crystal structure (4,4'-$(C_5H_4N)_2(CH_2)_3)Zn_2(HPO_3)_2 \cdot 2.5H_2O$, **2**.

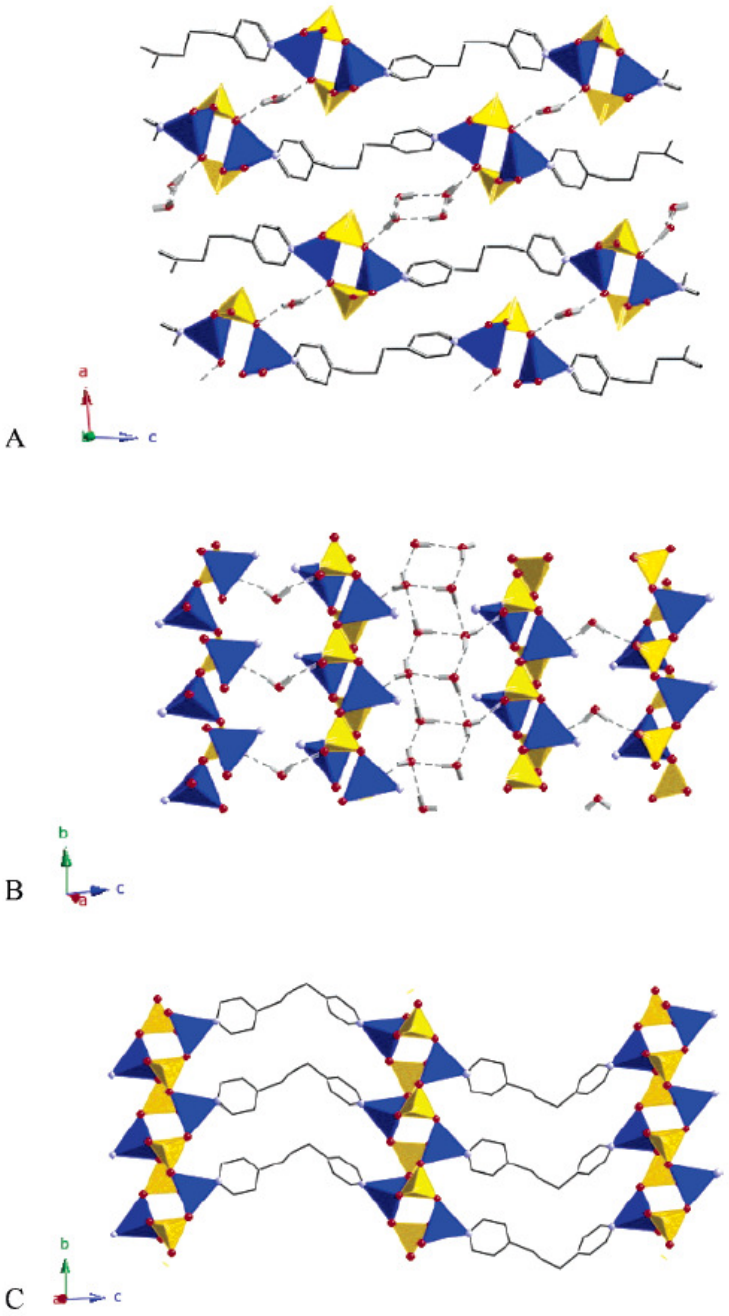

Figure 2.9: Three views of the structure of **2**. (A) A side-on view of the stacking of the two-dimensional hybrid sheets. The layers are separated, in an alternation manner, by isolated water molecules and a chain of hydrogen-bonded waters. (B) A view of the layer formed by the Z_2P_2 ladders and the hydrogen-bonded water molecules. (C) A view of the two-dimensional hybrid sheets formed from Zn_2P_2 ladders and the bridging TMDP ligands.

The structure of **2** is shown in Figure 2.9, the composition of which is (4,4'-$(C_5H_4N)_2(CH_2)_3$)$Zn_2(HPO_3)_2 \cdot 2.5H_2O$. One-dimensional ladders of $Zn(HPO_3)$ are connected by 1,3-dipyridylpropane ligands to form two-dimensional hybrid sheets, as shown in Figure 2.9C. The neutral sheets are separated by interlayer water molecules, as shown in Figure 2.9A, as viewed down the $Zn_2(HPO_3)_2$ ladders. The stacking arrangement can be described as 1A:4H_2O:1B:1H_2O where 2.9A and 2.9B refer to different orientations of the two-dimensional sheets. The stoichiometry is five water molecules per two Zn_2P_2 four-rings and the layers are separated, in an alternating manner, by isolated water molecules and a chain of hydrogen bonded water molecules. The water molecules and the $Zn_2(HPO_3)_2$ ladders form a hydrophilic sheet connected by hydrogen bonds, as shown in Figure 2.9B.

2.8.3. Crystal structure (4,4'-$(C_5H_4N)_2(CH_2)_3)Zn_2(HPO_3)_2 \cdot 3H_2O$, **3**.

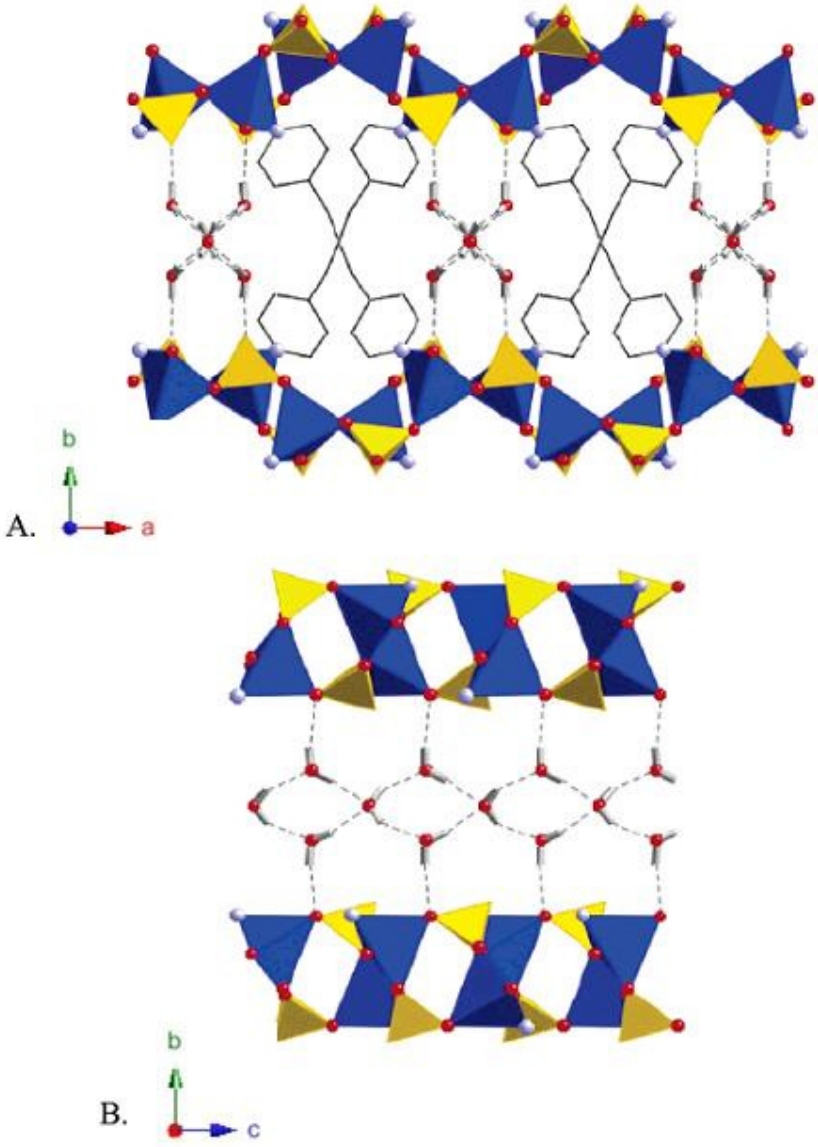

Figure 2.10: (A) View down the channels formed in **3** from the 4.8^2 layers and the TMDP pillars. Zinc atoms are represented in dark blue, phosphorus in yellow, oxygen in red, and nitrogen in light blue. Water fills the channels. (B) A view parallel to hydrogen-bonded chain of water molecules that fill the channels.

Efforts to generate **2** by performing the reaction at higher pH led to the formation of a new compound, **3**. The structure of **3** is similar in some respects to the structure of **1**. Specifically in **3**, neutral 4.8^2 sheets are pillared by TMDP groups that bridge zinc atoms in adjacent layers, whereas in **1** the 4.8^2 sheets are pillared by inorganic $(Zn(HPO_3)_2)^{2-}$ chains (compare Figures 2.10A and 2.8A.) The resulting interstitial space between pillars is quite large and accommodates a chain of hydrogen-bonded water molecules. The distance between closest phosphite hydrogen atoms in adjacent layers is 8.130 Å, and the distance between closest oxygen atoms is 9.244 Å. A view of the hydrogen-bonded chain of water molecules is given in Figure 2.10B. One central water molecule is connected by hydrogen bonds to four water molecules in a tetrahedral arrangement. The other crystallographically unique water molecule is connected to two water molecules in the chain and is a hydrogen-bond donor to the zinc phosphite sheet. The oxygen-oxygen distances between hydrogen-bonded water molecules within the chain are in the range 2.799-2.889 Å, and the closest distance between oxygen atoms of water and phosphite oxygen is 2.837 Å. The TGA shows that water can be removed under relatively mild conditions. A nitrogen BET surface area measurement on a sample of **3** dried at 120 °C gives a nominal surface area of 5.2 m^2g^{-1}. This value suggests that the pores vacated by water collapse upon dehydration. A similar structure, with 4,4'-bipyridine as the organic pillar, has recently been reported.[68]

2.8.4. Crystal structure (4,4'-$(C_5H_4N)_2(CH_2)_3)Zn_2(HPO_3)_2$·phenol, **4**.

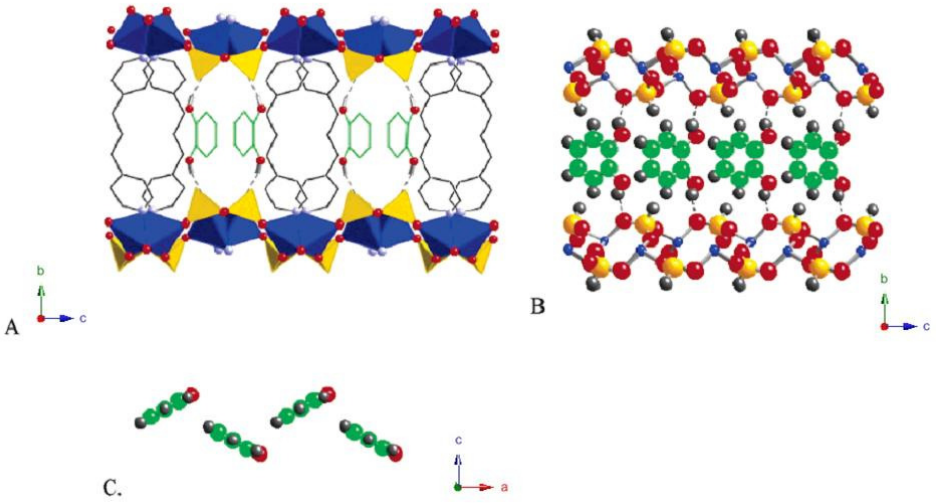

Figure 2.11: (A) View down the channels formed in **4** from the 4.8^2 layers and the TMDP pillars. Zinc atoms are represented in dark blue, phosphorus in yellow, oxygen in red, and nitrogen in light blue. Phenol fills the channels. (B) A view parallel to the molecular wire of phenols. The orientation of the phenol is disordered; each oxygen position is 50% occupied. The phenol oxygen is alternatively hydrogen bonded to the upper and lower zinc phosphite layers. (C) A view orthogonal to the view in B to show the C-H-π interaction in the phenol chain.

When the synthesis of **3** is conducted in the presence of phenol as a potential template molecule, we find that phenol is preferentially then water molecules incorporated into the structure to give **4** (Figure 2.11). The incorporation of a neutral molecule other than water or solvent is rare in the preparation metal-organic frameworks. Although, the neutral 4.8^2 layer pattern is retained, these sheets are flatter than in either **1** or **3**. As in **3,** the TMDP ligand serves as a pillar between adjacent ZnPO layers. The propyl portion of the pillars is more parallel, and the pyridine bonds to the concave rather than the convex portion of the ZnPO layer. The nearest-neighbor phosphite hydrogen atoms between layers are 6.755 Å apart, and the distance between closest oxygen atoms is 8.614 Å. Thus, the layers are closer together

than in **3**. The pillars define channels in the structure that are filled with phenol. The phenol is disordered with half the OH groups directed toward one layer and the other half directed toward the adjacent layer. The projection of phenol shown in Figure 2.4 thus looks like catechol. (Catechol, however, leads to a different ZnPO structure, as shown below.) The phenol guests line up to form a molecular wire with nearest-neighbor C-C distances of 3.767 Å. The closest distance between phenol oxygen and ZnPO oxygen is 2.881 Å. Similar molecular wires have been proposed to form upon the impregnation of nitroaniline into the non-centrosymmetric zeolite, ALPO-5.[120, 121]

2.8.5. Crystal structure (4,4'-$(C_5H_4N)_2(CH_2)_3)_2Zn_2(HPO_3)_2\cdot(catechol)_2$, **5**.

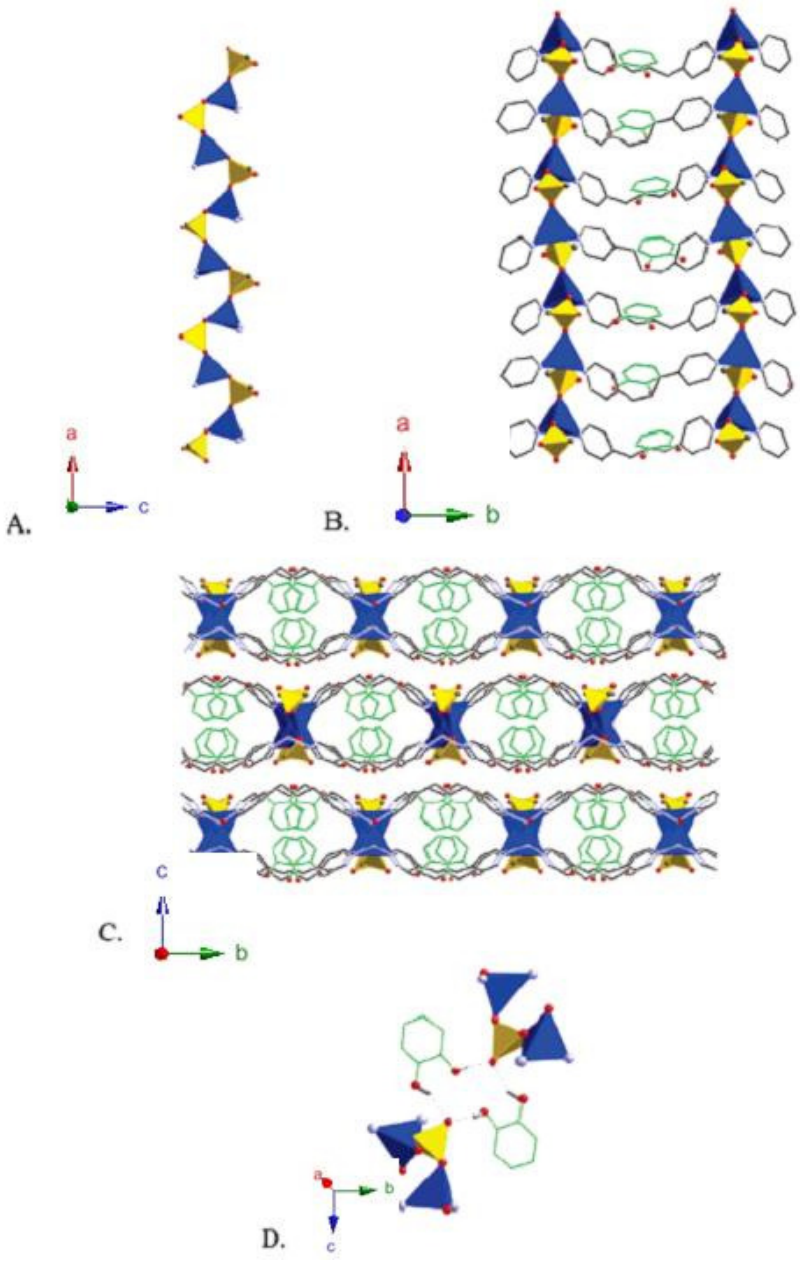

Figure 2.12: (A) View of the one-dimensional ZnPO chains in **5**. (B) A view of the hybrid sheet formed from the ZnPO chains linked by the TMDP ligands. (C) A view of the stacking of the hybrid sheets. The catechol ligand is shown in green. This projection gives the impression of a hydrophobic cavity. (D) A representation of the hydrogen-bonding contacts between two catechols and two phosphites.

The disorder of phenol in **4** suggests that catechol could fit in the network cavities. Catechol is indeed incorporated as a template into the same hybrid host structure observed in **4**; however, the catechol group disrupts the formation of the 4.8^2 sheets by strongly hydrogen bonding to the P=O group. Thus, the phosphite is only two-connected in the structure. This limits the connectivity of ZnPO to two dimensions. Zinc is also two connected in the ZnPO portion of the structure with the remaining two coordination sites occupied by nitrogen from the TMDP ligand. The ZnPO chains are shown in Figure 2.11A; these chains can be visualized as being 'cut' from a 4.8^2 sheet. The connection of these chains into sheets linked by TMDP is shown in Figure 2.11B, and the stacking of sheets is shown in Figure 2.11C. The projection of the stacked sheets gives the impression of cavities that hold the catechol guests. The sheets, however, are simply wavy, and the catechol is tucked into the trough of the wave; the hydrophobic portion of the catechol is directed toward the propyl backbone on the TMDP ligand, and the hydroxyl groups are directed toward the phosphite of an adjacent sheet. The nearest-neighbor oxygen contacts between catechol and phosphite are shown in Figure 2.5D. The hydrogen bonding is limited to islands of two catechols and two phosphites and does not extend through the entire structure. Catechol is reported to cocrystallize with 2-hydroxylphenyl phenylphosphonate; in these structures, catechol and the phosphonate, which has two hydrogen bond acceptors, form a chain that extends throughout the structure.[122]

2.8.6. Crystal structure (4,4'-$(C_5H_4N)_2(CH_2)_3)Zn_2(HPO_3)_2(H_2O)$, **6**.

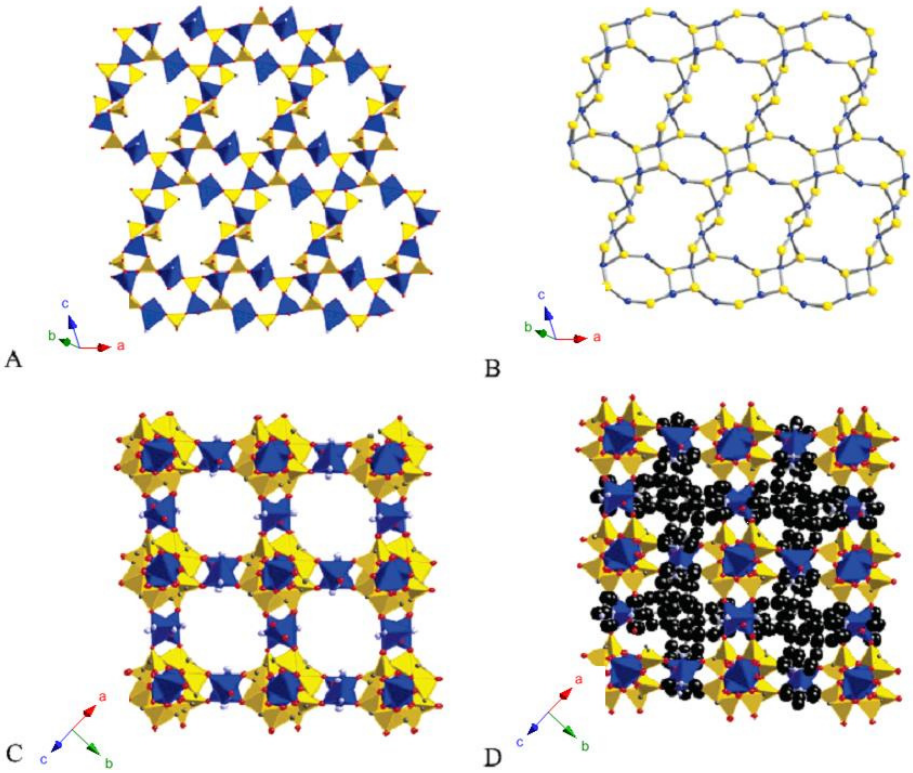

Figure 2.13: (A) View of one of two identical orthogonal sheets of zinc phosphite in 6. Zinc atoms are represented in dark blue, phosphorus in yellow, and oxygen in red. (B) An alternative representation of the view in (A) in which only the zinc and phosphorus positions are shown. The sheet structure is formed from intersecting 4-ring chains and 4.8 ladders to give 16-rings. (C) A view that shows the intersection of the sheets represented in (A) to give new 16-rings. (D) An identical projection of the structure of 6 as given in (C) with the carbon atoms of the TMDP ligand added to show the hybrid composite formed by TMDP and zinc phosphite.

Different views of the structure of **6** are shown in Figure 2.13. The structure is composed of identical intersecting sheets, shown in Figures 2.13A and 2.13B to give a square motif, as shown in Figure 2.13C. The sheets are constructed from anionic $Zn(HPO_3)_2^{2-}$ chains connected by Zn^{2+} ions to give a layer that contains 4-rings, 8-rings, and 16-rings. The zinc

atoms in the chains, Zn2, are tetrahedrally coordinated to four phosphite oxygen atoms; the zinc that connects the chains. Zn1 is five connected and has a distorted trigonal bipyramidal geometry. Zn(1) is bonded to two phosphite oxygen atoms, two nitrogen atoms from different TMDP ligands, and one water oxygen atom (this water position is fractionally occupied according to the disorder model used to refine the structure.) (Figure 2.14). One nitrogen atom and the water molecule are in the axial position with an N1-Zn1-O7B angle of 166.15(19)°. The equatorial atoms, N2, O6, and O2, are nearly coplanar with angles of 115.78(7)°, 119.92(7)°, and 114.94(6)°. The TMDP ligands and Zn2 combine to make TMDP -Zn chains that extend through the entire structure. The TMDP ligands completely fill the pores of the neutral ZnPO framework. A view of the composite ZnPO framework interwoven with ZnTMDP polymers is shown in Figure 2.13C.

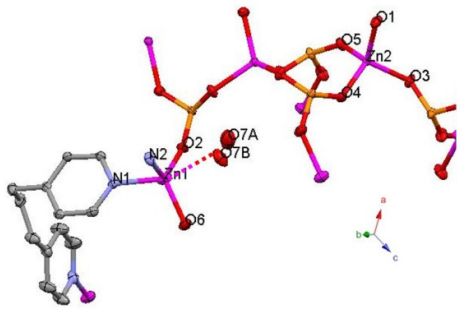

Figure 2.14: The Zn1 atom is bonded to O2 and O6 atoms from phosphites, N1 and N2 atoms from different TMDP ligand, and one water O7(O7A and O7B) atom. The Zn2 atom is bonded to O1, O3, O4 and O5 atoms from phosphites.

2.8.7. Crystal structure (4,4'-$(C_5H_4N)_2(CH_2)_3$)Zn2$(HPO_3)_2\cdot(C_6H_6O_2)$, **7**.

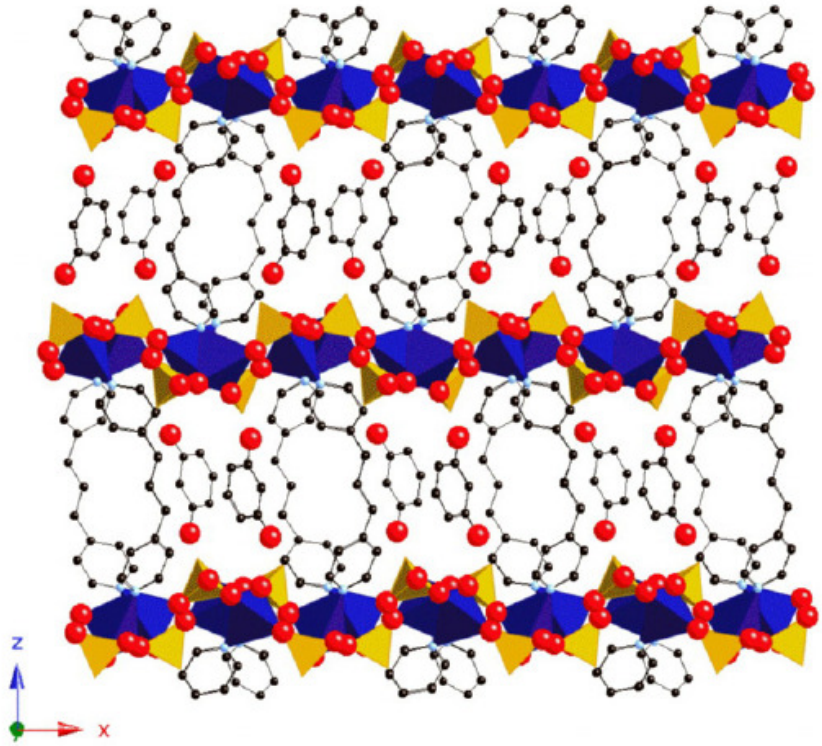

Figure 2.15A: A view down the *b* axis of **7**. Resorcinol fills the channels generated by the trimethylene-dipyridine pillars.

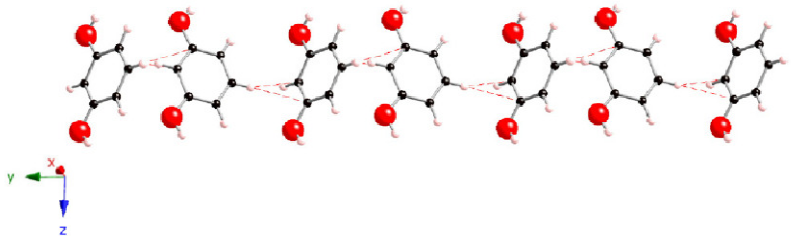

Figure 2.15B: A view of the resorcinol chain that fills the channels in **7**. The closest CH–C distances between adjacent resorcinol molecules are 2.609 and 2.694 Å.

The reaction of zinc phosphite with TMDP in the presence of resorcinol leads to a pillared layer structure of composition (4,4'-$(C_5H_4N)_2(CH_2)_3$)Zn2$(HPO_3)_2\cdot(C_6H_6O_2)$. The

structure of **7** shows the most common structural theme for this class of inorganic/organic hybrid. Namely, the zinc phosphite forms neutral sheets with a connectivity of 4.8^2 that are linked by trimethylene-dipyridine pillars. The resulting channels are filled by the templating aromatic alcohol. Similar structures are observed for TMDP-Zn-HPO_3 hybrids templated by phenol and hydroquinone (see below). The resorcinol tilts in the interstitial space to accommodate the spacing limitation dictated by the length of the pillar. The tilting leads to a twofold screw axis parallel to the channels. The space group, $P2_12_12_1$, requires three mutually perpendicular screw axes. The resorcinol hydroxyl groups show strong hydrogen bonding to phosphite oxygen atoms. A cross-section of the channels filled with resorcinol is shown in Figure 2.15A, and Figure 2.15B shows the chain of resorcinol molecules. Each resorcinol forms two hydrogen bonds with two crystallographically unique phosphite oxygen atoms. Hydrogen bonding parameters are given in table 2.3. Further, as in the phenol templated structure and the hydroquinone templated structure, short C–H–C contacts are observed between resorcinol molecules in the chain. In accommodating this structure TMDP adopts *a*, *g*, *a*, *c* conformation with a calculated energy expense of only 0.3 kcal mol^{-1}.

Compound **7** crystallizes in the chiral space group $P2_12_12_1$. The flexibility of the ligand, TMDP, enables the ligand to accommodate the twofold screw axis that runs parallel to the ligand axis. Thus, TMDP can accommodate chiral structural motifs. This was recently demonstrated in the co-crystallization of TMDP with *R*-binaphthol to form a chiral framework in which chiral chains of (TMDP-*R*-binaphthol) intertwine to give a double helix motif.[82]

2.8.8. Crystal structure (4,4'-$(C_5H_4N)_2(CH_2)_3)Zn_2(HPO_3)_2 \cdot 2(C_6H_5NO_3)$, **8**.

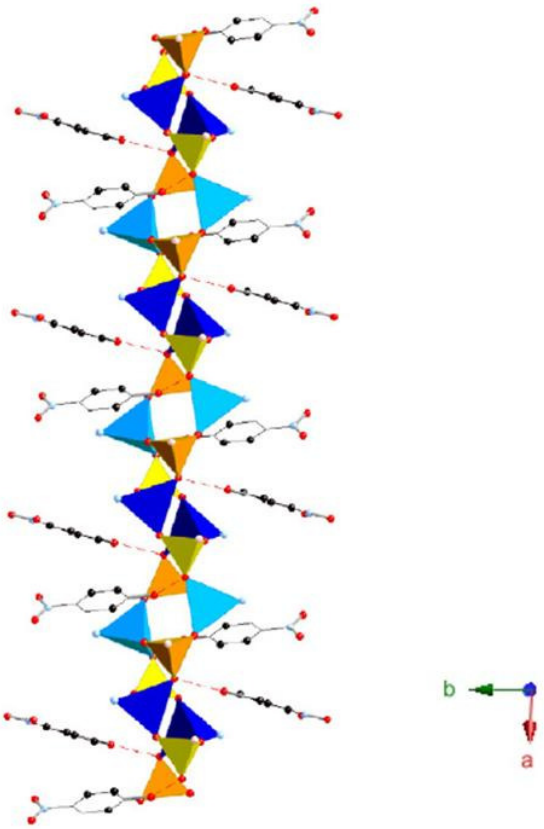

Figure 2.16A: A view of the zinc phosphite chain in 8 stabilized by hydrogen bonding to nitrophenol. The crystallographically unique zinc ions are represented by dark and light blue tetrahedral. Each tetrahedral site is three-connected in the ladder of 4-rings.

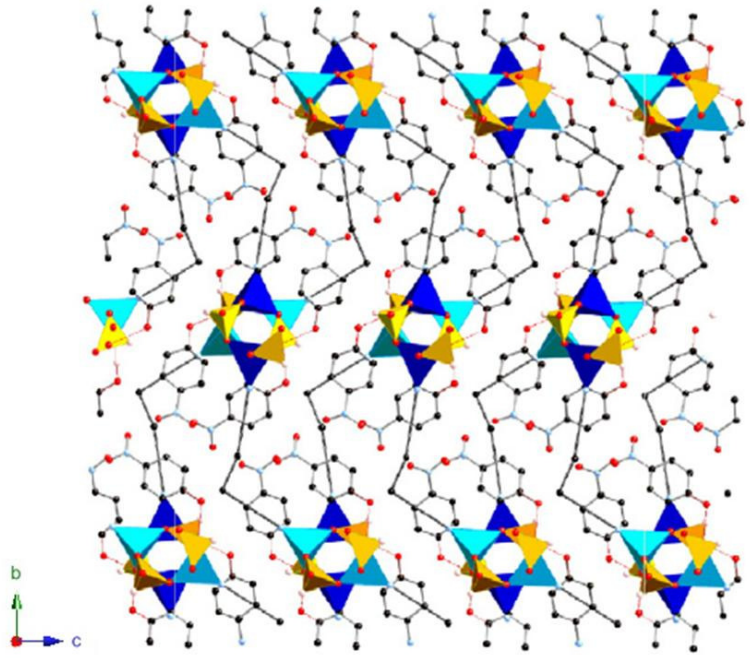

Figure 2.16B: A view perpendicular to the zinc phosphite 4-ring chains. The chains are linked into a three-dimensional network by bridging trimethylene-dipyridine. For clarity the bridging ligands are shown schematically.

The most unique of the hybrid structures of zinc phosphite with TMDP is templated by nitrophenol and has a composition of $(4,4'\text{-}(C_5H_4N)_2(CH_2)_3)Zn_2(HPO_3)_2 \cdot 2(C_6H_5NO_3)$. Two views of the structure are given in Figure 2.16A and Figure 2.16B. The inorganic motif is that of a twisted ladder stabilized by hydrogen bonding to nitrophenol. The twisted ladder with hydrogen bonded nitrophenol groups is shown in Figure 2.16A. Trimethylene-dipyridine connects the twisted ladders into a three-dimensional network structure as shown in Figure 2.16B. To accommodate the nitrophenol in the structure, TMDP is distorted significantly from its most stable conformation. The observed conformation is *c*, *g*, *a*, *s* which is calculated to have an energy 1.5 kcal mol^{-1} higher than the unstable conformation of the free ligand.

2.8.9. Crystal structure (4,4'-$(C_5H_4N)_2(CH_2)_3)_2Zn_4(HPO_3)_4 \cdot 2(C_6H_6O_2)$, **9**.

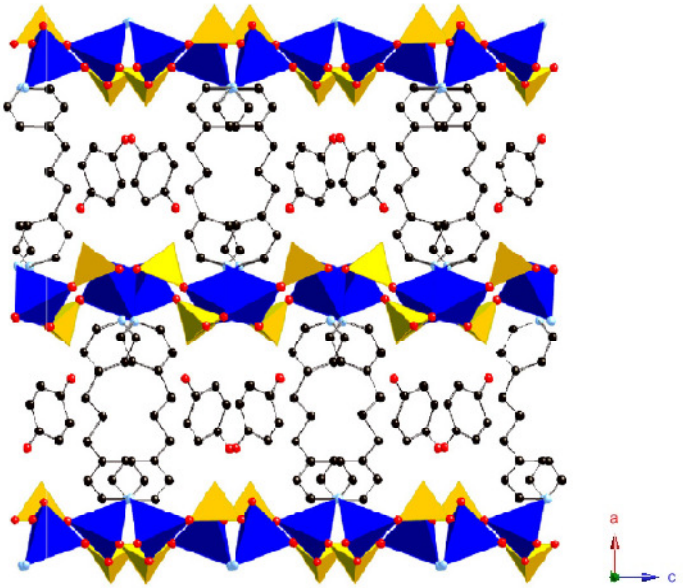

Figure 2.17A: A view down the *b* axis of **9**. Hydroquinone fills the channels generated by the trimethylene-dipyridine pillars.

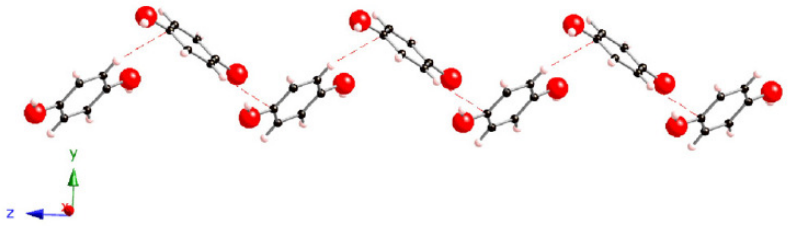

Figure 2.17B: A view of the hydroquinone chain that fills the channels of **9**. The closest CH–C distance between adjacent hydroquinone molecules is 2.785 Å.

Hydroquinone, like phenol and resorcinol, templates a layered structure of composition (4,4'-$(C_5H_4N)_2(CH_2)_3)_2Zn_4(HPO_3)_4 \cdot 2(C_6H_6O_2)$. The zinc phosphite layer is a neutral 4.8^2 net and the layers are pillared by trimethylene-dipyridine. The hydroquinone forms chains in the channels with short CH – aromatic ring contacts (*d*(H16–C14) = 2.785 Å). The two hydroxyl groups in one hydroquinone are hydrogen bonded to phosphite oxygen atoms in adjacent

layers; hydrogen bonding contacts are given in Table 2.3. The trimethylene-dipyridine ligand adopts *s*, *a*, *a*, *g* conformation with the last dihedral angle C-C-N-C (ϕ_1') of 158.25° (measure from Mercury), being nearly *anti* with respect to the trimethylene link. This is the most distorted conformation of TMDP in this series of compounds; still it lies just 2 kcal mol^{-1} above the most stable conformation (Figure 2.17A and Figure 2.17B).

2.8.10. Crystal structure (4,4'-$(C_5H_4N)_2(CH_2)_3$)$Zn(HPO_3)\cdot 2(C_6H_5BrO)$, **10**.

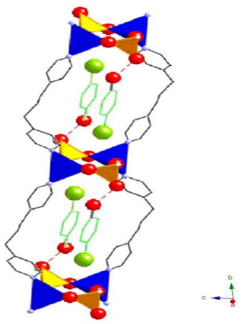

Figure 2.18A: A representation of the double chains of alternating Zn2P2 4- rings and trimethylene-dipyridine. The associated bromophenol is shown in green.

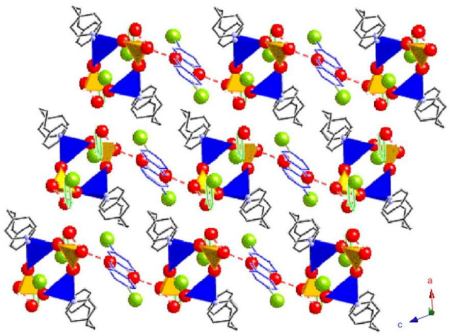

Figure 2.18B: A projection of the packing diagram of **10**. The bromophenols that are caged by the double chain of two trimethylene-dipyridine and Zn_2P_2 four rings are shown in green. The bromophenols that pack between double chains are shown in blue.

The zinc phosphite hybrid templated by bromophenol forms linear chains of Zn_2P_2 squares linked by trimethylene-dipyridine. Each zinc atom is coordinated to two pyridine nitrogen atoms and two phosphite oxygen atoms. Each tetrahedral atom in the squares is two-connected in the inorganic square. Adjacent squares are eclipsed and the effect of the linking ligands is to make a square prism with just two connectors between the square faces. The "vacant" edges are occupied by bromophenol molecules, indicated in green in Figure 2.18A. The bromine atoms are directed toward the hydrophobic center of the square prism, the OH groups are directed away from the center and are hydrogen bonded to the phosphite oxygen atoms that are also directed away from the zinc phosphite squares. All three P–O bond lengths are nearly identical so it is not possible to assign the exo cyclic phosphite oxygen as a phosphoryl group. The chains stack in a nearly closest packed array, as shown in Figure 2.18B, and the interstitial space between chains is occupied by additional bromophenol molecules. These are also hydrogen bonded to the exocyclic phosphite oxygen with distances: O5–O3 2.617 Å and H5–O3 1.817 Å.

Table 2.3: Hydrogen bonds in hybrid network series **I.**

1		**2**	
N1-O5	2.721(3)	O7-O9	1.815(6)
N1-H1B-O5	169[a]	O7-O9	2.799(7)
		O7-O9	2.890(6)
		O9-O2	2.779(6)
		O8-O4	2.837(5)
		O7-H7E-O9	169(6)
		O7-H7F-O9	176(8)
		O9-H9B-O7	155(8)
		O9-H9A-O2	158(8)
		O8-H8E-O4	156(5)

3		**4**	
O4-O5	2.809(3)	O4-O2	2.875(5)
O5-O4	2.821(3)	O4-H4-O2	150[a]
O5-O3	2.805(3)		
O4-H4B-O5	152(7)		
O5-H5B-O4	166(4)		
O5-H5B-O3	172(3)		

5		**7**	
O6-O8	2.736(5)	O7-O4	2.780(2)
06-O10	2.638(4)	O8-O2	2.745(2)
O3-O9	2.772(5)	O7-H7-O4	175(3)
O3-O7	2.648(4)	O8-H8-O2	164(2)
O7-O8	2.673(5)		
O6-H8C-O8	150[a]		
06-H10A-O10	163[a]		
O3-H9C-O9	147[a]		
O3-H7-O7	164[a]		
O7-H8-O8	114[a]		

8		**9**	
O1-O10	2.6605(17)	O2-O1	2.7958(17)
O4-O8	2.7020(17)	O2-O3	2.7123(13)
O1-H1-O10	168.4	O1-N1	2.7173(14)
O4-H4-O8	159.9	O2-H2-O1	153.0(13)
		O2-H2-O3	112.0(11)
		O1-H1-N1	161.6(15)

10	
O4-O3	2.634(2)
O5-O3	2.617(2)
O4-H4-O3	158.0
O5-H10-O3	158.6

[a] No esd is given because the hydrogen-bond positions in these compounds were calculated and not defined.

2.9 Discussion of templates in hybrid network series **I**

Aromatic alcohols are uniquely suited as hydrogen bond donors in the formation of network solids. For example merocyanine dyes co-crystallize with phenolic derivatives to give materials with non-linear optical properties.[123] The use of the aromatic alcohols in the preparation of zinc phosphites is described by us[85], demonstrates the ability of this class of compound to alter the structure of zinc phosphite hybrids during their synthesis under hydrothermal conditions. In most cases it is a bridging Zn–O–P oxygen atom that acts as the hydrogen bond acceptor. In a few cases the aromatic alcohol effectively pulls a phosphite oxygen atom into a terminal position. Most notably this occurs with catechol and bromophenol as templates. Further, the shortest hydrogen bond contacts are observed in the catechol and the bromophenol templated materials. Non-aromatic hydrogen bond donors have not yet been used successfully as templates in this class of hybrid network. Phosphine oxides are often added as a potential hydrogen bond acceptor to aid the crystallization of potential hydrogen bond donors.[124, 125] Phenols can also aid the crystallization of potential hydrogen bond acceptors.[125, 126]. Phosphites and aromatic alcohols appear to have an affinity that promotes the crystallization of these unique hybrid structures.

2.10 Summary of hybrid network series **I**

Zinc phosphite hybrids constructed with the flexible linker 4, 4'-trimethylenedipyridine (TMDP) form a wide variety of framework structures. These hybrid structures are unique in their ability to incorporate guest molecules that have hydrogen-bond donor capacity. These guest molecules are the aromatic alcohols, phenol, catechol, resorcinol, hydroquinone, 1,2,3-trihydroxybenzene, nitrophenol, bromophenol, and flurophenol. The aromatic alcohols interact with the framework by hydrogen bonding to oxygen atoms that bridge zinc and phosphorous atoms in the inorganic portion of the network. Calculations of PM5 parameters demonstrate that TMDP can adopt a wide variety of conformations with a minimal energy expense. With a different ligand, the systems may have the potential to incorporate small-molecule pharmaceuticals including chiral guests. If chiral groups could be incorporated, it may be possible to induce the formation of enantiopure helical ZnPO chains in a hybrid structure.

Chapter 3

Series II: Hybrid structures containing rigid ligand

4, 4'-bisimidazolylbiphenyl (BIB)

3.1 Introduction of Hybrid structure series **II**

It is well known the bisimidazole ligands have been widely used in the preparation of hybrid structure constructions. Carlucci et al. reported that the flexible ligand 4-bis(imidazole-1-ylmethyl)benzene (bix) (Scheme 3.1A), when coordinated with $CoSO_4$ salts (Figure 3.1 shows the coordination rings), forms an open-channel entangled architecture with nanoporous behavior.[127] The species they report is a highly unusual hybrid material containing both 1D and 3D arrays within the same crystal structure. Additionally, the solvent molecules that are present in the as-synthesized complex can be removed completely from the cavities, and then reinstated in a reversible process.

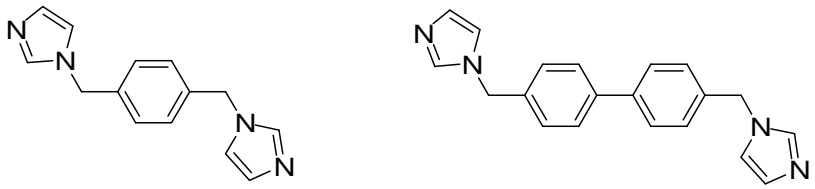

A B

Scheme 3.1: A) 4-bis(imidazole-1-ylmethyl)benzene (bix). B) 4,4′-bis(imidazole-1-ylmethyl)biphenol (bimb).

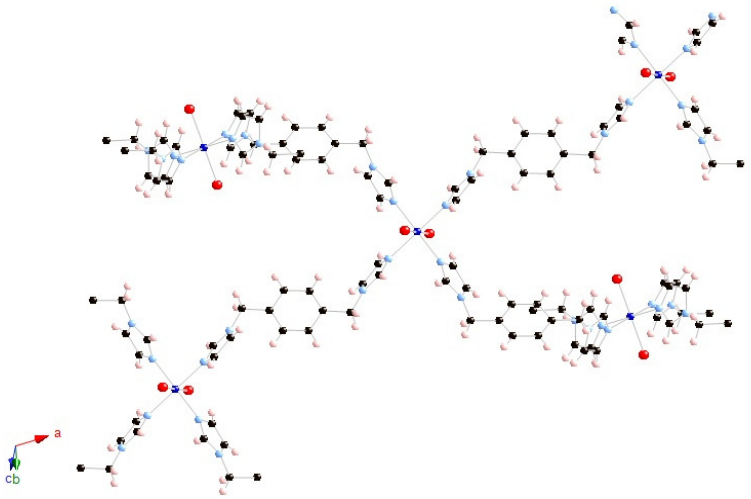

Figure 3.1: Rings are constructed by 4-bis(imidazole-1-ylmethyl)benzene (bix) in hybrid structure $[Co(bix)_2(H_2O)_2](SO_4)\bullet 7H_2O$.[127] (Dark blue = Co, red = oxygen, black = carbon, light blue = nitrogen, pink = hydrogen.)

Another example, reported by Fei et al,[128] shows a hybrid metal-organic framework structure $[Mn(bimb)_3][ClO_4]_2\bullet 2H_2O$ (Figure 3.2) incorporating manganese ions and the novel ligand 4,4′-bis(imidazole-1-ylmethyl)biphenol (bimb) (Scheme 3.1B).[128] They expected magnetic interaction between the neighboring Mn(II) ions, however the magnetic susceptibility results indicated that there is no interaction because of the long intermetallic distance created by the bimb ligands.[128]

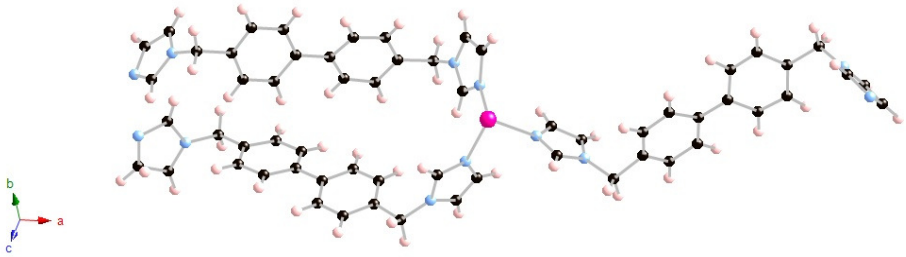

Figure 3.2: Cationic moiety of hybrid structure $[Mn(bimb)_3][ClO_4]_2\bullet 2H_2O$.[128] (Purple = Mn, light blue = nitrogen, black = carbon)

Inspired by these resent results, we investigated the coordination chemistry of a similar bifunctional ligand 4,4'-bisimidazolylbiphenyl (BIB) (Scheme 3.2). The reaction of copper nitrate, copper sulfate, and nickel acetate with 4,4'-bisimidazolylbiphenyl (BIB) in the presence of phosphoric acid/phosphorous acid leads to the formation of five new hybrid structure with interesting structure topologies.

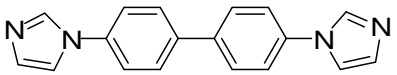

Scheme 3.2: Ligand 4,4'-bisimidazolylbiphenyl (BIB).

3.2 Ligand rigidity

As we know, ligand flexibility leads to many possible conformations in hybrid structure. Hybrid structures with cavities generated by flexible templates are not stable enough for gas absorption because the guest molecule removal tends to cause the collapse of the pores. Permanent porosity hybrid is important for gas absorption. Rigid channels allow guest molecules access and are robust enough to withstand guest removal. The rigidity of hybrid structures depends primarily on the rigidity of the ligand backbone. Ligands with less orientation freedom are rigid. Further, rigid ligands reduce the structure variety available for the formation of networks, which, in particular helps one to predict structures. Examples of rigid ligands include 2,4,6-tri(pyridin-4-yl)-1,3,5-triazine, benzene-1,3,5-tricarboxylic acid, 4,4'-bipyridine, 4-(2,3,5,6-tetrafluoro-4-(pyridin-4-yl)phenyl)pyridine, and isonicotinic acid (Scheme 3.3). Kondo et al. reported a 3D framework $Co_2(4,4'\text{-bipy})_3(NO_3)_4 \bullet xH_2O$ with channel shaped cavities in which small molecules could reside.[129] Kepert et al. reported a robust framework $Ni(4,4'\text{-bipy})_{3/2}(NO_3)_2$[130] which shows both ethanol-loaded and desolvated forms with a small relaxation of the structure upon guest loss (Figure 3.3).[130] These two examples show that rigid ligands are important in the construction of porous hybrid

structures.

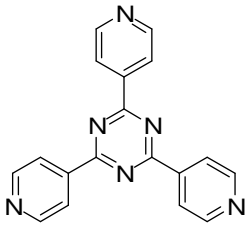

2,4,6-tri(pyridin-4-yl)-1,3,5-triazine

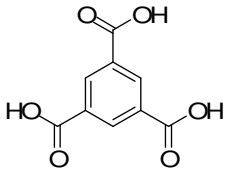

benzene-1,3,5-tricarboxylic acid

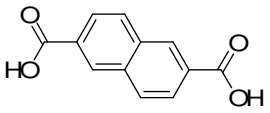

naphthalene-2,6-dicarboxylic acid

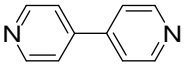

4,4'-bipyridine

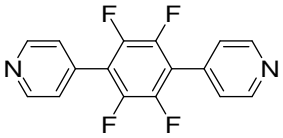

4-(2,3,5,6-tetrafluoro-4-(pyridin-4-yl)phenyl)pyridine

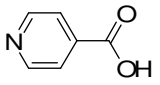

isonicotinic acid

Scheme 3.3: Examples of some rigid ligands.

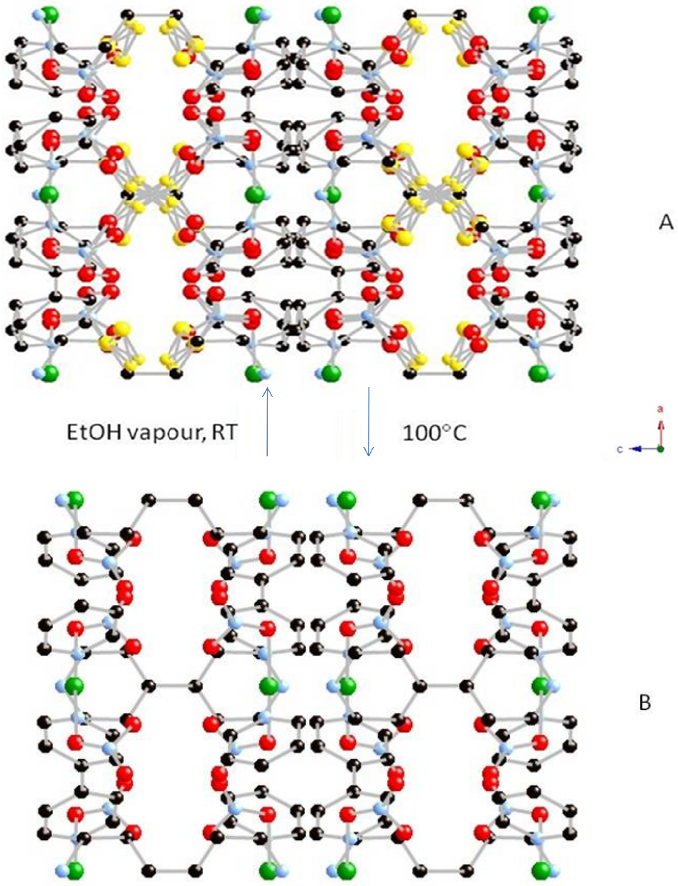

Figure 3.3: Structure projections down the a-axis, showing removal of disordered ethanol molecules from Ni(4,4'-bipy)$_{3/2}$(NO$_3$)$_2$•EtOH to give Ni(4,4'-bipy)$_{3/2}$(NO$_3$). (EtOH are in gold color). The desolvated structure B contains channels that occupy 20% of crystal volume. Adjacent layers are shown in yellow and red, with the C and disordered O atoms of the guest as green and blue spheres.[130]

The ligand, 4,4'-bisimidazolylbiphenyl is relatively rigid and has only rotational flexibility about the long axis of the molecule. The nitrogen lone pairs are directed 36° off the long axis regardless of the dihedral angles. If the dihedral angle between lone pairs is 0° then the angle subtended by the nitrogen atoms is 72°; if the dihedral is 180° then the nitrogen lone pairs are directed in opposite, parallel directions (Scheme 3.4). The crystal structure of BIB, co-crystallized with water, has a dihedral angle between the nitrogen lone

pairs of 180°, a planar biphenyl core, and slight twisting between the terminal imidazole rings and the adjacent phenyl rings.

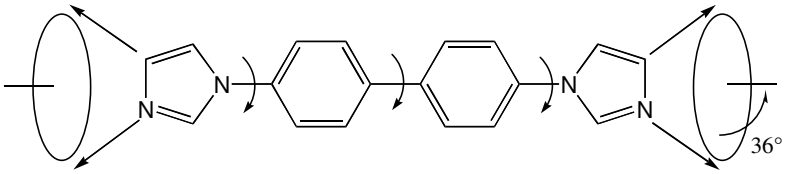

Scheme 3.4: Rotation flexibility about BIB.

There are crystallographically unique BIB molecules in structures $[Cu_4(H_2PO_4)_2(HPO_4)_2(C_{18}N_4H_{14})_4(OH)]NO_3 \bullet 2(H_2O)$, **11** and $[Cu_5(H_2PO_4)_4(HPO_4)_2(C_{18}N_4H_{14})_5](NO_3)_2 \bullet (H_2O)_2$, **12**. The dihedral angles between nitrogen lone pairs range from 142.9 to 180° and the dihedral angles between the planar five membered and six membered rings are in the range of 0 to 28°. The orientation of the imidazole groups appears to be dictated by the geometric arrangement of the inorganic part of the structure.

3.3 BIB structure with Cu(II) and Ni(II)

It is well known that isolated transition metal ions and organic bridging ligands can form hybrid structure. Metal ions, such as Cu^{2+} and Ni^{2+} have well-defined geometries that fulfill the formation of hybrid structures.

3.3.1 Cu(II) ions in hybrid structures

Copper has a valance electron configuration of $4s^1 3d^{10}$ and Cu^{2+} has a d^9 electronic configuration. Lone electron pairs from organic bridging ligands can coordinate with Cu^{2+}. The Cu^{2+} ion adopts a variety of coordination geometries, including square planer, square

pyramidal, octahedral, and tetrahedral[131-135], each of which has been observed in hybrid structure.[136-139]

Cai et al. reported a four coordinate Cu(II) ion in the metal complex $[Cu(acactn)H_2O]_2$ [H_2acactn = bis(actylacetone)trimethylenediimine].[138] In this complex structure (Figure 3.4), each Cu(II) ion is coordinated to two N and two O atoms of the ligand (H_2acactn) in a square planar geometry.[138]

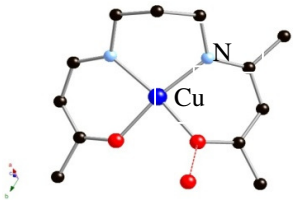

Figure 3.4: Four coordinated Cu(II) (blue) ions in complex $[Cu(acactn)H_2O]_2$ [H_2acactn = bis(actylacetone)trimethylenediimine].[139]

Five coordinate Cu(II) is common in hybrid structure. Zhang et al. reported a hybrid structure $CuSO_4(pia)•2CH_3OH•H_2O$ [pia = N, N′-(1,2-phenylene)diisonicotinamide], in which the Cu(II) ion is bonded to two different molecules of pia and two sulfate anions (Figure 3.5).[139] The O atoms from SO_4^{2-} are located at the axial position of the distorted square pyramidal geometry of the Cu(II) ion.[139]

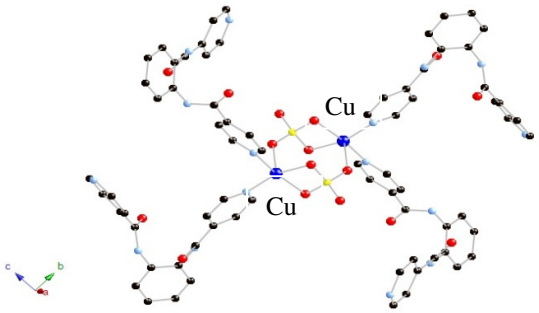

Figure 3.5: Five coordinated Cu(II)(blue) in hybrid structure $CuSO_4(pia)•2CH_3OH•H_2O$ [pia = N, N′-(1,2-phenylene)diisonicotinamide].[139](The CH_3OH and H_2O molecules are not shown in this figure.)

Six coordinated Cu(II) ions are very common in hybrid structure. Noro et al. reported a network structure $[Cu(GeF_6)(4,4'\text{-pipyridine})_2]\bullet 8H_2O$, in which the Cu(II) atom has octahedral geometry with four N atoms of 4, 4′-bipyridine ligands in the equatorial plane, and two O atoms of H_2O molecules at the axial sites (Figure 3.6).[137]

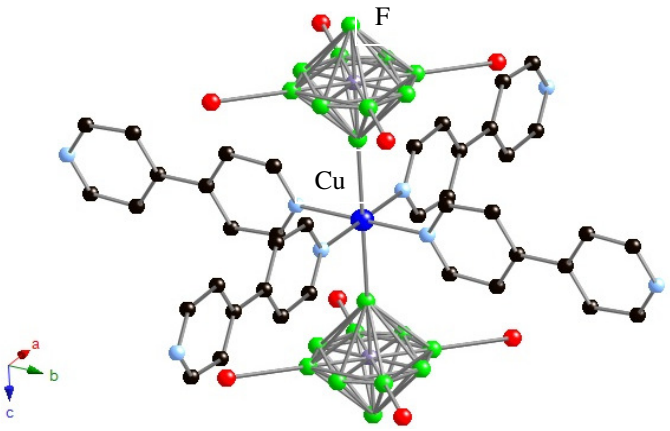

Figure 3.6: Six coordinated Cu(II) (blue) in network structure $[Cu(GeF_6)(4,4'\text{-pipyridine})_2]\bullet 8H_2O$.[137]

3.3.2 Ni(II) ions in hybrid structures

The valence electron configuration of Ni is: $4s^2 3d^8$. The most common oxidation state of nickel is +2, although 0, +1, +3 and +4 Ni ions present in complexes have been observed. Ni^{2+} has a d^8 electronic configuration. The Ni^{2+} ion can adopt a variety of coordination geometries in hybrid structure.

Three coordinate Ni(II) is observed in complex $(2,4,6\text{-}Me_3NN)Ni(NO)$, which was reported by Puiu et al. One of the two independent molecules in the asymmetric unit reveals trigonal-planar coordination at Ni(II) (Figure 3.7).[140]

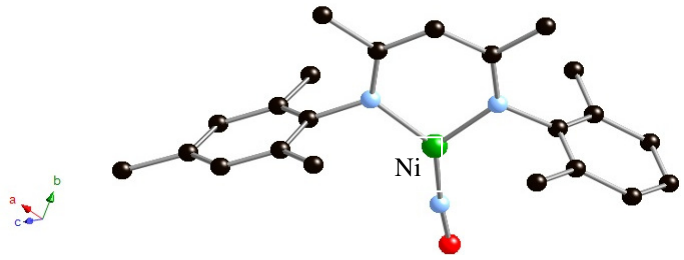

Figure 3.7: Three coordinated Ni(II) in complex (2,4,6-Me_3NN)Ni(NO).[140]

There are numerous complexes and hybrid structures containing four coordinated Ni(II) ions. Zhu et al. reported a series of Ni(II) complexes, one them being $[(2,6\text{-}Me_2C_6H_3)NC(CH_3)C(H)C(Ph)O]_2Ni$.[141] The crystal structure of this complex contains four coordinated Ni(II) ions (Figure 3.8).[141] Each Ni(II) ion is coordinated to two N and O atoms to form a distorted square planar coordination geometry.[141]

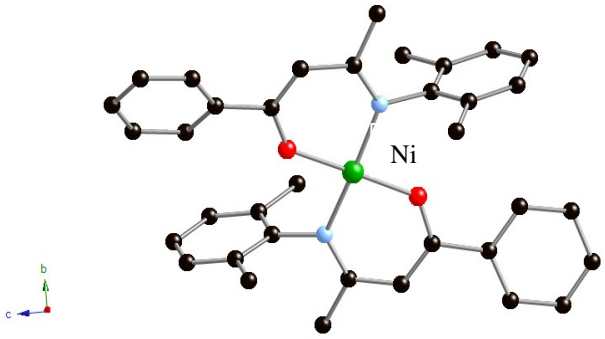

Figure 3.8: Four coordinated Ni(II) (dark green) ion in complex $[(2,6\text{-}Me_2C_6H_3)NC(CH_3)C(H)C(Ph)O]_2Ni$.[141]

Five and six coordinated Ni(II) ions have been reported by many researchers.[142] Examples include $NiCl_2(L^m)$, L^m = 2,6-bis[3′, 4′, 5′-tri(alkoxy)phenyliminomethyl]pyridine, in which the Ni(II) ions are in a distorted trigonal bipyramidal geometry.[142] The pyridyl N atom and two Cl atoms are in the trigonal plane, and the two imine N atoms are in the axial positions (Figure 3.9).[142] A six coordinated Ni(II) ion in a network was reported by Goher et al. The structure of $[Ni(4\text{-ethylpyridine})_4(N)_3](PF_6)$ consists of 1D nickel-azido chains, and

isolated by PF_6^- anions.[143] Each Ni(II) ion is coordinated to four N atoms from four different pyridine ligands and two N atoms from two different μ-1,3-azide bridges in an octahedral geometry (Figure 3.10).[143]

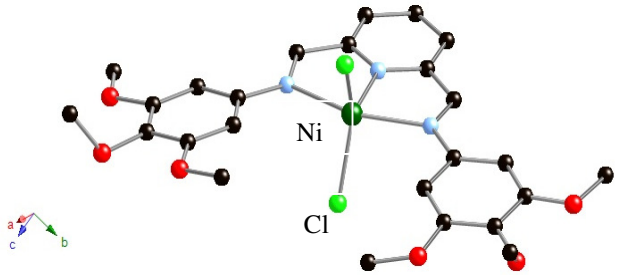

Figure 3.9: Five coordinated Ni(II) (dark green) in complex $NiCl_2(L^m)$, L^m = 2,6-bis[3′, 4′, 5′-tri(alkoxy)phenyliminomethyl]pyridine.[142]

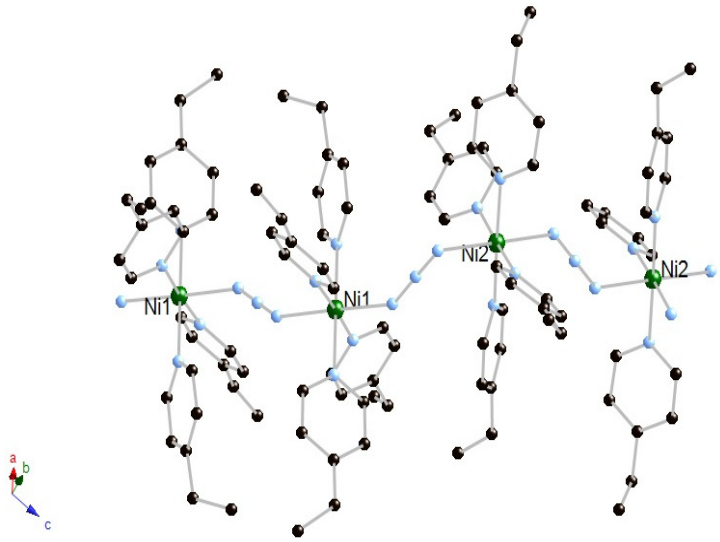

Figure 3.10: Six coordinated Ni(II) in a hybrid chain $[Ni(4\text{-ethylpyridine})_4(N)_3]^+$.[143]

3.4 Experimental Section

3.4.1 Synthesis of the BIB ligand

The hybrid structure series **II** is constructed from the 4,4'-bisimidazolylbiphenyl (BIB) ligand and transition metal ions.

The synthesis of the BIB ligand (Scheme 3.5): 4,4′-dibromobiphenol (6.24g, 20.0 mmol), imidazole (5.76g, 84.0 mmol), potassium carbonate (8.78g, 63.0mmol), and anhydrous copper sulfate (0.064g, 0.4 mmol) were mixed in a 250 mL round bottom glass flask and heated to 180 °C under argon protection for 12 to 14 hours. The reaction mixture burns a light blue color. Three portions of deionized water, 150mL, were used to wash the crude products. The crude product is white after washing. The product was then recrystallized from ethanol (200 mL). Yield: 81% based on 4,4′-dibromobiphenol. ^{1}H NMR (400 MHz; solvent $CDCl_3$) δ 7.26 (2H, s), 7.35 (2H, s), 7.49-7.51 (4H, m), 7.70-7.72 (2H, m) (NMR spectra are in the Appendix C). The crystal structure of the BIB ligand will be included in the hybrid structure **II** discussion section.

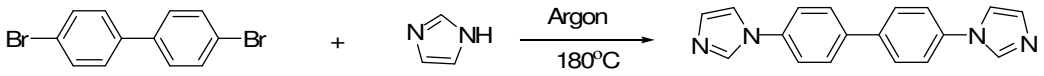

Scheme 3.5: Synthesis of the BIB ligand.

3.4.2 Synthesis of hybrid structure series **II**

All commercially available chemicals were reagent grade and were used as received without further purification. Thermogravimetric measurements were performed on a TGA Q500 thermal analyzer under flowing N_2 with a heating rate of 10 °C min^{-1}. TGA traces for the BIB ligand and the hybrid structure series **II** presented herein are included in the Appendix A.

$[Cu_4(H_2PO_4)_2(HPO_4)_2(C_{18}N_4H_{14})_4(OH)]NO_3•2(H_2O)$, **11**. Copper nitrate tetrahydrate (242.0 mg, 1.0 mmol), BIB (429.5 mg, 1.5 mmol), phosphoric acid (85 wt. % aqueous solution, 230.6 mg, 2.0 mmol), and 6 mL water were added to a heavy-wall glass tube, which was then immersed in liquid nitrogen and sealed under vacuum. The pH of the reaction solution was 5.0. The glass tube was placed in a furnace and held at 130°C for 3 days. The mixture was then filtered under gravity. Yield was approximately 50%, based on Cu(II).

$[Cu_5(H_2PO_4)_4(HPO_4)_2(C_{18}N_4H_{14})_5](NO_3)_2•(H_2O)_2$, **12**. Copper nitrate tetrahydrate (242.0 mg, 1.0 mmol), BIB (286.0 mg, 1.0 mmol), phosphoric acid (85 wt. % aqueous solution, 230.6 mg, 2.0 mmol), sodium hydroxide (60.0 mg, 1.5 mmol), and 6 mL water were added to a heavy-wall glass tube, which was then immersed in liquid nitrogen and sealed under vacuum. The pH of the reaction solution was 4.0. The glass tube was placed in a furnace and held at 130°C for 3 days. The mixture was then filtered under gravity. Yield was approximately 30%, based on Cu(II).

$(C_{18}H_{14}N_4)CuSO_4•H_2O$, **13**. Copper sulphate (160.0 mg, 1.0 mmol), BIB (286.0 mg, 1.0 mmol) and 6mL water were added to a heavy-wall glass tube and sealed under vacuum. The pH of the reaction solution was 4.3. The glass tube was placed in an oven for 3 days at 130°C. Blue crystals of **13** were collected by filtration. Yield was approximately 35%, based on Cu(II).

$(C_{18}H_{14}N_4)_3Ni_3(H_2PO_4)_2(HPO_4)_2 \bullet 4H_2O$, **14**. Nickel acetate tetrahydrate (248.8 mg, 1.0 mmol), BIB (286.0 mg, 1.0 mmol), phosphoric acid (85 wt. % aqueous solution, 230.6 mg, 2.0 mmol), and 6 mL water were added to a heavy-wall glass tube and sealed under vacuum. The pH of the reaction solution was 3.0. The glass tube was placed in an oven for 3 days at 130°C. Colorless crystals of **14** were collected by filtration. Yield was approximately 30%, based on Ni(II).

$(C_{18}H_{14}N_4)_2Ni(H_2PO_3)_2$, **15**. Nickel acetate tetrahydrate (248.8 mg, 1.0 mmol), BIB (286.0 mg, 1.0 mmol), phosphorous acid (164.0 mg, 2.0 mmol), and 6 mL water were added to a heavy-wall glass tube and sealed under vacuum. The pH of the reaction solution was 3.5.The glass tube was placed in an oven for 3 days at 130°C. Colorless crystals of **15** were collected by filtration. Yield was approximately 80%, based on Ni(II).

3.5 Crystal structure of hybrid structure series **II**

$[Cu_4(H_2PO_4)_2(HPO_4)_2(C_{18}N_4H_{14})_4(OH)]NO_3 \bullet 2(H_2O)$, **11**.

Hybrid structure **11** is not unambiguously determined by the crystallographic data alone. A representation of the copper phosphate 8-ring in **11** is shown in Figure 3.11. The 8-ring is required to be cationic since there is one extra framework nitrate ion in the lattice for each ring. In Figure 3.11 the 8-ring is represented as $[Cu_4(H_2PO_4)_2(HPO_4)_2(OH)]^+$ (the two OH sites are each 50% occupied); copper is assumed to be in the +2 oxidation state. All but two of the phosphate proton positions were found in electron density difference maps; two protons were added to the phosphate groups to balance the charge as required by the presence of nitrate and copper(II), however the exact location of the hydrogen atoms was not determined conclusively from the X-ray diffraction data. In the absence of magnetic data to prove otherwise it is possible for the oxidation state of two copper ions to be assigned as +3 and the two extra protons would not be required. Magnetic measurements, however, are consistent with the presence of only copper (II). Within the copper phosphate 8-ring there

are two well-defined square planar copper atoms, Cu1. The copper positions labeled Cu2 have a fifth coordination site partially occupied by a hydroxyl group. This copper-oxygen contact is very long, 2.434(6) Å. The 8-ring encapsulates the hydroxyl group with the long Cu-O bond and hydrogen bonding between H9A and O2, dH9-O2 1.99(1) Å.

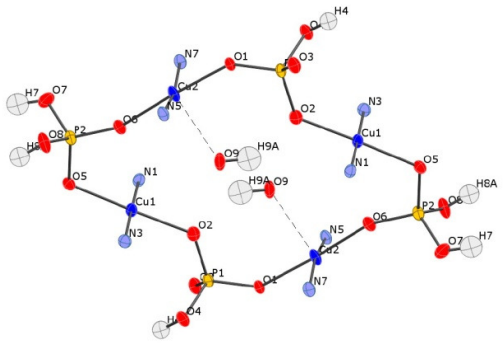

Figure 3.11: A thermal ellipsoid plot (50% probabilities) generated in CrystalMaker of the 8-ring in hybrid structure **11**.

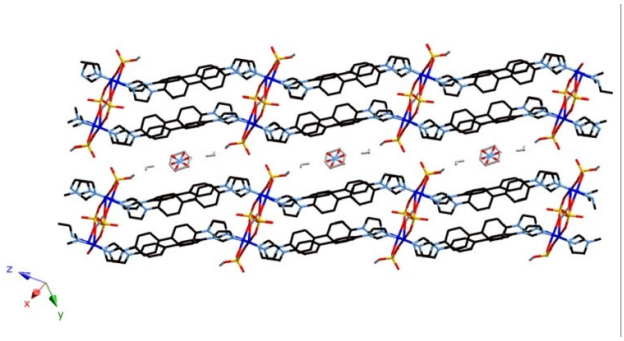

Figure 3.12: A representation of the parallel chains of BIB alternating with copper phosphate 8-rings. The nitrate ions lie on an inversion center and are disordered.

The copper phosphate 8-rings are connected at copper by four parallel BIB ligands to form a rod-like arrangement of alternating ligand and copper phosphate. Each copper is bonded to pair of trans imidazole groups. The parallel arrangement of ligands is shown in Figure 3.12. The rods are packed tightly such that the 8-rings are slightly offset. The rods are connected by hydrogen bonding directly and through water and nitrate ions that separate the rods. The packing of two rods is shown in Figure 3.12.

$[Cu_5(H_2PO_4)_4(HPO_4)_2(C_{18}N_4H_{14})_5](NO_3)_2 \bullet (H_2O)_2$, **12**.

As in hybrid structure **11**, 8-rings are present in **12**, however these are now fused to form one-dimensional copper-phosphate chains. A representation of the chain is given in Figure 3.13. The distance between Cu3-Cu3, across the 8-ring, is 5.2436(9) Å; this is compressed compared to the 8-ring in **11**. Accordingly, the 8-ring in hybrid structure **12** is empty while in **11** a hydroxyl group is present. The 8-rings are fused at Cu1, which has a distorted octahedral structure, to form the chains. The Cu1-N and Cu1-O distances are 2.017(3) and 1.953(2) Å respectively while the apical Cu1-O distance is 2.691(3)Å. The pendent copper, Cu2, is relatively close to Cu3 and gives the appearance of a singly bridged copper dimer. The distance between copper atoms, 3.3167(6) Å, however, is significantly longer than observed in typical carboxylate bridged copper dimers, which have copper-copper distances in the range 2.44-2.81 Å. The copper phosphate chains are hydrogen bonded through nitrate ions and water to form sheets. The sheets are connected by BIB to form a dense three-dimensional structure. A side-on view of the sheets with a schematic representation of the BIB links is given in Figure 3.14.

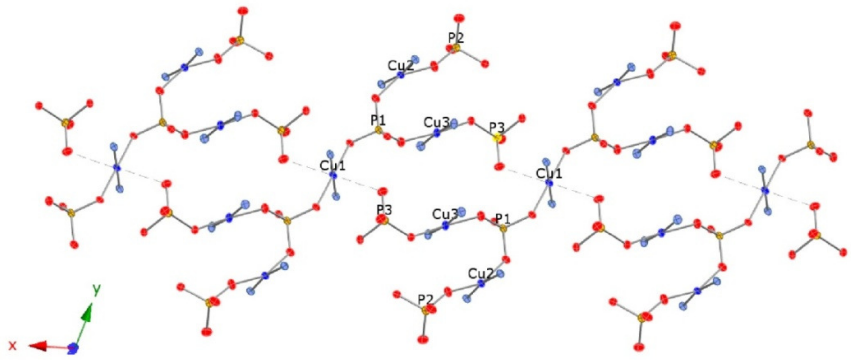

Figure 3.13: A thermal ellipsoid plot of the copper phosphate chain in **12**.

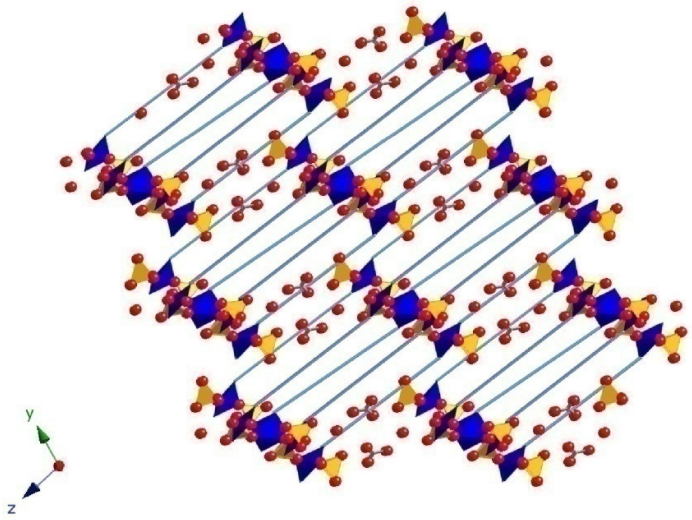

Figure 3.14: A schematic representation of the three dimensional structure of **12**. The BIB ligands are shown as blue rods connecting imidazole nitrogen atoms. The view is down the copper-phosphate chains that run parallel to the z-axis; the inorganic sheet.

$(C_{18}H_{14}N_4)CuSO_4 \cdot H_2O$, **13**.

Hybrid structure **13** crystallizes in the orthorhombic space group $P2_12_12_1$. The asymmetric unit contains a single square pyramidal Cu^{2+} ion that is bound to two nitrogen atoms from two different BIB ligands (N1-Cu1 2.000(2) Å, N3-Cu1 1.987(2) Å), two oxygen atoms from two different SO_4^{2-} anions (Cu1-O1 2.005(2) Å, Cu1-O2 2.009(2) Å), and one axial H_2O molecule (Cu1-O5 2.213(2) Å). Each SO_4^{2-} anion displays tetrahedral geometry. Two oxygen atoms from a SO_4^{2-} ion coordinate to two different Cu(II) ions, thus bridging the metals centers to create a 1D inorganic chain (Figure 3.15a) in which the distances between neighboring Cu^{2+} ions is 4.690 Å. The $CuSO_4$ chains are then linked via BIB ligands to form corrugated 2D hybrid sheets (Figure 3.15b). Hydrogen bonds between SO_4^{2-} anions and coordinated H_2O molecules on neighboring 2D hybrid sheets connect the sheets to form a 3D structure (Table 3.1, Figure 3.15c). The 2D hybrid sheet stacking is of the AAA type. The interlayer distance is approximately 6.4 Å.

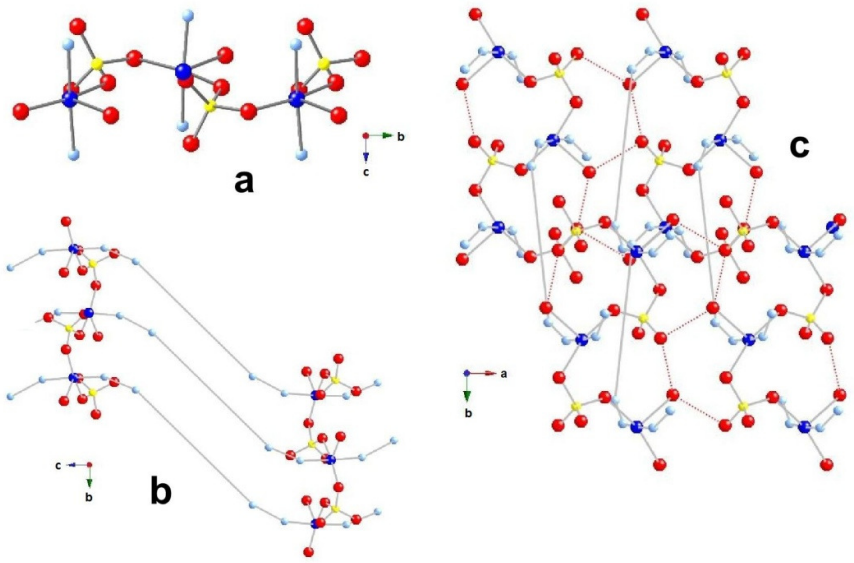

Figure 3.15: (a) The $CuSO_4$ 1D inorganic chain observed in $(C_{18}H_{14}N_4)CuSO_4 \cdot H_2O$, **13**. (Cu = dark blue; N = light blue; O = red); (b) The 2D hybrid structure sheet constructed from $CuSO_4$ chains and BIB ligands. For clarity, BIB ligands are shown as N-N-N-N lines; (c) The 3D structure of **13**, with hydrogen bonds shown as dashed lines.

$(C_{18}H_{14}N_4)_3Ni_3(H_2PO_4)_2(HPO_4)_2 \cdot 4H_2O$, **14**.

In hybrid structure **14** there are two crystallographically independent Ni^{2+} centers, both of which have octahedral coordination geometry (Figure 3.16a). Atom Ni1 is coordinated to two nitrogen atoms from two separate BIB molecules (N1-Ni1 2.083(3) Å, N3-Ni1 2.097(3) Å), three oxygen atoms from two partially deprotonated phosphoric acid molecules ($H_2PO_4^-$ and HPO_4^{2-}) (Ni1-O1 2.140(2) Å, O1-Ni1 2.084(2) Å, O6-Ni1 2.049(2) Å), and one water molecule (O5-Ni1 2.093(2) Å). Adjacent Ni1 atoms are bridged by two $H_2PO_4^-$ entities. The Ni1-Ni1 distance is 3.1574(8) Å, which is considerably greater than twice the ionic radius of Ni^{2+} (1.66Å),[16] indicating the absence of any Ni1-Ni1 bonding interaction. The $[Ni_2(H_2PO_4)_2]^{2+}$ units are connected to the second symmetry independent nickel ion (Ni2) via HPO_4^{2-} dianions (Ni2-O7 2.039(2) Å), generating a charge neutral inorganic chain (Figure 3.16b). The nickel ion Ni2 is also bound to two nitrogen atoms from two different BIB

ligands (N5-Ni2 2.073(2) Å), and two water molecules (Ni2-O10 2.128(2) Å) (Fig.16a). Neighboring chains are linked by BIB ligands to form 2D hybrid sheets (Figure 3.17). These 2D sheets are hydrogen bonded to each other to form a 3D network (Table 3.1). The 2D sheets are in an AAA stacking arrangement, where the distance between neighboring sheets is approximately 7.9 Å.

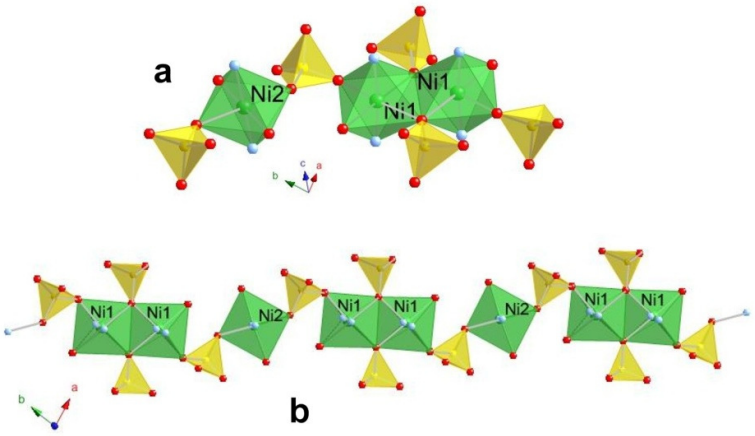

Figure 3.16: (a) A diagram showing the two Ni^{2+} environments observed in hybrid structure $(C_{18}H_{14}N_4)_3Ni_3(H_2PO_4)_2(HPO_4)_2{\cdot}4H_2O$, **14**; (b) A 1D inorganic chain seen in **14**.

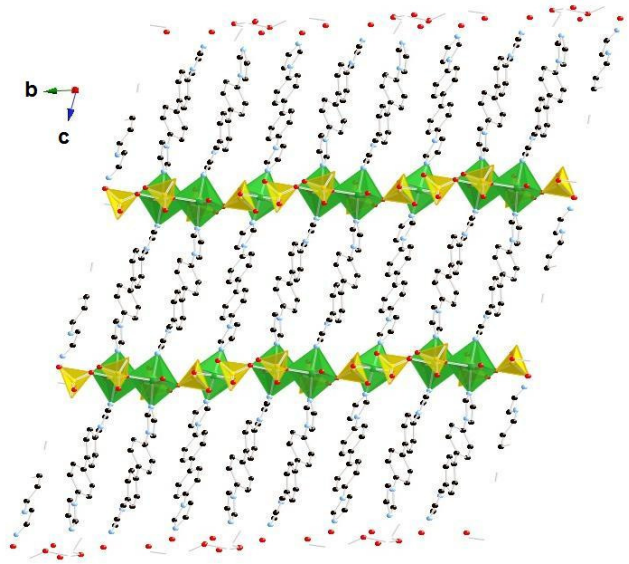

Figure 3.17: The 2D sheet seen in hybrid structure **14**.

$(C_{18}H_{14}N_4)_2Ni(H_2PO_3)_2$, **15**.

In hybrid structure **15** the Ni^{2+} ions have octahedral coordination geometry, the equatorial positions are occupied by nitrogen atoms from four separate BIB ligands (N1-Ni1 2.092(2) Å, N3-Ni1 2.087(2) Å), and two oxygen atoms from two different H_3PO_3 molecules situated at the axial positions (O1-Ni1 2.072(2) Å) (Figure 3.18). The BIB ligands link the $Ni(H_2PO_3)_2$ units to form 2D hybrid sheets (Figure 3.19 and 3.20). $H_2PO_3^-$ anions in adjacent sheets are hydrogen bonded to each other to form a 3D hybrid structure (Table 3.1). Within the 3D hydrogen bonded network there are diamond shaped 'voids', with an edge length of 17.8 Å (Figure 3. 20). However, the structure are interdigitated within the crystal structure, and consequently these spaces are filled (Figure 3.21). If one were to imagine the hydrogen bond between the 2D hybrid layers being replaced by covalent chemical bonds, then the crystal structure observed for **15** is reminiscent of a three-fold interpenetrated framework.

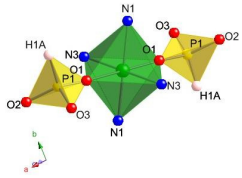

Figure 3.18: The inorganic units observed in complex **15** showing the octahedral geometry of the Ni^{2+} ion.

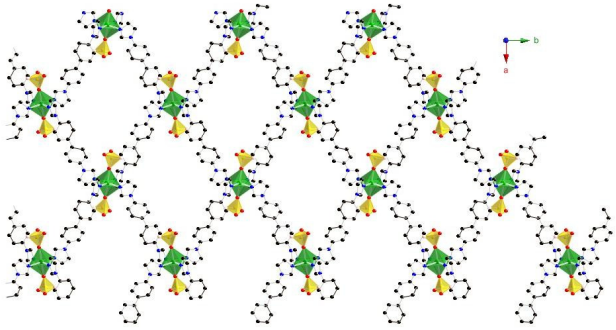

Figure 3.19: Diagram showing the BIB ligands linking the $Ni(H_2PO_3)_2$ units within hybrid structure **15** to form 2D hybrid sheets that lay parallel to the crystallographic *ab*-plane.

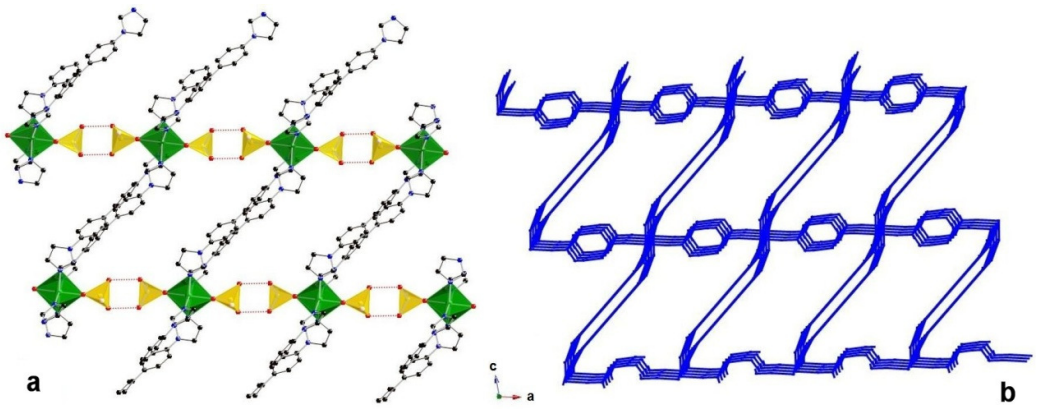

Figure 3.20: (a) A side-on view of 2D hybrid sheet seen in hybrid structure $(C_{18}H_{14}N_4)_2Ni(H_2PO_3)_2$ (**15**) demonstrating how hydrogen bonds (shown as dashed lines) link the sheet; (b) schematic representation of the hybrid sheets shown in (a).

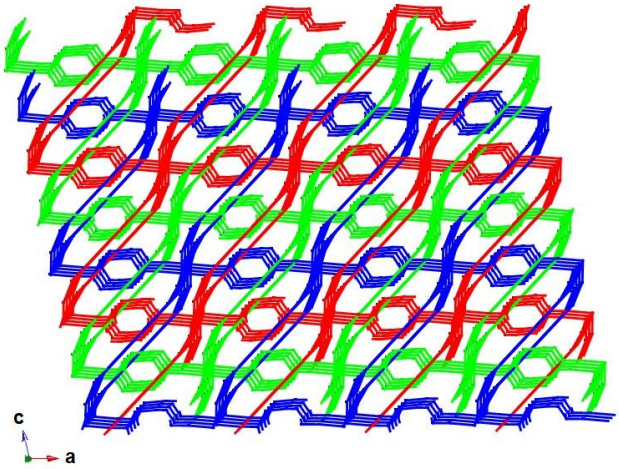

Figure 3.21: Schematic showing the three interdigitated networks in hybrid network **15**.

Table 3.1: Hydrogen bond information for hybrid structures **11**, **12**, **13**, **14**, and **15**.

Complex	**Hydrogen bond**	**d(D-H) (Å)**	**d(H···A) (Å)**	**d(D···A) (Å)**	**<(DHA) (°)**
11	O9-H9A···O9^{ix}	0.823(18)	1.36(3)	1.894(8)	118(3)
	O4-H4···O6^{xi}	0.797(17)	1.904(18)	2.700(2)	176(3)
	O10-H10B···O3^{xii}	0.842(18)	1.811(19)	2.636(3)	166(3)

	O10-H10A···O13^{x}	0.801(17)	2.160(19)	2.952(6)	170(3)
	O8-H8···O10^{vii}	0.801(17)	1.844(19)	2.631(3)	167(3)
12	O2-H2A···O8^{xiii}	0.84^{a}	1.82^{a}	2.646(3)	167^{a}
	O6-H6A···O1^{xiv}	0.84^{a}	1.86^{a}	2.609(3)	146.9^{a}
	O12-H12A···O15^{xiv}	0.84^{a}	2.07^{a}	2.595(3)	120.1^{a}
	O12-H12A···O13^{xiv}	0.84^{a}	2.55^{a}	3.291(4)	147^{a}
	O12-H12A···N11^{xiv}	0.84^{a}	2.65^{a}	3.297(4)	135.3^{a}
	O7-H7A···O16^{xv}	0.84^{a}	2.626(3)	2.626(3)	152.1^{a}
	O16-H16A···O12^{xv}	0.818(17)	2.264(18)	3.297(4)	154(3)
	O11-H11A···O5	0.84^{a}	2.02^{a}	3.020(4)	155.4^{a}
	O11-H11A···O6	0.84^{a}	2.59^{a}	3.137(3)	123.6^{a}
	O16-H16B···O14	0.884(17)	1.883(18)	2.715(4)	156(3)
13	O5-H5A···O4^{i}	0.81(3)	2.06(3)	2.829(3)	158(3)
	O5-H5A···O1^{i}	0.81(3)	2.53(3)	3.166(3)	136(3)
	O5-H5A···S1^{i}	0.81(3)	2.81(3)	3.605(2)	166(3)
	O5-H5B···O4^{ii}	0.91(3)	1.96(3)	2.865(3)	174(3)
	O5-H5B···S1^{ii}	0.91(3)	2.87(3)	3.656(3)	146(2)
14	O9-H9A···O8^{iii}	0.80(2)	1.67(2)	2.458(3)	169(4)
	O10-H1A···O8^{iv}	0.84(2)	1.81(2)	2.636(3)	166(3)
	O10-H1B···O4^{v}	0.85(2)	2.24(2)	3.081(3)	170(3)
	O2-H2A···O3^{v}	0.79(2)	1.81(2)	2.599(3)	172(4)
	O4-H4A···O6^{vi}	0.82(2)	1.70(2)	2.515(3)	173(3)
	O5-H5A···O7	0.86(2)	1.77(2)	2.609(3)	166(3)
	O5-H5B···O3^{vi}	0.82(2)	2.07(2)	2.887(3)	172(3)
15	O3-H3A···O2^{iii}	0.84	1.80	2.603(3)	160.1

Symmetry codes:

(i) -x+1,y+1/2,-z+3/2; (ii) x,y+1,z; (iii) -x+1,-y,-z; (iv) -x,-y,-z; (v) -x,-y-1,-z; (vi) -x+1,-y-1,-z; (vii) x-1,y,z-1; (viii) x+1,y,z+1; (ix) -x+1,-y+2,-z; (x) -x+1,-y+1,-z+1; (xi) -x,-y+2,-z; (xii) -x+1,-y+2,-z+1; (xiii) -x-1, -y, -z; (xiv) x-1, y, z; (xv) -x, -y+1, -z+1.

[a] No esd is given because the hydrogen-bond positions in these compounds were calculated and not refined.

Crystallography

Data for all complexes were collected on an Oxford Diffraction Gemini diffractometer at 100K with Mo Kα radiation (λ = 0.71073 Å). All data processing was performed using CrysAlisPro, and structural solutions and refinements were conducted with SHELX via the WinGX graphical interface software.[117, 119, 144] Structural solutions were obtained by direct methods, and refinement performed on F^2 by least-squares techniques. All non-hydrogen atoms were refined anisotropically. Hydrogen atoms on the BIB ligands are placed at calculated positions. Hydrogen atoms associated with $H_2PO_4^-$ and HPO_4^{2-} groups (hybrid structures **11**, 1**2** and **15**), HPO_3^{2-} (hybrid structure **14**), NO_3^- (hybrid structures **11** and **12**), SO_4^{2-} (hybrid structure **13**) and bound water molecules (hybrid structures **11**, **12**, **13** and **15**), were located in the difference Fourier maps and are restrained to chemically reasonable positions. A summary of all crystallographic data is given in Table 3.2.

Table 3.2: Crystal data and structure refinement parameters for BIB and **11-15**.

	BIB	**11**
Empirical formula	$C_{18}H_{16}N_4O$	$C_{72}H_{67}N_{17}O_{22}P_4Cu_4$
M_w	304.35	1900.47
T/K	100	100
Space group	C*2/c*	P-*1*
a/Å	20.6024(1)	10.987(1)
b/Å	9.3996(6)	11.1631(9)
c/Å	8.3612(5)	15.902(2)

α/degree	90	103.393(8)
β/degree	111.766(6)	100.277(8)
γ/degree	90	104.714(8)
V/Å^3	1503.7(2)	1775.8(3)
Z	4	1
μ/mm^{-1}	0.087	1.367
R1[a][I>2σ(I)]	0.0507	0.0447
wR2[b][I>2σ(I)]	0.1050	0.1154

	12	**13**
Empirical formula	$C_{90}H_{84}N_{22}O_{32}P_6Cu_5$	$C_{18}H_{16}N_4O_5SCu$
M_w	2489.31	463.95
T/K	100	100
Space group	P-*1*	P$2_12_12_1$ Flack = -0.002(10)
a/Å	10.5206(5)	7.4490(5)
b/Å	13.7206(6)	7.7741(6)
c/Å	17.5966(5)	29.3227(19)
α/degree	101.118(3)	90
β/degree	98.242(4)	90
γ/degree	107.119(4)	90
V/Å^3	2327.0(2)	1698.1(2)
Z	1	4
μ/mm^{-1}	1.329	1.453
R1[a][I>2σ(I)]	0.0416	0.0312
wR2[b][I>2σ(I)]	0.1042	0.428

	14	**15**

Empirical formula	$C_{54}H_{56}N_{12}O_2P_4Ni_3$	$C_{36}H_{32}N_8O_6P_2Ni$
M_w	1493.12	793.33
T/K	100	100
Space group	P-*1*	P$2_1/c$
a/Å	8.7639(3)	10.9865(6)
b/Å	12.3703(4)	17.9797(11)
c/Å	14.1822(4)	8.7605(6)
α/degree	72.026(3)	90
β/degree	82.868(2)	101.706(6)
γ/degree	79.364(3)	90
V/Å^3	1433.77(8)	1691.73(18)
Z	1	2
μ/mm^{-1}	1.178	0.73
R1[a][I>2σ(I)]	0.0400	0.0368
*w*R2[b][I>2σ(I)]	0.0808	0.0690

[a]$R1 = \Sigma \, ||F_o| - |F_c|| / \Sigma |F_o|$. [b]$wR2 = \{\Sigma[w(F_o^2 - F_c^2)^2] / \Sigma[w(F_o^2)^2]\}^{1/2}$,

where $w = 1/[\sigma^2(F_o)^2 + (aP)^2 + bP]$, $P = [(F_o)^2 + 2(F_c)^2]/3$.

3.6 Motifs and coordination environment about metal ions in Hybrid structure series **II**

Hybrid structure series **I** has some structural motifs that are shared by more than one crystal structure. The major reason for this result is the similar starting materials that were used for synthesizing these hybrid structures. The starting materials for hybrid structure **I** include: zinc metal ions (Zn^{2+}), TMDP ligand, inorganic acid (H_3PO_3), and water. Reaction variables included temperature, pH value, and template molecules. Compared to hybrid structure series **I**, the starting materials of hybrid structure series **II** were different for each network which created a variety of different motifs and coordination environments in these

network structures.

Both **11** and **12** are prepared by the same hydrothermal method except that the pH value was different for the reaction solutions. Sodium hydroxide was used in the synthesis of **12** to increase the pH value from 3.0 to 4.5. In crystal structures **11** and **12**, a similar copper 8 ring motif is observed. The first, **11**, consists of a novel cationic copper phosphate 8-ring (Scheme 3.6A) composed of four copper atoms and four phosphate groups that encapsulate an hydroxide ion; these are linked into chains by four parallel BIB groups. This structure is the first in which isolated copper 8-rings form nodes in a network solid. The second structure, **12**, is formed at higher pH, and is similarly constructed from copper phosphate 8-rings with tails (Scheme 3.6B) that are further linked into inorganic chains by the "fusion" of 8-rings at one of the copper sites. These chains, in turn, are linked into a three dimensional cationic network by the bridging ligand. The structures demonstrate the tendency of the BIB ligand to support the formation of cationic frameworks[145] with extra framework anions to balance the charge.

Hybrid structure **13** contains an inorganic chain (Scheme 3.6C) which is constructed by $CuSO_4$ compound. In the synthesis, no H_3PO_3 or H_3PO_4 was added to the reaction solution; SO_4^{2-} acted as a bridging unit in this network. All these inorganic chains are linked by BIB ligands to form a hybrid structure.

Both hybrid structures **14** and **15** are synthesized from the same starting materials except for the inorganic acid. The addition of H_3PO_3 to the reaction solution yields complex **15**, in which there is a single Ni^{2+} coordination environment within the inorganic chain, and the crystal structure is composed of three interdigitated networks. Yet, if H_3PO_4 is employed in the reaction, complex **14** results in which the inorganic chains exhibit two distinct Ni^{2+} coordination environments (Figure 3.20 and Scheme 3.6D). Consequently, these chains cross-link in a manner dissimilar to **15**, resulting in 2D hybrid sheets with a different topology (Figures 3.21, 3.23 and Scheme 3.6E). The smaller 'holes' in the sheet structures in **14** with respect to those in **15** prevents network interdigitation.

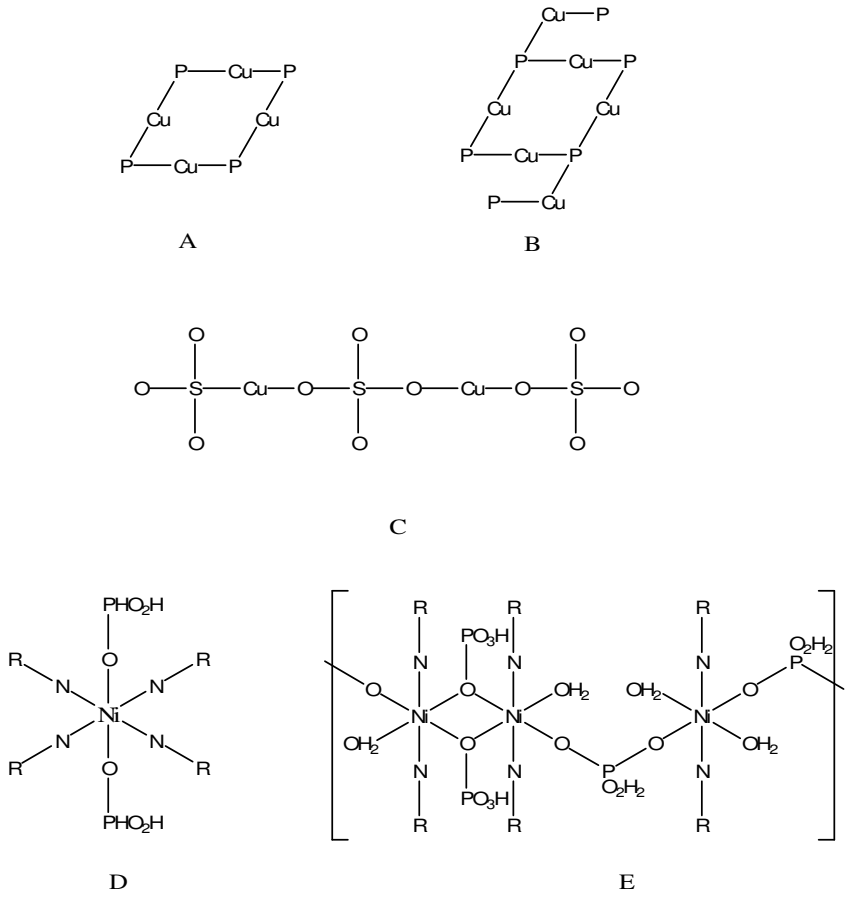

Scheme 3.6: A) Copper 8 ring in hybrid structure **11**. B) Copper 8 ring with tails in hybrid structure **12**. C) $CuSO_4$ chain in hybrid structure **13**. D) Single coordination environment of Ni(II) ions in hybrid structure **15**. E) The Ni(II) coordination environment in hybrid structure **14**.

3.7 Magnetic measurement of hybrid structure **11** and **12** in series **II**

The ambiguity in the determining the oxidation state in **11** by crystallography alone necessitated an investigation of the magnetic behavior of the copper in this compound. Figure 26 and 27 show plots of χT and χ^{-1} vs T for both **11** (Figure 3.22) and **12** (Figure 3.23). The respective g-values are 2.38 and 2.29. These values are consistent with only copper(II) present in both compounds. As indicated above, the presence of copper(II) requires two

additional protons to be included in the refinement of **11**. At very low temperature in **11** the upswing in the plot of χT may indicate a slight ferromagnetic coupling. There is no significant magnetic coupling between copper sites in **12** even though there is a relatively short contact between two of the copper ions in this structure.

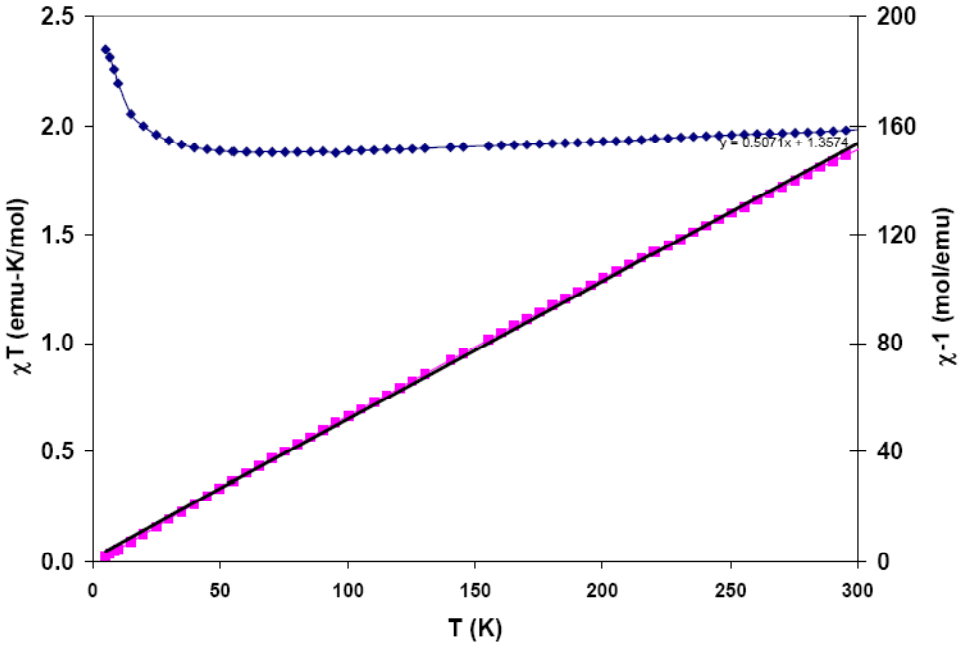

Figure 3.22: Plots of χT and χ^{-1} vs T for hybrid structure **11**. χT = 1.97 emu-K/mol for four copper ions. g_{ave} = 2.29. There may be slight evidence for ferromagnetic coupling at low temperature.

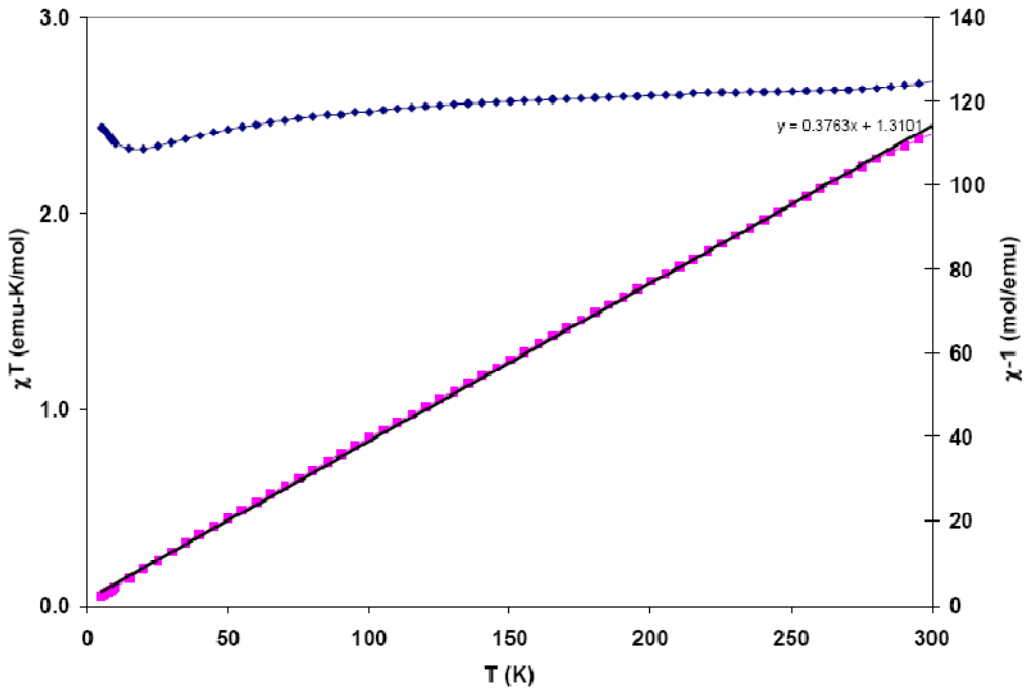

Figure 3.23: Plots for χT and χ^{-1} vs T for hybrid structure **12**. $\chi T = 0.53$ for five copper ions. $g_{ave} = 2.38$.

3.8 Summary of hybrid structure series **II**

The synthesis and structural characterization of five hybrid structure were reported incorporating the rigid ligand BIB. From the study of hybrid structure series **II**, it can be concluded that BIB ligand has propensity to coordinate with Cu(II) and Ni(II) ions to construct hybrid structures displaying topological diversity.

Chapter 4

Other Hybrid Networks

4.1 Background

It has been demonstrated that hybrid networks can be synthesized to form appropriate building blocks by metal-ligand coordination.[13] Further, a wide variety of organic bridging ligands can be utilized in hybrid network synthesis. We have successfully prepared a series of 4, 4'-trimethylenedipyridine (TMDP) and 4, 4'-bisimidazolybiphenyl (BIB) hybrid networks. In addition, we have explored many other ligands, includes 1, 2, 4-triazole, picolinic acid (2-pyridinecarboxylate), 4-(2-(1H-imidazol-1-yl)ethyl)pyridine, tartaric acid and terephthalic acid (Scheme 4.1). Hybrid network structures incorporating these ligands are discussed in this chapter.

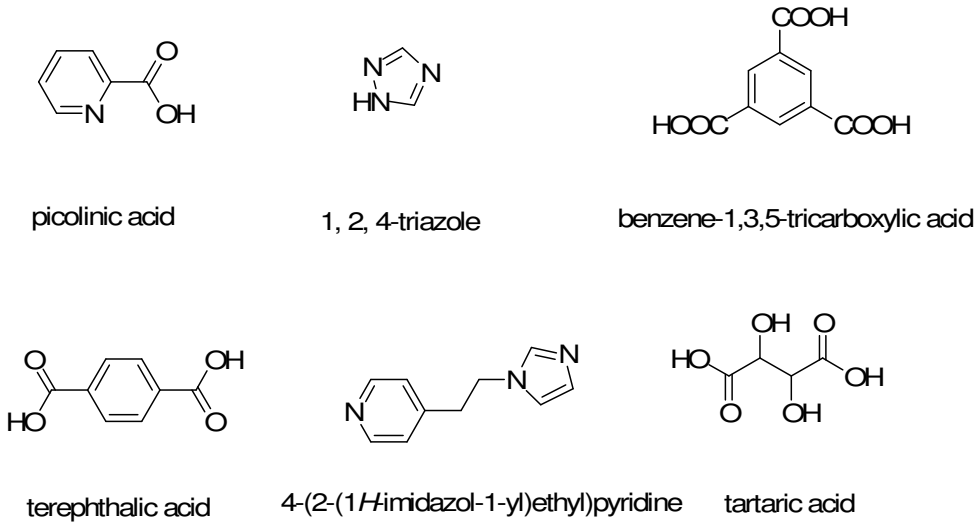

Scheme 4.1: Ligands used in the formation of hybrid networks reported in this chapter.

4.2 Experimental Section

All commercially available chemicals are reagent grade and used as received without further purification. Thermogravimetric measurements were performed on TGA Q500 thermal analyzer under following N_2 with the heating rate of 10°C min^{-1}. TGA traces for the hybrid networks are included in the Supporting Material. Diffraction data for hybrid networks were collected on an Oxford Diffraction Gemini diffractometer at 100K/293K with Mo K_α radiation (λ = 0.71073 Å). All data processing was performed using CrysAlisPro, and structural solutions and refinements were conducted SHELX via WinGx graphical interface software.[117, 119, 144] Structural solutions were obtained by direct methods, and refinement performed on F^2 by least-squares techniques. All non-hydrogen atoms were refined anisotropically. A summary of all crystallographic data is given in Table 4.1.

Table 4.1: Crystal data and structure refinement parameters for **16-20**.

	16	**17**
Empirical formula	$C_6H_6NO_3Cu_{0.5}$	$C_{40}H_{28}N_6O_{24}Zn_5$
M_w	171.89	1367.63
T/K	293	293
Space group	P-*1*	P2_1/*c*
a/Å	5.1029(17)	8.6985(15)
b/Å	7.5333(11)	13.039(3)
c/Å	9.1037(12)	19.187(5)
α/degree	76.002(12)	90
β/degree	85.149(11)	94.08(2)
γ/degree	72.267(13)	90
V/$Å^3$	323.41(8)	1691.73(18)
Z	1	2

μ/mm^{-1}	1.719	2.838
R1[a][I>2σ(I)]	0.0306	0.0332
*w*R2[b][I>2σ(I)]	0.0731	0.0823

	18	**19**
Empirical formula	$C_{14}H_{15}N_9O_6Zn_2$	$C_{20}H_{24}N_8O_7Cu$
M_w	536.09	552.01
T/K	100	293
Space group	C*2/c*	C*c*
a/Å	12.2878(8)	14.2015(4)
b/Å	24.2101(9)	9.9216(3)
c/Å	7.7879(5)	17.3455(5)
α/degree	90	90
β/degree	125.342(10)	111.983(3)
γ/degree	90	90
V/Å^3	1889.86(19)	2266.32(11)
Z	4	4
μ/mm^{-1}	2.595	1.025
R1[a][I>2σ(I)]	0.0589	0.0437
*w*R2[b][I>2σ(I)]	0.1235	0.1101

	20
Empirical formula	$C_4H_4O_6Na_2$
M_w	194.05
T/K	293
Space group	P*bca*
a/Å	10.1187(6)
b/Å	10.0093(6)

c/Å	13.0688(9)
α/degree	90
β/degree	90
γ/degree	90
V/Å^3	1323.62(14)
Z	8
μ/mm^{-1}	0.287
R1[a][I>2σ(I)]	0.0252
wR2[b][I>2σ(I)]	0.0686

[a]$R1 = \Sigma \, ||F_o| - |F_c|| / \Sigma |F_o|$. [b]$wR2 = \{\Sigma[w(F_o^2 - F_c^2)^2] / \Sigma[w(F_o^2)^2]\}^{1/2}$,

where $w = 1/[\sigma^2(F_o)^2 + (aP)^2 + bP]$, $P = [(F_o)^2 + 2(F_c)^2]/3$.

4.3 Hybrid network $(C_6H_4NO_2)Cu_{0.5}H_2O$, **16** constructed from 2-pyridinecarboxylate (PYCA)

Pyridine with addtional functional groups is commonly used in hybrid network construction. The ligand, 2-pyridinecarboxylate has been reported in some metal complexes.[146-148] However, so far this ligand has not been used in hybrid network constructions. Huang et al. reported a complex $(Et_4N)[MnCl_2(PYCA)_2]$, in which the PYCA ligand coordinates to the Mn^{3+} ion forming a chelating five-membered ring (Figure 4.1).[149]

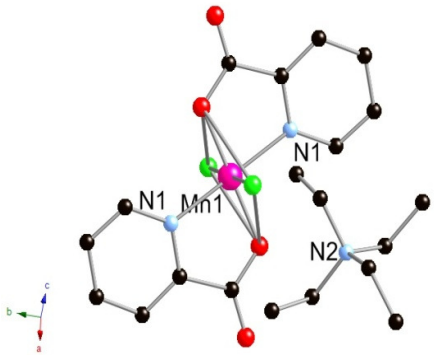

Figure 4.1: The metal complex of $(Et_4N)[MnCl_2(PYCA)_2]$.[149]

Synthesis of hybrid network $(C_6H_4NO_2)Cu_{0.5}•H_2O$, **16.**

$(C_6H_4NO_2)Cu_{0.5}•H_2O$, **16**: Copper nitrate tetrahydrate (242.0 mg, 1.0 mmol), 1,2-bis(2-pyridyl)-ethylene (182.2 mg, 1.0 mmol), phosphoric acid (85 wt. % aqueous solution, 230.6 mg, 2.0 mmol), and 6 mL water were added to a Teflon-line steel antoclave. The mixture was heated at 150°C for 3 days, cooled down to room temperature, filtered and washed with deionized water. Blue crystals were obtained. Yield: approximately 80% based on Cu(II).

In the hydrothermal synthesis of hybrid network $(C_6H_4NO_2)Cu_{0.5}•H_2O$, 1,2-bis(2-pyridyl)-ethylene was oxidized by the phosphoric acid. The product of this reaction is 2-pyridinecarboxylate (picolinic acid), which acts as the bridging ligand in the hybrid network that is formed. In some cases the starting materials are oxidized by nitrate in the reaction mixture.

Crystal Structure hybrid network $(C_6H_4NO_2)Cu_{0.5}•H_2O$, **16.**

Hybrid network $(C_6H_4NO_2)Cu_{0.5}•H_2O$ crystallized in the triclinic space group *P*-1. The asymmetric unit contains an octahedral Cu^{2+} ion that is bound to two nitrogen atoms from two different ligands (Cu1-N1 1.9643(14) Å), four oxygen atoms from four different PYCA ligands (Cu1-O1 1.9643(11) Å, Cu1-O2 2.6955(11) Å) (Figure 4.2A). Each PYCA ligand has three coordination sites: two oxygen atoms of the carboxylate group, and one nitrogen atom of the pyridyl group. One of the oxygen atoms and one nitrogen atom coordinate to one Cu^{2+} ion, and the other oxygen atom coordinate to an adjacent Cu^{2+} ion. The distance between neighboring Cu^{2+} ions is 5.103 Å. Two PYCA ligands in each unit coordinate to the Cu^{2+} center in the *trans* manner with the pyridyl nitrogen atoms and the carboxylic oxygen atoms being in the *trans* position with respect to each other (Figure 4.2B). Thus the PYCA ligand bridges the metal centers to form a 1D hybrid chain (Figure 4.2C). Hydrogen bonds between the carboxylate group of the PYCA ligand and the coordinated H_2O molecule connect

neighboring 1D hybrid chains to form 2D sheets (Figure 4.3) in the crystal structure. Hydrogen bonding parameters are given in Table 4.2.

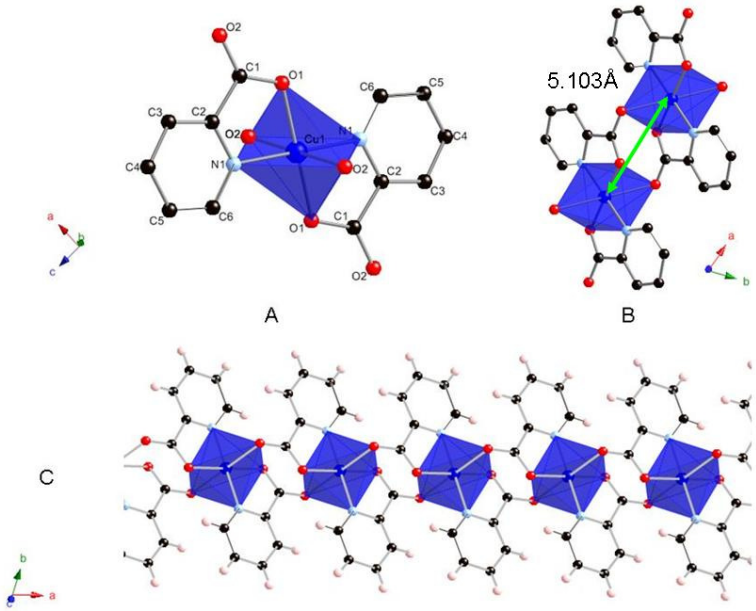

Figure 4.2: Crystal structure of $(C_6H_4NO_2)Cu_{0.5}•H_2O$, **16**. A). Coordination environment of the Cu^{2+} ion (Cu = dark blue; N = light blue; O = red). B) One unit of $(C_6H_4NO_2)Cu_{0.5}•H_2O$. C) The 1D hybrid chain seen in the hybrid network.

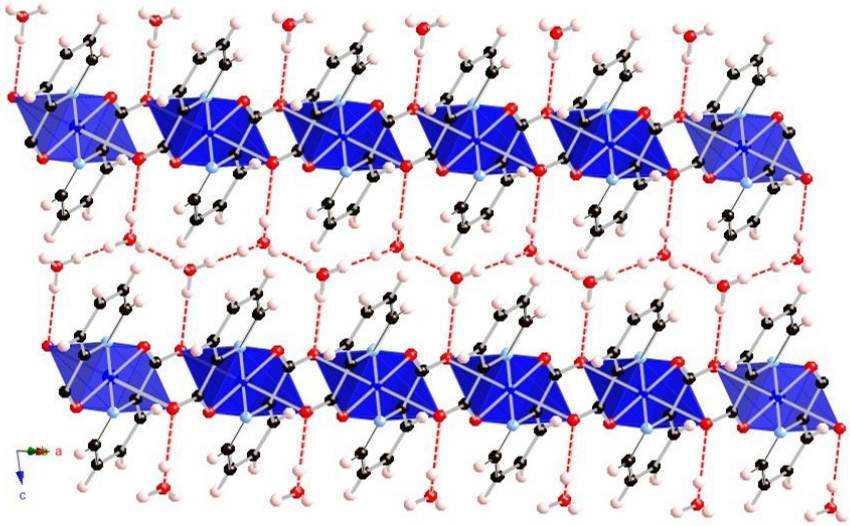

Figure 4.3: The 2D structure of $(C_6H_4NO_2)Cu_{0.5}•H_2O$, **16** with hydrogen bonds shown as red dash lines.

Table 4.2: Hydrogen bonds for hybrid network $(C_6H_4NO_2)Cu_{0.5}•H_2O$, **16** [Å and °].

D-H...A	d(D-H)	d(H...A)	d(D...A)	<(DHA)
O(3)-H(3B)...O(3)^{i}	0.95	2.04	2.830(3)	139.9
O(3)-H(3C)...O(3)^{ii}	0.80	2.01	2.805(3)	172.2
O(3)-H(3A)...O(2)	0.79	2.13	2.9062(19)	168.9

Symmetry codes:

i: -x+1,-y,-z-1; ii: -x+2,-y,-z-1.

4.3 Hybrid network $(C_2H_2N_3)_2(C_9H_4O_6)_4Zn_5•4H_2O$ (**17**) and $(C_2H_2N_3)_2(C_2H_3N_3)(C_8H_4O_4)Zn_2•2H_2O$ (**18**)

The 1,2,4-triazole ligand is one of the smallest and simplest organic bridging ligands used in network construction. The 1,2,4-triazole ligand can act as a neutral bridging ligand which bonds to two metal ions, or as an anionic bridging ligand that bonds to up to three metal centers (Scheme 4.2). Furthermore, the triazole ligand can combine with other inorganic or organic compounds and act as a building unit in the formation of hybrid networks.[150]

Scheme 4.2:Two-coordinated and three-coordinated triazoles.

Ouellette et al. reported a series of hybrid network structures containing the triazole

ligand.[150] The 3D hybrid network Zn(1,2,4-triazole)$_2$ contains tetrahedrally coordinated Zn(II) ions.[150] Each Zn(II) is bonding to two N atoms from four different triazole ligands (Figure 4.4).[150] The 1,2,4-triazole bridges to two Zn^{2+} ions, the N2 atom is not bonded to any Zn^{2+} ions. Another crystal structure reported by these authors is Zn(1,2,4-triazole)Br, which is 2D hybrid network.[150] Each Zn^{2+} center bonds to three nitrogen atoms from three different triazolate ligands and a terminal bromine ligand. All three nitrogen sites on the triazolate bond to metal ions (Figure 4.5).[150] The triazole ligands have different coordination numbers in these two structures.

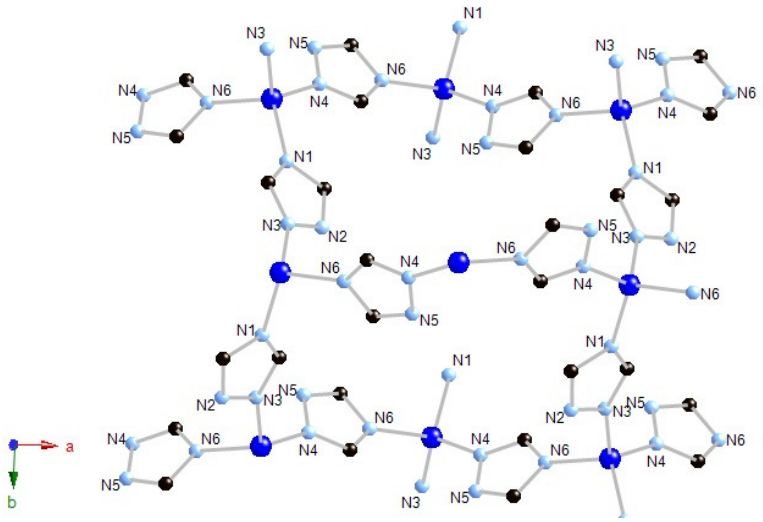

Figure 4.4. Hybrid network Zn(1,2,4-triazole)$_2$ (Zn is in dark blue).[150]

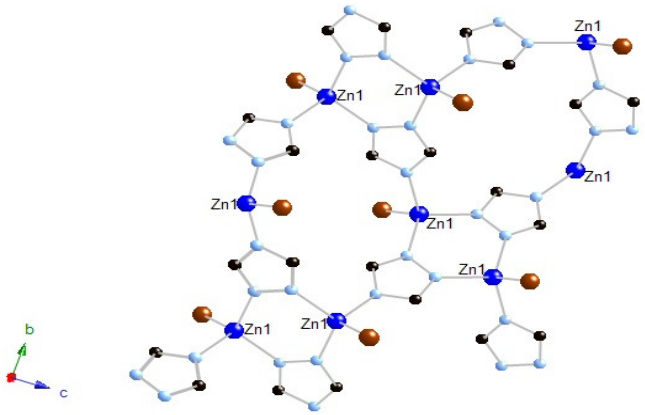

Figure 4.5. 2D hybrid network Zn(1,2,4-triazole)Br (Zn is in dark blue).[150]

We synthesized two 3D hybrid networks that contain the 1,2,4-triazole ligand, $(C_2H_2N_3)_2(C_9H_4O_6)_4Zn_5•4H_2O$, **17** and $(C_2H_2N_3)_2(C_2H_3N_3)(C_8H_4O_4)Zn_2•2H_2O$, **18**. These two hybrid network structures **17** and **18** contain the same 1,2,4-triazole ligand. The triazole ligand is three coordinated in hybrid network **17**, and two/three mixed coordinated in **18**. The steric effects between neighboring N atoms on the triazole ligands is not strong enough to avoid coordination bond formation. Furthermore, triazole ligand can coordinate with metal ions in the presence of co-ligands such as benzene carboxylate. Other co-ligands can be used to design and synthesize more hybrid network structures.

Synthesis of hybrid network **17** and **18**

$(C_2H_2N_3)_2(C_9H_4O_6)_4Zn_5•4H_2O$, 17: Zinc acetate dihydrate (219.5 mg, 1.0 mmol), 1,2,4-triazole (138.1 mg, 2.0 mmol), 1,3,5-tricarboxylic acid (210.1 mg, 1.0 mmol), and 6 mL water were added to a Teflon-line steel antoclave. The mixture was heated at 180°C for 3 days, cooled down to room temperature, filtered and washed with deionized water. Colorless crystals were obtained. Yield: approximately 60% based on Zn(II).

$(C_2H_2N_3)_2(C_2H_3N_3)(C_8H_4O_4)Zn_2•2H_2O$, 18: Zinc acetate dihydrate (219.5 mg, 1 mmol), 1,2,4-triazole (138.1 mg, 2.0 mmol), terephthalic acid (166.1 mg, 1.0 mmol), and 6 mL water were added to a Teflon-line steel antoclave. The mixture was heated at 150°C for 3 days, cooled down to room temperature, filtered and washed with deionized water. Colorless crystals were obtained. Yield: approximately 50% based on Zn(II).

Crystal structure of hybrid networks **17** and **18**

Hybrid network structure $(C_2H_2N_3)_2(C_9H_4O_6)_4Zn_5•4H_2O$ (**17**) contains three different coordination geometries for the Zn^{2+} ions (Figure 4.6). The Zn1 ion has octahedral geometry, four water molecules are located in the equatorial positions (Zn1-O13 2.158(3) Å,

Zn1-O14 2.068(2) Å), two oxygen atoms from two different carboxylates are at the axial positions (Zn1-O2 2.061(2) Å). The second coordination geometry for the Zn^{2+} ion is tetrahedral. The Zn2 ion is bound to three oxygen atoms from three different carboxylate groups (Zn2-O1 2.005(2) Å, Zn2-O8 2.005(2) Å, Zn2-O10 1.938 Å), and one nitrogen atom from a triazole ligand (Zn2-N2 2.006(3) Å). The Zn3 ion has distorted trigonal bipyramidal geometry. The Zn3 is bonded to two nitrogen atoms from two different triazole ligands (Zn3-N1 2.011(3) Å, Zn3-N3 2.032(2) Å), two oxygen atoms from the same carboxylate (Zn3-O3 2.073 Å, Zn3-O4 2.271(2) Å), and another oxygen from a different carboxylate (Zn3-O7 2.003(2) Å). The triazole ligand is three coordinated in this crystal structure. The size effect does not forbid the coordination bond formation between the nitrogen atom and metal ion. Two triazole ligands coordinate to two Zn ions in *trans* positions to form a ring in which the distance between the two Zn^{2+} ions is 3.812 Å. The organic acid, 1,3,5-tricarboxylate benzene acts as co-ligand in the crystal structure. One of the carboxylate groups is deprotonated and coordinates to the same Zn3 ion to form distorted trigonal bipyramidal geometry. The second deprotonated carboxylate group coordinates to two Zn1 and Zn2 ions, respectively. The third carboxyale group retains its hydrogen atom. The Zn^{2+} ions, triazole ligands, and 1,3,5-tricarboxylate benzene form 2D hybrid sheets (Figure 4.7). The co-ligand, 1,3,5-tricarboxylate benzene links neighboring 2D sheets to a form a 3D hybrid network (Figure 4.8). Hydrogen bond parameters are given in Table 4.3.

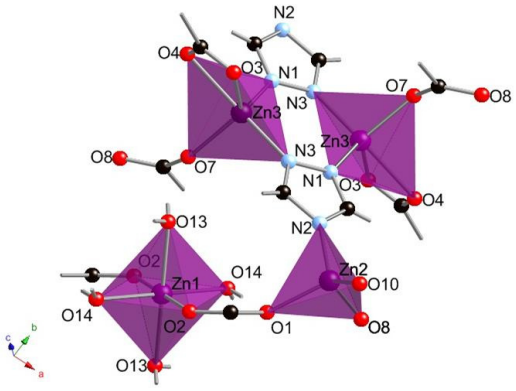

Figure 4.6: Coordination geometries of Zn^{2+} ions in hybrid network $(C_2H_2N_3)_2(C_9H_4O_6)_4Zn_5 \cdot 4H_2O$, **17** (purple = Zn; red = O; light blue = N; black = C).

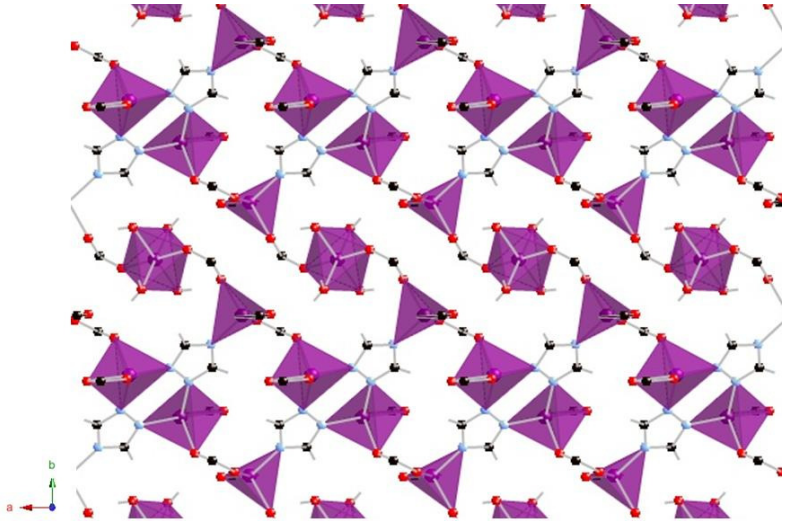

Figure 4.7: The 2D hybrid sheet in hybrid network $(C_2H_2N_3)_2(C_9H_4O_6)_4Zn_5 \bullet 4H_2O$, **17**.

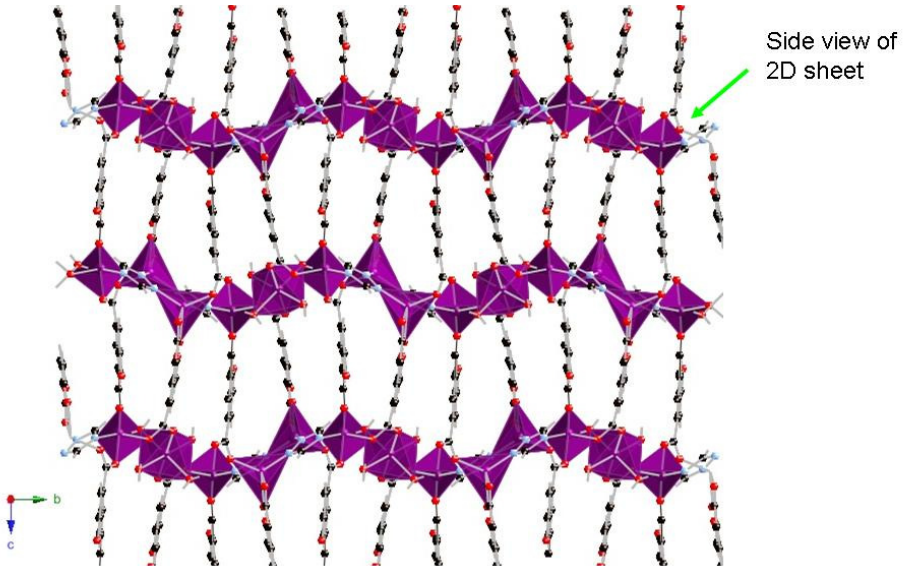

Figure 4.8: The 3D hybrid network $(C_2H_2N_3)_2(C_9H_4O_6)_4Zn_5 \bullet 4H_2O$, **17**.

Table 4.3: Hydrogen bonds for hybrid network $(C_2H_2N_3)_2(C_9H_4O_6)_4Zn_5 \bullet 4H_2O$, **17** [Å and °].

D-H...A	d(D-H)	d(H...A)	d(D...A)	<(DHA)
O(6)-H(6)...O(3)^{i}	0.82	1.89	2.655(3)	154.2

O(12)-H(12)...O(9)[i]	0.82	1.81	2.597(3)	160.7
O(13)-H(13A)...O(10)[ii]	0.813(18)	2.63(4)	3.157(3)	124(3)
O(13)-H(13B)...O(5)[ii]	0.813(19)	2.032(19)	2.839(4)	172(4)
O(14)-H(14B)...O(5)[ii]	0.815(18)	2.18(3)	2.887(4)	145(4)
O(14)-H(14A)...O(1)[iii]	0.817(18)	1.94(2)	2.704(3)	156(4)
O(13)-H(13A)...O(7)	0.813(18)	2.13(2)	2.891(3)	157(4)
O(14)-H(14B)...O(11)[iii]	0.815(18)	2.62(4)	3.133(4)	122(3)

Symmetry codes:

i: x+1,y,z; ii: x-1,y,z; iii: -x+1,-y+2,-z.

The hybrid network $(C_2H_2N_3)_2(C_2H_3N_3)(C_8H_4O_4)Zn_2 \bullet 2H_2O$ (**18**) crystallized in the monoclinic space group *C*2/c. The are two different coordination geometries for the Zn^{2+} ions in the asymmetric unit (Figure 4.9). The Zn1 ion has tetrahedral geometry, and is bound to two nitrogen atoms from two different triazole ligands (Zn1-N2 2.014(6)Å), and two oxygen atoms from two different carboxylates (Zn1-O1 2.030(5) Å). The Zn2 ion has octahedral geometry. All six nitrogen atoms are from six different triazole ligands. The triazole ligand has two different oxidation states in the crystal structure, $(C_2H_2N_3)^-$ and $C_2H_3N_3$. The $(C_2H_2N_3)^-$ anion is three-coordinated, and the neutral molecule $C_2H_3N_3$ molecule is two-coordinated. The dicarboxylate ligand is diprotonated, and acts as a co-ligand in the network construction. Each of acid group available to coordinate only one oxygen atom to the metal. The triazole ligands and Zn^{2+} ions form 2D layers (Figure 4.10). The co-ligand benzene dicarboxylate links ajacent 2D layers to form a 3D hybrid network (Figure 4.11). Hydrogen bonding information is given in Table 4.4.

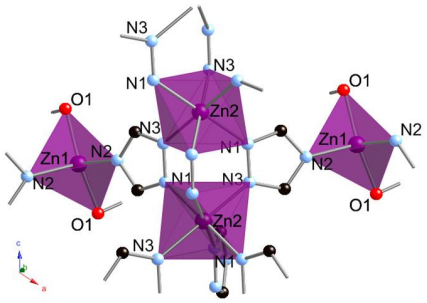

Figure 4.9: The Zn^{2+} coordination geometries in hybrid network $(C_2H_2N_3)_2(C_2H_3N_3)(C_8H_4O_4)Zn_2 \bullet 2H_2O$, **18**.

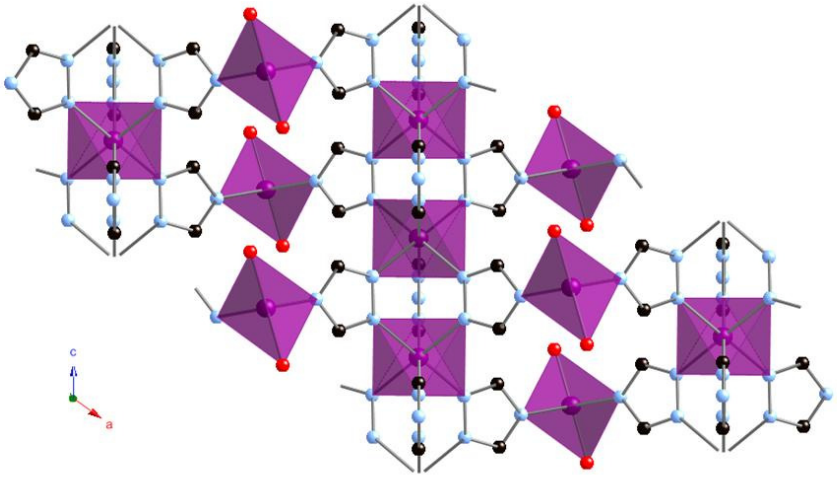

Figure 4.10: The 2D layer in hybrid network $(C_2H_2N_3)_2(C_2H_3N_3)(C_8H_4O_4)Zn_2 \bullet 2H_2O$, **18**.

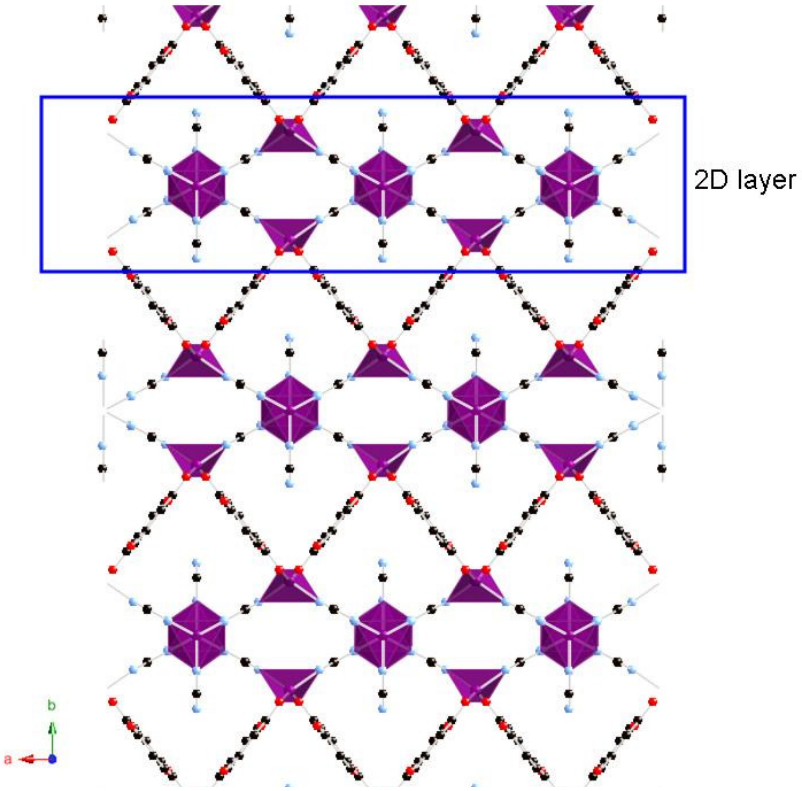

Figure 4.11: The 3D hybrid network $(C_2H_2N_3)_2(C_2H_3N_3)(C_8H_4O_4)Zn_2 \bullet 2H_2O$, **18**.

Table 4.4: Hydrogen bond information for hybrid network $(C_2H_2N_3)_2(C_2H_3N_3)(C_8H_4O_4)Zn_2 \bullet 2H_2O$, **18** [Å and °].

D-H...A	d(D-H)	d(H...A)	d(D...A)	<(DHA)
O(12)-H(12B)...O(2)^{i}	0.85(2)	2.74(15)	3.068(13)	105(11)
O(11)-H(11B)...O(1)	0.83(2)	2.02(4)	2.844(11)	172(24)

Symmetry code:

i: -x+1/2,-y+1/2,-z+1

4.4 Hybrid network $(C_{10}H_{11}N_3)_2Cu(NO_3)_2 \bullet H_2O$, **19.**

Unsymmetric ligand 4-(2-(1H-imidazol-1-yl)ethyl)pyridine

We synthesized an unsymmetric ligand 4-(2-(1H-imidazol-1-yl)ethyl)pyridine (Scheme 4.3) and used this ligand in hybrid network construction.

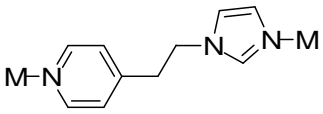

Scheme 4.3: Two coordinated 4-(2-(1H-imidazol-1-yl)ethyl)pyridine ligand.

Experimental section

Preparation of 4-(2-(1H-imidazol-1-yl)ethyl)pyridine ligand (Scheme 4.4)

The starting mixture containing 52.5 g (0.50 mol) of 4-vinylpyridine, 30.6 g (0.45 mol) of imidazole and 1.1 g of glacial acetic acid, this mixture was placed in a round bottom flask, then stirred and heated to a temperature of 130°C under an argon protection, and then maintained at this temperature for 5-6 hours. The mixture was then cool down to room temperature and left to stand overnight. A white solid was obtained. This solid was dissolved in 150 mL methylene dichloride, extracted with charcoal, filtered through Celite and concentrated under vacuum. The crude product was crystallized from a mixture of methylene dichloride and pentane in a 1:2 ratio. A colorless crystalline product was obtained.[151] The yield was approximately 60% based on imidazole. ^{1}H NMR (400 MHz; solvent $CDCl_3$) δ 3.02 (2H, m), 4.22 (2H, m), 6.82 (1H, m), 6.93 (2H, m), 7.04 (1H, m), 7.52 (1H, s), 8.45 (2H, m) (Appendix C).

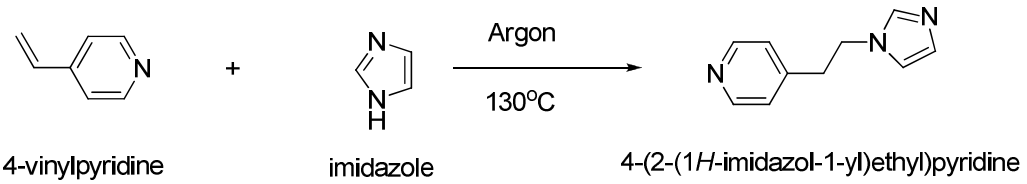

Scheme 4.4: Synthesis of the 4-(2-(1H-imidazol-1-yl)ethyl)pyridine ligand.

Synthesis of hybrid network $(C_{10}H_{11}N_3)_2Cu(NO_3)_2•H_2O$, **19.**

Typically, hydrothermal synthesis is commonly used in hybrid network construction. However, the hybrid network $(C_{10}H_{11}N_3)_2Cu(NO_3)_2•H_2O$, **19** was synthesized *via* an interfaced crystallization method. The reason for this is that the unsymmetric ligand 4-(2-(1H-imidazol-1-yl)ethyl)pyridine decomposes at approximately 120°C. Hydrothermal synthesis is not appropriate for preparing hybrid networks with this ligand because of its low decomposition temperature. However, tnterfacial technique, at room temperature, were successful, and we were able to synthesize this 1D network.

$(C_{10}H_{11}N_3)_2Cu(NO_3)_2•H_2O$, 19: The ligand 4-(2-(1H-imidazol-1-yl)ethyl)pyridine (171.0 mg, 1.0 mmol) was dissolved in 2.0 mL chloroform, copper nitrate tetrahydrate (121.0 mg, 0.5 mmol) was dissolved in 2.0 mL water. The copper nitrate solution was slowly layered on top of the chloroform solution. The layered solution stayed at room temperature for 6 days. Big blue crystals were collected from the interface between the two layers. Yield: approximately 30% based on Cu(II).

Crystal structure of hybrid network $(C_{10}H_{11}N_3)_2Cu(NO_3)_2•H_2O$, **19.**

Hybrid network $(C_{10}H_{11}N_3)_2Cu(NO_3)_2•H_2O$ crystallized in the monoclinic space group *C*c. The Cu^{2+} ion has octahedral geometry (Figure 4.12), and is bound to two nitrogen atoms from two imidazole groups (Cu1-N1 2.007(4) Å), two pyridyl nitrogen atoms (Cu1- N4 2.018(4) Å), and two oxygen atoms from two different nitrate anions (Cu1- O1 2.5407(35) Å, Cu1- O5 2.5836(34) Å). The asymmetric ligand 4-(2-(1H-imidazol-1-yl)ethyl)pyridine links Cu^{2+} ions into a 1D hydrid chain (Figure 4.13). Figure 4.14 shows the hydrogen bond network in the crystal structure (Table 4.5).

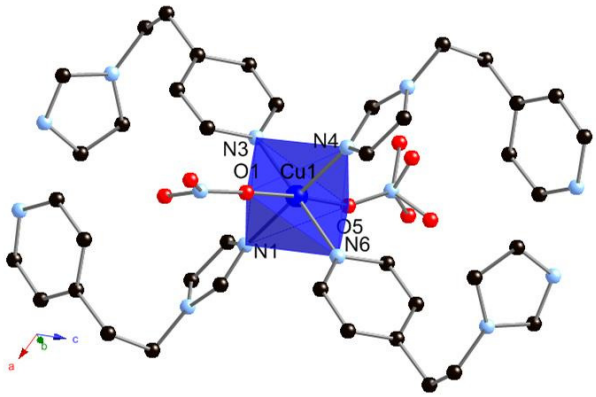

Figure 4.12: Octahedral geometry of the Cu^{2+} ions in hybrid network $(C_{10}H_{11}N_3)_2Cu(NO_3)_2{\bullet}H_2O$, **19**.

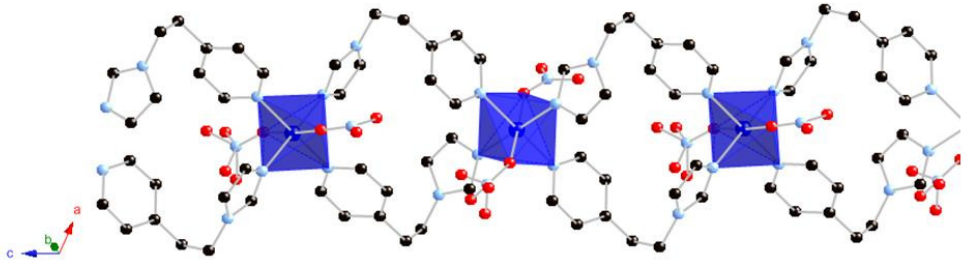

Figure 4.13: The 1D hybrid network $(C_{10}H_{11}N_3)_2Cu(NO_3)_2{\bullet}H_2O$, **19**.

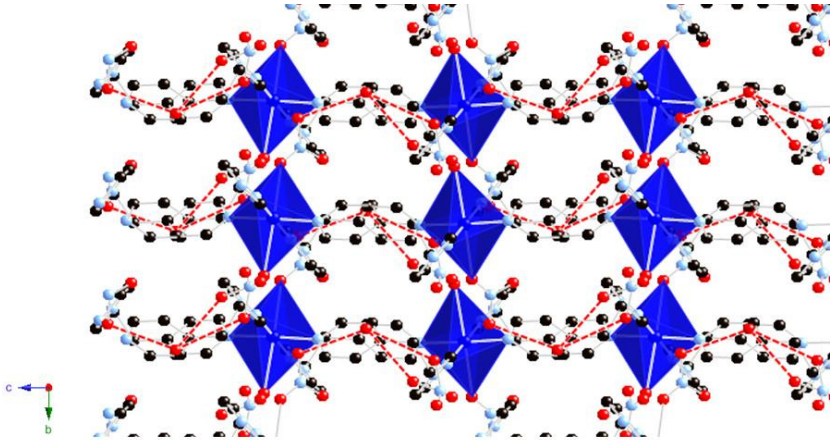

Figure 4.14: Hydrogen bonds in hybrid network $(C_{10}H_{11}N_3)_2Cu(NO_3)_2{\bullet}H_2O$, **19**.

Table 4.5: Hydrogen bonds for hybrid network $(C_{10}H_{11}N_3)_2Cu(NO_3)_2 \bullet H_2O$, **19** [Å and °].

D-H...A	d(D-H)	d(H...A)	d(D...A)	<(DHA)
O(1S)-H(1S)...O(6A)^{i}	0.859(10)	2.18(4)	2.954(8)	149(7)
O(1S)-H(1S)...O(6B)^{i}	0.859(10)	2.57(6)	3.160(12)	126(6)
O(1S)-H(2S)...O(3)^{ii}	0.860(10)	2.64(7)	3.045(8)	110(6)

Symmetry transformations used to generate equivalent atoms:

i: x,y-1,z; ii: x,-y,z+1/2.

4.5 Network $(C_4H_4O_6)Na_2$, **20.**

Tartaric acid (Scheme 4.5) is a white crystalline organic acid. It occurs naturally in many plants, particularly in grapes, bananas, and tamarinds, and is one of the main acids found in wine. It is added to other foods to give a sour taste, and is used as an antioxidant. Salts of tartaric acid are known as tartrates. The complexes formed from aqueous solutions of metal ions and tartaric acid are reported widely in the literatures.[152, 153] One such example is the Cu-tartrate complex shown in Figure 4.15.[152]

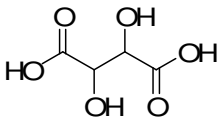

Scheme 4.5: Tartaric acid.

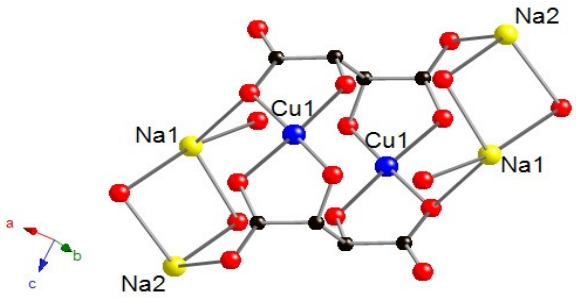

Figure 4.15: Structure of the Cu-tartrate anion.[152]

Experimental section

$(C_4H_4O_6)Na_2$, 20: L(+)-Tartaric acid (150.1 mg, 1.0 mmol), sodium hydroxide (80.0 mg, 2.0 mmol), manganese acetate tetrahydrate (245.1 mg, 1.0 mmol), and 6 mL water were added to a Teflon-line steel antoclave. The mixture was heated at 130°C for 3 days, cooled down to room temperature, filtered and washed with deionized water. Colorless crystals were obtained. Yield: approximately 80% based on Na(I).

Crystal structure of rac-$(C_4H_4O_6)Na_2$, **20.**

Although we were trying to make a manganese tartrate network, a new phase of sodium tartrate was obtained. Also, under the high temperature reaction conditions, the L(+)-tartaric acid turned to rac-tartaric acid.

The network rac-$(C_4H_4O_6)Na_2$ crystallized in the orthorhombic space group *P*bca. Each Na^+ ion is coordinated to six oxygen atoms from tartrate anions (O1-Na1 2.5300(10) Å, O2-Na1 2.4516(10) Å, O3-Na1 2.3559(10) Å, O4-Na1 2.3848(10) Å, O6-Na1 2.2949(10) Å, O1-Na2 2.3347(10) Å, O2-Na2 2.3094(10) Å, O3-Na2 2.4976(10) Å, O5-Na2 2.5229(10) Å, O6-Na2 2.4113(10) Å). Chemically, each tartrate bonds to two Na^+ cations (Figure 4.16). Figure 4.17 shows that this hybrid network structure is well packed (Na1-Na2 3.3867(7) Å, Na1-Na1 3.4233(10) Å, Na2-Na2 3.5783(10) Å). Hydrogen bonding information is given in

Table 4.6.

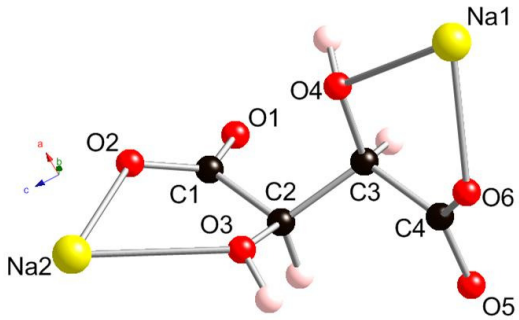

Figure 4.16: Coordination between Na^+ and tartrate acid in hybrid network rac-$(C_4H_4O_6)Na_2$, **20**.

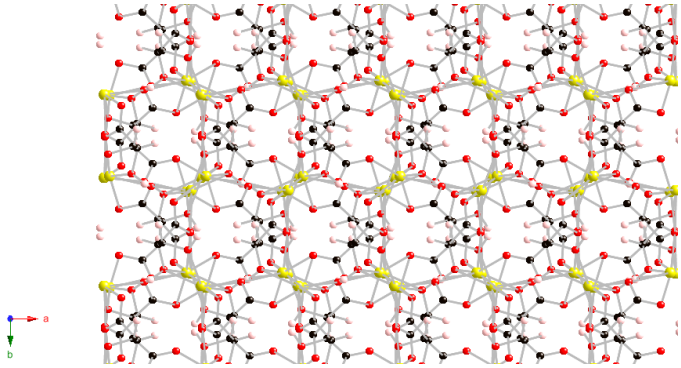

Figure 4.17: Crystal structure of network $(C_4H_4O_6)Na_2$, **20**.

Table 4.6: Hydrogen bonds for hybrid network $(C_4H_4O_6)Na_2$, **20** [Å and °].

D-H...A	d(D-H)	d(H...A)	d(D...A)	<(DHA)
O(3)-H(3)...O(1)^{i}	0.885(16)	1.771(16)	2.6511(13)	172.9(15)
O(4)-H(4)...O(5)^{ii}	0.875(16)	1.797(16)	2.6641(13)	170.7(16)

Symmetry codes:

i: x-1/2,y,-z+3/2; ii: -x,y+1/2,-z+3/2.

Discussion

In the Cambridge Structural Database (CSD), there are a large variety of metal-tartrate structures. Our hybrid network structure rac-$(C_4H_4O_6)Na_2$ is a new tartrate network, which is submitted to the CCDC database.

Chapter 5

Hydrogen-bonded networks and π-π stacking interactions

5.1 Introduction

It is well known that non-covalent interactions between molecules or ions can be used to build crystalline materials. Interactions between molecules such as hydrogen bonds, π-π stacking interactions, halogen-halogen interactions, van der Waals forces, etc., are observed in a wide variety of organic crystal structures. Although these forces are weaker than covalent bonds, they are important for the periodic assembly of building units in crystal structures. In this chapter, hydrogen bonds and π-π stacking interactions within organic crystals will be discussed.

5.1.1 Hydrogen-bonded networks

Hydrogen-bonded networks have potential applications in the design of crystalline solids for separations, catalysis, and electronic uses.[154-157] The strength and direction of hydrogen bonds play an important role in organic crystal construction. However, the definition of a "hydrogen bond" is not obvious. Hydrogen bonds can be considered as an electrostatic interaction between hydrogen bond donors and acceptors. Hydrogen bond donors are usually electronegative atoms that have one or more covalently bonded hydrogen atoms. Hydrogen bond acceptors are atoms that interact with a hydrogen atom bound to a hydrogen bond donor. There are several geometric parameters used to define a hydrogen bond (Scheme 5.1).[158] The summary of the three classes of hydrogen bonds (strong, moderate and weak) are shown in Table 5.1.[158]

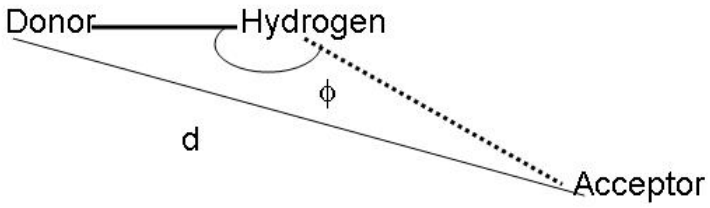

Scheme 5.1: The geometric parameters used to define a hydrogen bond.

Table 5.1: Three classes of hydrogen bonds.[159, 160]

Parameters	Strong	Moderate	Weak
Bond energy (kJ/mol)	60-190	20-60	<20
Distance range (Å)	2.2-2.5	2.5-3.0	3.0-4.0
Angle range (°)	175-180	130-180	90-180
Examples	F-H…F	O-H…N	N-H…O

Graph-set analysis perhaps is the most useful means of identifying hydrogen-bonded patterns.[158] Four simple categories of hydrogen-bonding patterns are important in describing the recognition between molecules.[158] Different molecules with similar functional groups may have similar hydrogen-bonding characteristics when evaluated by graph-set analysis.[158] (Table 5.2)

Table 5.2: Graph-set analysis terminology.[158] (Reproduced by permission of the Royal Society of Chemistry. http://dx.doi.org/10.1039/DOI.) (Permission is in Appendix E)

Degree (of a pattern)	The number of atoms in the pattern
Designator, G (of a pattern)	One of four letters designating the type of pattern: C (chain), R (ring), S (intramolecular pattern), D "discrete" patterns.
Descriptor G_d^a (n) (of a pattern)	A notation summarizing the pattern: *G*:

	the pattern designator; *d*: a subscript describing the number of donors in the pattern; *a*: a superscript describing the number of acceptors in the pattern; n: the degree of the pattern.

The examples shown in Scheme 5.2 display four patterns and their corresponding descriptors. A chain that is composed of four atoms (1 in Scheme 5.2) is described as C(4). There is no subscript and superscript, this means that there is one donor and one acceptor group in this pattern. A ring pattern is shown in 2 (Scheme 5.2), the pattern contains 8 atoms, two of them are hydrogen bond donors and two of them are hydrogen bond acceptors, so the pattern is described as $R_2^2(8)$. There are six atoms involved in the intramolecular hydrogen bond in 3 (Scheme 5.2), so the descriptor is S(6). Example 4 (Scheme 5.2) shows a discrete hydrogen bond pattern (D). In many crystal structures, the hydrogen-bonding network may contain a number of different patterns. For example, scheme 5.3 shows a schematic of the N-methylaniline structure.[158] In this structure, the basic graph set is $R_1^2(4)$. All these rings are linked to form a chain with pattern $C_1^2(8)$,so the complete designator for this pattern is $C_1^2(8)[R_1^2(4)]$.[158]

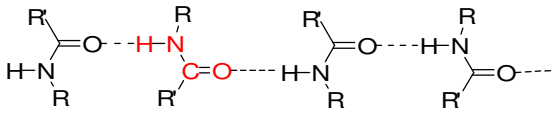

1

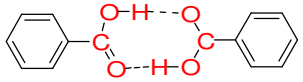

2

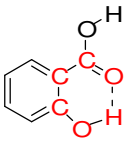

3

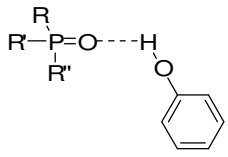

4

Scheme 5.2: Examples of hydrogen-bonding patterns. 1: C(4); 2: $R_2^2(8)$; 3: S(6); 4: D.

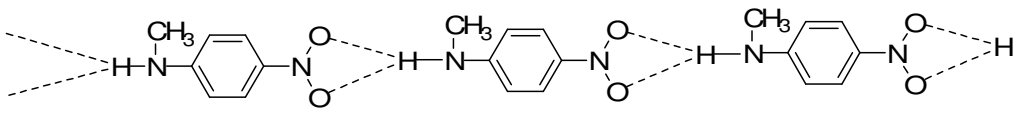

Scheme 5.3: The N-methylnitroaniline structure with pattern $C_1^2(8)[R_1^2(4)]$.

5.1.2 π-π stacking interactions

In this chapter, the π-π stacking interactions between benzene, pyridine and imidazole rings will be discussed. Atoms of these rings are sp^2 hybridized, and the delocalized electrons form π clouds above and below the ring.[161] Typically, there are two types of π-π stacking interactions (Scheme 5.4). When the rings are perpendicular to each other the arrangement is more energetically favorable than when the two rings are parallel because this situation allows for a maximum interaction between the electron clouds. As with hydrogen bond interactions, there is no strict definition for π-π stacking interactions. Scheme 5 shows two geometrical parameters associated with parallel π-π stacking interactions. In accordance with published literature we will consider values of less than 4.0Å to be a π-π stacking interactions.[161] The angle between the perpendicular line and centroids line shows the degree of ring slippage from the totally eclipsed arrangement.

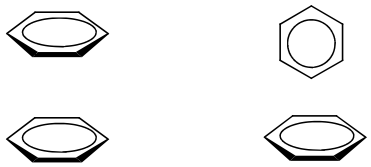

Scheme 5.4: Two types of ring interactions. (A) Rings are parallel. (B) Rings are perpendicular to each other.

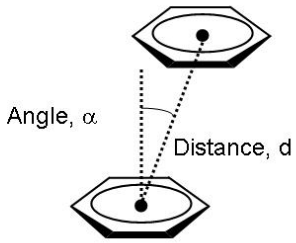

Scheme 5.5: The geometric parameters that define π-π stacking interactions.

5.2 The 4,4'-trimethelenedipyridine (TMDP) crystals

During the attempts to synthesize hybrid network series **I** (**chapter 2**), some reaction yielded hydrogen-bonded crystals instead. TMDP is capable of forming co-crystals with other organic compounds, such as hydroquinone, benzene-1,2,3-triol, and 4-nitrophenol (Scheme 5.6).

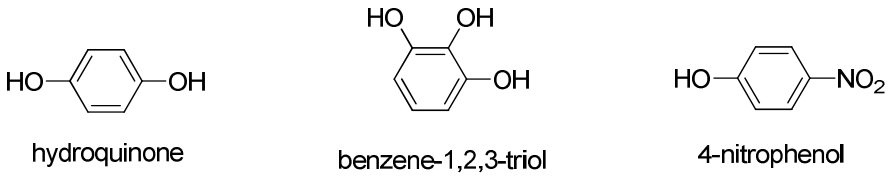

Scheme 5.6: Examples of organic molecules that crystallize with TMDP.

5.2.1 Crystal structures TMDP with hydroquinone: $(C_{13}H_{14}N_2)_2(C_6H_6O_2)_3 \bullet 2H_2O$ (**21**) and $(C_{13}H_{14}N_2)(C_6H_6O_2)$ (**22**)

When we synthesized hybrid network different synthesis conditions lead to the formation of some hydrogen-bonded crystals.

Experimental section for hydrogen-bonded networks **21** and **22**

$(C_{13}H_{14}N_2)_2(C_6H_6O_2)_3 \bullet 2H_2O$ (**21**): Zinc acetate dihydrate (220.0 mg, 1.0 mmol),

phosphorous acid (164.0 mg, 2.0 mmol), hydroquinone (220 mg, 2.0 mmol), TMDP (300.0 mg, 1.5 mmol), and 6 mL water were added to a heavy-walled glass tube that was sealed under vacuum. The tubes were placed in an oven for 7 days at 130°C. The colorless crystals were collected after filtration. Hydrogen-bonded network **1** was the only crystalline material obtained from this synthesis, no hybrid network formation was observed.

$(C_{13}H_{14}N_2)(C_6H_6O_2)$ (**22**): Phosphorous acid (164.0 mg, 2.0 mmol), hydroquinone (220 mg, 2.0 mmol), TMDP (300.0 mg, 1.5 mmol), and 6 mL water were added to a heavy-walled glass tube that was sealed under vacuum. The tubes were placed in an oven for 7 days at 130°C. The colorless crystals were collected after filtration. In a similar manner to hydrogen-bonded network **21**, **22** was the only crystal obtained from this synthesis, no hybrid network formation was observed.

Crystal structure of hydrogen-bonded network **21** (Figure 5.1) and **22** (Figure 5.2)

$(C_{13}H_{14}N_2)_2(C_6H_6O_2)_3 \bullet 2H_2O$, **21**: The structure crystallized in the triclinic space group *P*-1. The asymmetric unit contains one TMDP, one and half hydroquinone molecules and one water molecule. Two kinds of motifs are shown in scheme 5.7. The first motif shows hydroquinone hydrogen bonding to the TMDP ligand to form a C_2^2 (19) chain pattern. The second motif is another chain, which is composed of water and hydroquinone molecules with pattern C_2^2(9). Hydrogen bonds between TMDP, hydroquinone, and water molecules connect the molecules together (hydrogen bond information is table 5.1) to form a 3D network

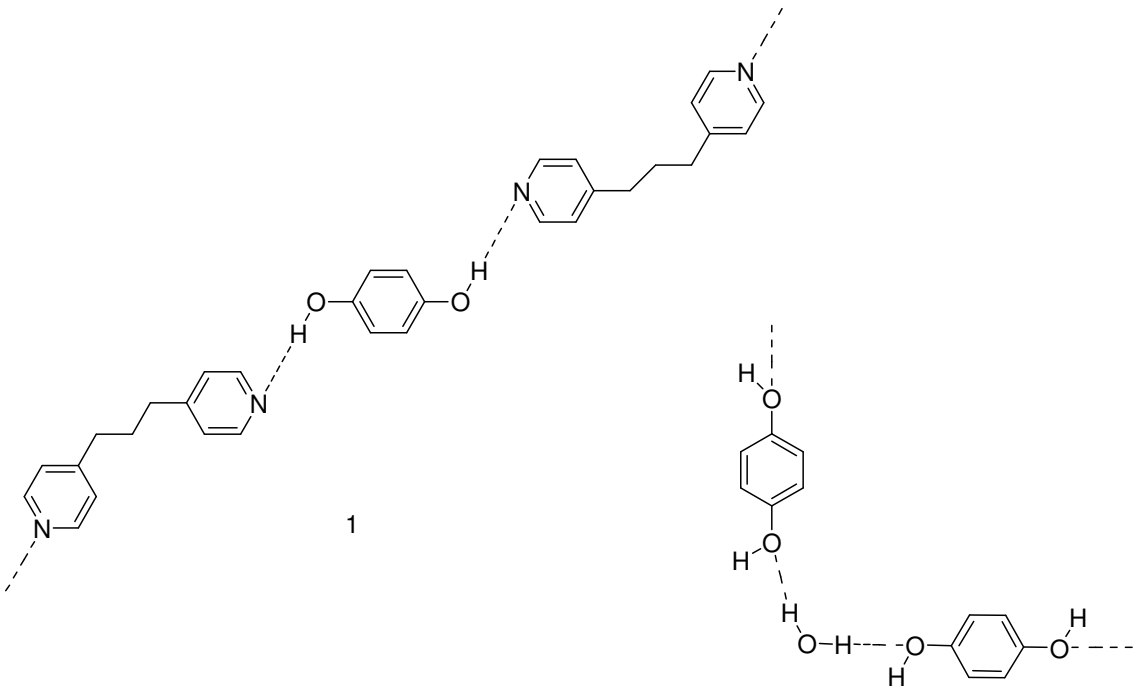

Scheme 5.7: Two motifs in hydrogen-bonded network **21**. Motif 1 is $C_2^2(19)$ packing pattern; motif 2 is $C_2^2(9)$ packing pattern.

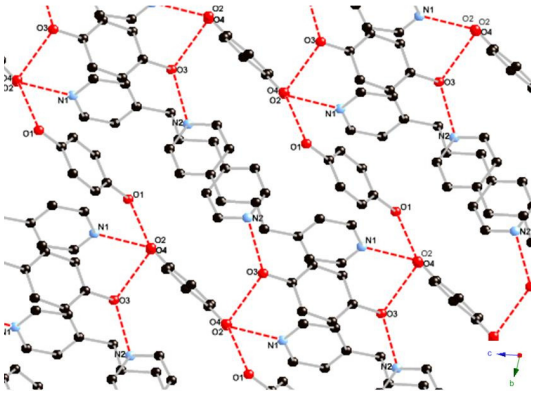

Figure 5.1: Crystal structure of hydrogen-bonded network **21**.

$(C_{13}H_{14}N_2)(C_6H_6O_2)$, **22**: Compared to **21**, crystal **22** contains the same organic molecules (TMDP and hydroquinone) but it does not contain water. Hydrogen bonds between

TMDP and hydroquinone connect these molecules to form a 1D chain. There is only one hydrogen bonding motif (pattern $C_2^2(19)$) in this crystal structure (Scheme 5.8). Hydrogen bond information is in table 5.1. Figure 5.6 shows the crystal structure.

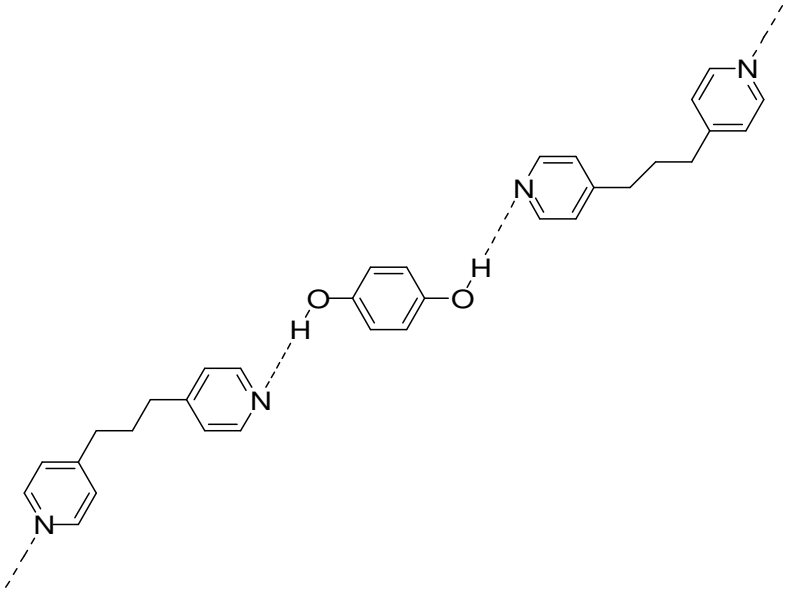

Scheme 5.8: Motif with packing pattern $C_1^1(19)$ in hydrogen-bonded network **22**.

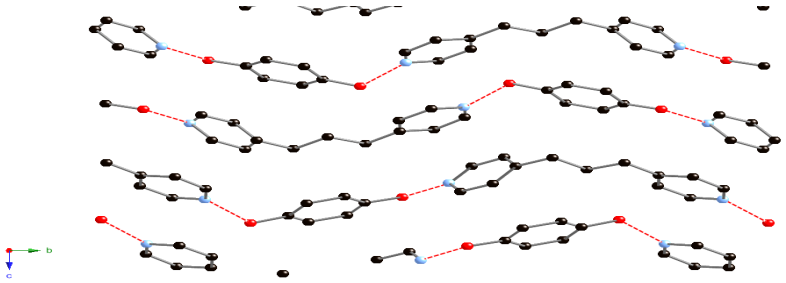

Figure 5.2: Crystal structure of hydrogen-bonded network **22**.

Discussion of hydrogen-bonded network **21** and **22**

During the synthesis of **21**, the zinc ion did not coordinate to the ligand TMDP and is therefore not incorporated in the crystal structure. Synthesis of **22** was performed with similar starting materials to **21** except that a different metal ion was used, however, the product of the

reaction turned out to be a similar. A common 1D chain motif with pattern $C_2^2(19)$ is observed in both crystal structures.

5.2.2. Crystal structures TMDP with 1,2,3-trihydroxide benzene $(C_{13}H_{14}N_2)(C_6H_6O_3)$ (**23**) and $(C_{13}H_{16}N_2)_2(C_6H_6O_3)_6(HO_3P)_2(H_2O)_7$ (**24**)

Experimental section of hydrogen-bonded network **23** and **24**

$(C_{13}H_{14}N_2)(C_6H_6O_3)$, **23**: Zinc acetate dihydrate (220.0 mg, 1.0 mmol), phosphorous acid (164.0 mg, 2.0 mmol), 1,2,3-trihydroxide benzene (258.0 mg, 2.0 mmol), TMDP (300.0 mg, 1.5 mmol), and 6 mL water were added to a heavy-walled glass tube that was sealed under vacuum. The tubes were placed in an oven for 7 days at 130℃. The colorless crystals were collected after filtration.

$(C_{13}H_{16}N_2)_2(C_6H_6O_3)_6(HO_3P)_2(H_2O)_7$, **24**: Zinc acetate dihydrate (220.0 mg, 1.0 mmol), phosphorous acid (164.0 mg, 2.0 mmol), 1,2,3-trihydroxide benzene (258.0 mg, 2.0 mmol), TMDP (300.0 mg, 1.5 mmol), NaOH (60.0 mg, 1.5 mmol), and 6 mL water were added to a heavy-walled glass tube that was sealed under vacuum. The tubes stayed at room temperature for 6 days. The colorless crystals were collected after filtration.

Crystal structure of hydrogen-bonded network **23** (Figrue 5.3) and **24** (Figure 5.4)

$(C_{13}H_{14}N_2)(C_6H_6O_3)$ (**3**): Crystal **23** crystallized in space group $P2_1/n$. Motif 1 in Scheme 5.7 shows one of the hydrogen-bonded patterns, $R_6^6(44)$. Motif 2 shows C_2^2

(10) packing pattern between 1,2,3-trihydroxide benzene molecules to from 1D chain (Scheme 5.9). Hydrogen bonds between 1,2,3-trihydroxide benzene and TMDP form a 2D layer structure as shown in figure 5.3 (hydrogen bond information is given in table 5.1).

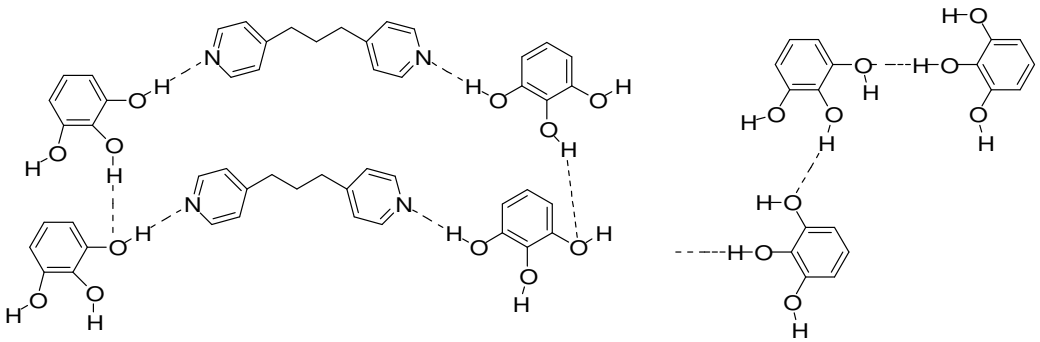

Scheme 5.9: Two motifs in hydrogen-bonded network **23**. Motif 1 is $R_6^6(44)$ packing pattern; motif 2 is $C_2^2(10)$ packing pattern.

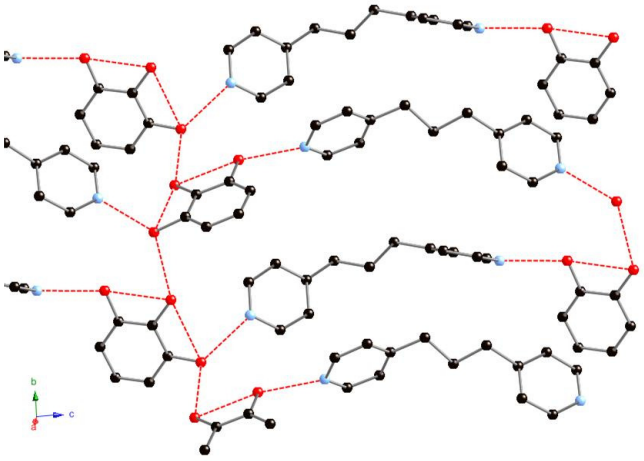

Figure 5.3: 2D hydrogen-bonded network observed in **23**.

$(C_{13}H_{16}N_2)_2(C_6H_6O_3)_6(HPO_3)_2(H_2O)_7$, **24** crystallized in space group $P2_1/n$. The asymmetric unit contains one TMDP molecule, three 1,2,3-trihydroxide benzene molecules, and one phosphite anion. One of the water molecules is sitting on the glide plane. Scheme 5.10 shows three important hydrogen bonding motifs $R_1^2(5)$, D, $R_2^1(7)$, respectively. Hydrogen bonds link all these molecules to form a 3D hydrogen-bonded network. Figure 5.8 shows the crystal structure of **24**.

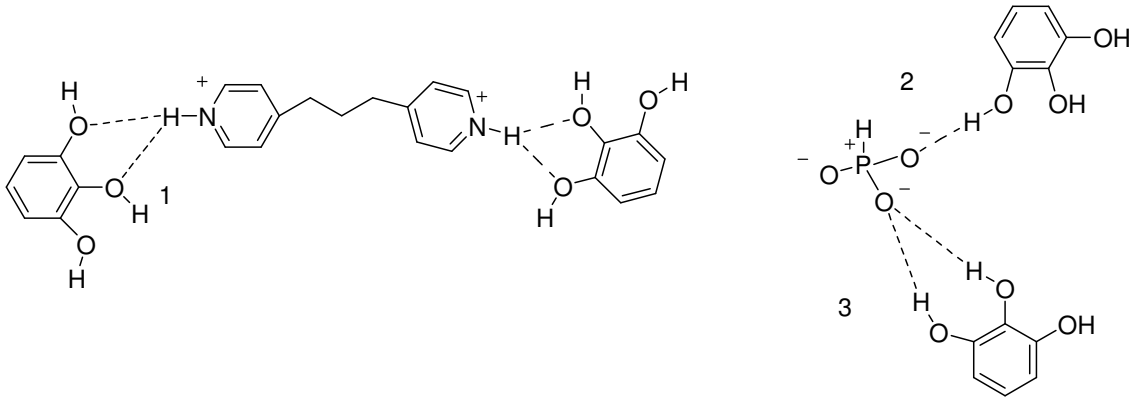

Scheme 5.10: Three motifs in hydrogen-bonded network **24**. 1: $R_1^2(5)$; 2: D; 3: $R_2^1(7)$.

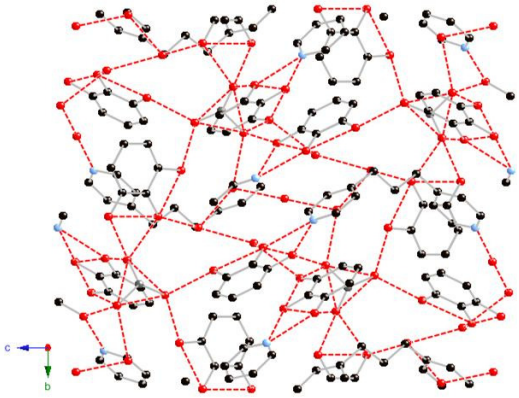

Figure 5.4: The 3D hydrogen-bonded network observed in **24.**

5.2.3. Crystal structures TMDP with nitrophenol: $(C_{13}H_{14}N_{2)})(C_6H_5NO_3)_2$, **25**.

The template molecule, nitrophenol, successfully co-crystallized in one of our hybrid network structures at 130°C (Chapter **2**). However, when the synthesis temperature was decreased to room temperature, the hydrogen-bonded network, **25**, formed instead. We therefore conclude that temperature is one of the key factors in hybrid network synthesis.

Experimental section of hydrogen-bonded trimer **25**

$(C_{13}H_{14}N_2)(C_6H_5NO_3)_2$, **25**: Zinc acetate dihydrate (220.0 mg, 1.0 mmol), phosphorous acid (164.0 mg, 2.0 mmol), nitrophenol (278.0 mg, 2.0 mmol), TMDP (300.0 mg, 1.5 mmol), and 6 mL water were added to a heavy-walled glass tube that was sealed under vacuum. The tubes were placed in a lab at room temperature for 7 days. The colorless crystals were collected after filtration.

Crystal structure of hydrogen-bonded trimer **25**

$(C_{13}H_{14}N_2)(C_6H_5NO_3)_2$, **25** crystallized in space group $P2_1/c$. Hydrogen bonds link TMDP and nitrophenol to form isolated trimers. The nitro group on each nitrophenol molecule terminates the hydrogen-bonded aggregate. Scheme 5.11 shows this type D hydrogen bond pattern. Figure 5.5 shows the trimer in the crystal structure.

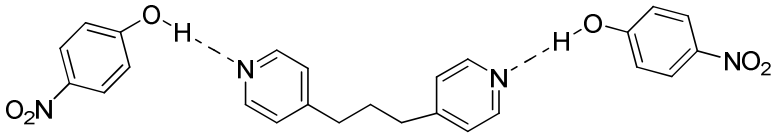

Scheme 5.11: Motif in hydrogen-bonded trimer **25**.

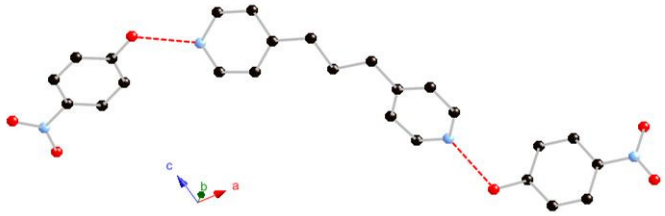

Figure 5.5: The 0D hydrogen-bonded trimer observed in **25**.

Table 5.3: Hydrogen bonds in hydrogen-bond networks **21**- **25** [Å and °].

D-H...A	d(D-H)	d(H...A)	d(D...A)	<(DHA)
Hydrogen-bonded network **21**				
O(1)-H(1A)...O(4)^{i}	0.889(16)	1.827(16)	2.7074(11)	170.5(15)
O(2)-H(2A)...N(1)	0.880(17)	1.828(17)	2.6794(11)	162.4(15)
O(3)-H(3A)...N(2)^{ii}	0.952(17)	1.735(17)	2.6836(11)	174.0(15)
O(4)-H(4B)...O(3)^{iii}	0.874(17)	1.925(17)	2.7905(11)	170.3(14)
O(4)-H(4A)...O(2)	0.873(16)	1.924(16)	2.7959(11)	176.2(15)
Hydrogen-bonded network **22**				
O(2)-H(9)...N(2)^{iv}	0.913(17)	1.817(17)	2.7075(10)	164.5(15)
O(1)-H(3)...N(1)^{v}	0.966(18)	1.804(18)	2.7376(11)	161.5(15)
Hydrogen-bonded network **23**				
O(2)-H(2)...O(1)^{vi}	0.880(15)	1.984(15)	2.7963(12)	153.0(13)
O(2)-H(2)...O(3)	0.880(15)	2.257(14)	2.7123(11)	112.0(11)
O(1)-H(1)...N(1)^{vii}	0.940(18)	1.810(17)	2.7174(13)	161.6(15)
Hydrogen-bonded network **24**				
N(1)-H(1A)...O(4)^{viii}	0.88	1.95	2.740(2)	148.7
N(1)-H(1A)...O(5)^{viii}	0.88	2.28	2.966(2)	134.5
N(2)-H(2A)...O(2)	0.88	2.07	2.785(2)	137.4
N(2)-H(2A)...O(1)	0.88	2.15	2.921(2)	145.7
O(1)-H(2B)...O(3)	0.72(3)	2.35(3)	2.7047(19)	112(2)
O(3)-H(3)...O(10)	0.84	1.81	2.6482(18)	171.2
O(4)-H(4A)...O(12)	0.84	1.83	2.6167(19)	156.2
O(7)-H(7)...O(12)	0.84	2.51	2.9243(19)	111.7
O(8)-H(8)...O(7)	0.84	2.52	2.9243(19)	111.1

O(5)-H(5B)...O(6)	0.89(3)	2.19(3)	2.717(2)	117.0
O(13)-H(13A)...O(14)	0.936(10)	1.990(17)	2.831(3)	149(2)
O(14)-H(14A)...O(13)	0.922(17)	2.08(2)	2.831(3)	138(2)
O(1)-H(1B)...O(11)^{ix}	0.84	1.88	2.7074(19)	164.8
O(6)-H(6)...O(11)^{i}	0.84	1.9	2.6505(19)	147.7
O(7)-H(7)...O(12)^{x}	0.84	1.86	2.673(2)	162.6
O(8)-H(8)...O(12)^{x}	0.84	1.79	2.603(2)	162.8
O(9)-H(9)...O(10)^{xi}	0.84	1.80	2.617(2)	163.6
O(2)-H(2B)...O(14)^{xii}	0.72(3)	2.10(3)	2.753(2)	151.0
O(14)-H(14B)...O(6)^{xiii}	0.948(17)	2.23(2)	2.912(2)	128(2)
O(13)-H(13B)...O(15)^{xiv}	0.954(10)	1.792(13)	2.710(3)	161(2)

Hydrogen-bonded network **25**

O(1)-H(1A)...N(1)^{xv}	0.98(2)	1.66(2)	2.6355(17)	172.4(19)
O(4)-H(4A)...N(2)^{xvi}	0.899(15)	1.757(16)	2.6484(17)	171(2)

Symmetry codes:

i: -1+x,y,z; ii: -1+x,y,-1+z; iii: -1+x,-1+y,z; iv: 1/2+x,-1/2-y,-1/2+z;

v: 1/2+x,1/2-y,-1/2+z; vi: 1/2-x,1/2+y,3/2-z; vii: 1/2-x,-1/2+y,3/2-z;

viii: x,y,-1+z; ix: 1/2+x,1/2-y,1/2+z; x: 3/2-x,1/2+y,1/2-z; xi: x,1+y,z;

xii: 3/2-x,-1/2+y,1/2-z; xiii: 1-x,1-y,z; xiv: x,1+y,z;

xv: x,3/2-y,1/2+z; xvi: 2-x,1/2+y,1/2-z.

No esd is given because the hydrogen-bond positions in these compounds were calculated and not refined.

5.3 The 4,4'-bisimidazolylbiphenyl (BIB) crystals

The BIB ligand has been successfully used in a series of hybrid network construction (**Chapter 3**). BIB also formed two hydrogen-bonded network structures that have interesting

structure topologies. We reported two structures of BIB in sctructure **26** and two network structures of BIB co-crystalized with water (**27**) and nitrate (**28**).

5.3.1 Crystal structure of BIB, **26** and BIB•H_2O, **27**.

Experimental section of BIB, **26** and BIB•H_2O, **27**.

The synthesis of BIB ligand is in **Chapter 3**. Two crystalline forms were obtained from the crystallization process. One form has no water molecules within the crystal, whereas the second form does.

Crystal structure of BIB, **26.**

The BIB ligand ($C_{18}H_{16}N_4$), **26** crystallized in space group *P*-1. There is no hydrogen bonding in the crystal structure. Instead, π-π stacking interactions dominate in this crystal structure (α = 25.96°, d = 3.763Å) (Scheme 5.12). Figure 5.6 shows the molecular structure of BIB.

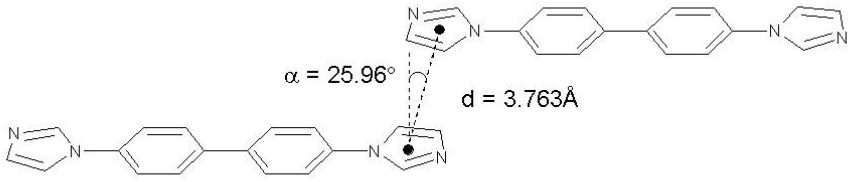

Scheme 5.12: The π-π stacking interactions in BIB crystal.

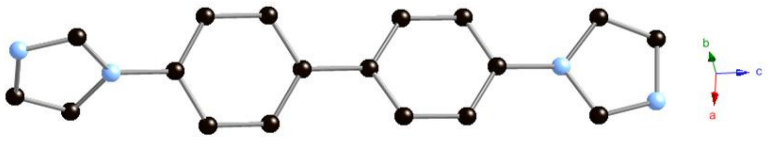

Figure 5.6: Crystal structure of BIB ligand.

$(C_{18}H_{16}N_4)\bullet H_2O$, **27** crystallized in space group *C*2/c. Hydrogen bonds between BIB and water molecules form a 1D chain (N-H...O = 2.843(2) Å). The packing motif is described by designator $C_2^2(18)$ (Scheme 5.13). Figure 5.7 shows the crystal structure **6**.

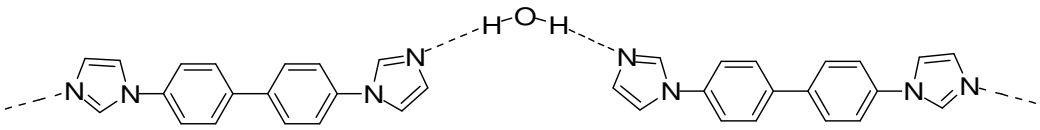

Scheme 5.13: Motif in hydrogen-bonded network **27**.

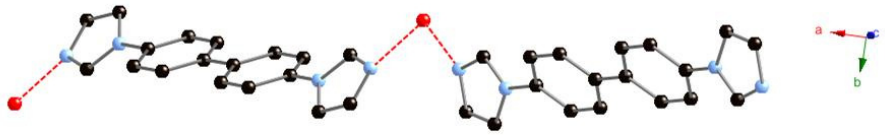

Figure 5.7: Crystal structure of the hydrogen-bonded network observed in **27**.

5.3.2 Crystal structure of BIB with nitrate anion $(C_{18}H_{16}N_4)(NO_3)_2$, **28.**

In our hybrid network synthesis, BIB ligand also formed a salt with an anion from the transitional metal compound used in the synthesis. All other starting materials remained in the solution.

Experimental section of hydrogen-bonded network **28**

$(C_{18}H_{16}N_4)(NO_3)_2$, **28**: Copper nitrate tetrahydrate (260.0 mg, 1.0 mmol), BIB (286.0 mg, 1.0 mmol), NaOH (60.0 mg, 1.5 mmol), and 6 mL water were added to a heavy-walled glass tube for 5 days at 130°C. The colorless crystals were collected after filtration.

Crystal structure of hydrogen-bonded network **28**

$(C_{18}H_{16}N_4)(NO_3)_2$, **28** crystallized in space group $P2_1/c$. The motifs in this crystal show $R_2^1(4)$ and D packing patterns (Scheme 5.14). Short contacts (2.835Å) are observed between oxygen atoms from different nitrate ions. The π-π stacking interactions play an important role in this crystal structures. Scheme 5.15 shows the geometric parameters associated with the π-π stacking interactions in this crystal: α = 17.34° and distance (d) = 3.765Å. Figure 5.8 shows the π…π stacking network in **28**. Hydrogen bond information is given in Table 2.

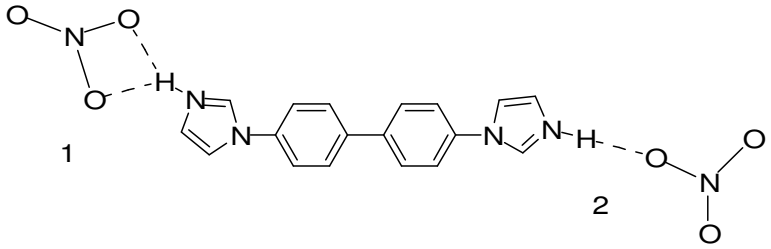

Scheme 5.14: Two motifs in hydrogen-bonded network **28**. Motif 1 is $R_2^1(4)$ packing pattern; motif 2 is D packing pattern.

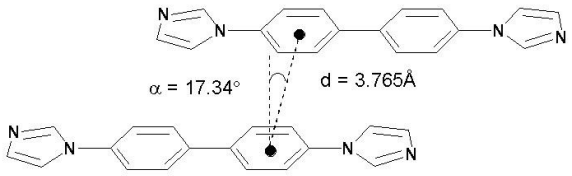

Scheme 5.15: The π-π stacking interactions in hydrogen-bonded network **28**.

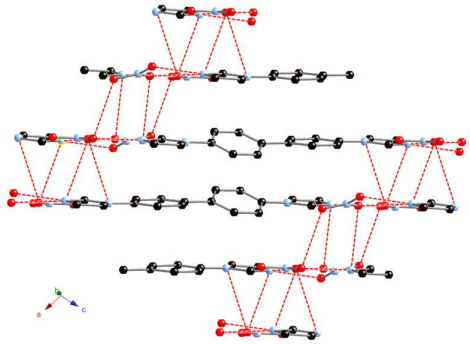

Figure 5.8: Crystal structure of **28** showing the π…π stacking network.

Table 5.4: Hydrogen bonds in the hydrogen-bonded network observed in **28** [Å and °].

D-H...A	d(D-H)	d(H...A)	d(D...A)	<(DHA)
N(4)-H(4A)...O(2)^{i}	0.97(2)	1.75(2)	2.701(2)	167.3(19)
N(4)-H(4A)...N(5)^{i}	0.97(2)	2.44(2)	3.324(3)	150.8(16)
N(4)-H(4A)...O(3)^{i}	0.97(2)	2.46(2)	3.115(2)	124.3(15)
N(1)-H(1A)...O(4)	0.91(2)	1.84(2)	2.744(2)	173(2)
N(1)-H(1A)...O(5)	0.91(2)	2.52(2)	3.048(2)	117.7(16)

Symmetry codes:

i: -x,-y,2-z.

Crystallography

Diffraction data for structures **21**-**27** were collected on an Oxford Diffraction Gemini diffractometer at 100 K with Mo Kα radiation (λ = 0.71073 Å). All data processing was performed using CrysAlisPro, and structural solutions and refinements were conducted with SHELX via the WinGX graphical interface software.[117, 119, 144] Structural solutions were obtained by direct methods, and refinement performed on F^2 by least-squares techniques. All non-hydrogen atoms were refined anisotropically. Unless stated otherwise, hydrogen atoms were located in the difference Fourier maps and are restrained to chemically reasonable positions. A summary of all crystallographic data is given in Table 5.5 (crystallographic data of tructure **27** is in **Chapter 3**).

Table 5.5: Crystal data and structure refinement parameters for 21-28.

	21	**22**
Empirical formula	$C_{44}H_{50}N_4O_8$	$C_{19}H_{22}N_2O_2$
M_w	762.88	308.37
T/K	100	100
Space group	P-*1*	P$2_1/n$
a/Å	8.5655(6)	5.8545(5)
b/Å	10.296(2)	18.1624(13)
c/Å	11.5624(14)	14.9741(12)
α/degree	78.743(13)	90
β/degree	88.626(8)	92.931(8)
γ/degree	87.169(10)	90
V/Å^3	998.7(2)	1590.1(2)
Z	1	4
μ/mm^{-1}	0.088	0.084
R1[a][I>2σ(I)]	0.0366	0.0391
*w*R2[b][I>2σ(I)]	0.1012	0.1046

	23	**24**
Empirical formula	$C_{19}H_{20}N_2O_3$	$C_{62}H_{84}N_4O_{31}P_2$
M_w	324.37	1443.27
T/K	100	100
Space group	P$2_1/n$	P$2_1/n$
a/Å	9.1505(7)	9.9813(7)
b/Å	9.7431(7)	16.8715(13)
c/Å	18.4635(12)	20.4207(12)
α/degree	90	90
β/degree	92.409(6)	94.968(6)

γ/degree	90	90
V/Å^3	1644.6(2)	3425.9(4)
Z	4	2
μ/mm^{-1}	0.089	1.156
R1[a][I>2σ(I)]	0.0382	0.0498
*w*R2[b][I>2σ(I)]	0.0877	0.1470

	25	**26**
Empirical formula	$C_{25}H_{24}N_4O_6$	$C_{18}H_{16}N_4$
M_w	476.48	762.88
T/K	100	100
Space group	$P2_1/c$	P-*1*
a/Å	27.9964(8)	9.4009(5)
b/Å	7.0286(2)	9.6350(5)
c/Å	11.6957(3)	17.5577(9)
α/degree	90	97.694(4)
β/degree	100.799(2)	94.579(4)
γ/degree	90	117.778(5)
V/Å^3	1375.93(14)	1375.93(14)
Z	4	4
μ/mm^{-1}	0.102	1.367
R1[a][I>2σ(I)]	0.0363	0.0447
*w*R2[b][I>2σ(I)]	0.0812	0.1154

	28
Empirical formula	$C_{18}H_{16}N_6O_6$
M_w	412.37

T/K	100
Space group	$P2_1/c$
a/Å	9.3180(6)
b/Å	15.8218(6)
c/Å	12.3876(7)
α/degree	90
β/degree	104.947(6)
γ/degree	90
V/Å^3	1764.48(17)
Z	4
μ/mm^{-1}	0.12
R1[a][I>2σ(I)]	0.0366
*w*R2[b][I>2σ(I)]	0.0805

[a]$R1 = \Sigma \, ||F_o| - |F_c|| / \Sigma |F_o|$. [b]$wR2 = \{\Sigma[w(F_o^2 - F_c^2)^2] / \Sigma[w(F_o^2)^2]\}^{1/2}$,

where $w = 1/[\sigma^2(F_o)^2 + (aP)^2 + bP]$, $P = [(F_o)^2 + 2(F_c)^2]/3$.

5.4 Summary of hydrogen-bonded networks

The graph set analysis[158] of these hydrogen-bonded networks shows the ability of organic ligands TMDP and BIB to form 0D, 1D, 2D and 3D networks with a wide variety of packing patterns. The subtle factors responsible for the different hydrogen-bonded networks are not fully understood. However, the study of the packing pattern of hydrogen-bonded networks helps us understand more about weak intermolecular interactions.

Chapter 6

Conclusions and future work

The principle goal of the research presented in this thesis was to coordinate difunctional ligands to transition metal ions for the construction of hybrid networks with porosity. We have demonstrated that flexible ligands such as 4, 4'-trimethylenedipyridine, TMDP (**Chapter 2**) tend to construct a wide variety of templated network structures, the architectures of which are directed by the templates. The interstitial space in hybrid materials constructed from flexible ligands occupied by the templates. And space is not sustained upon attempts to remove the templates. Rigid ligands, such as 4, 4'-bisimidazolybiphenyl, BIB (**Chapter 3**) can be used to construct 2D and 3D rigid networks that have large cavities. However the materials derived from BIB show that the large void space is filled by the formation of an interpenetrated structure. Generally it is difficult to control the structure of hybrid materials synthesis by tailoring the synthesis conditions, ligand rigidity, or the presence of template molecules to direct the growth of the networks. The ability to predict network structure from a given set of synthesis parameters remains elusive.

We investigated a number of potential templating molecules such as water, phenol, methanol, ethanol, etc and have found that aromatic alcohols act as templates for the generation of hybrid networks based on the TMDP ligand (**Chapter 2**). We believe that aromatic alcohols are successful templating molecules because of their ability to control the directionality of the structural units used in the creation of the hybrid networks. They are able to do this because they are rigid (i.e. have a well defined molecular shape), are capable of forming hydrogen bonds, and have the potential for $\pi\ldots\pi$ interactions with the components of the network. Unlike aromatic alcohols, aliphatic alcohols and amino acids do not template TMDP hybrid networks. This may be related poorer hydrogen bonding rigidity in the aliphatic alcohol systems, less molecular rigidity, or the lack of potential $\pi\ldots\pi$ interactions. In spite of our success in using templates to direct the construction of hybrid materials, we

cannot predict which template molecules will work, or what the topology of the resulting hybrid structure will be. A good example of this was presented in **chapter 2**, where we reported the structure of a 3D framework that was prepared using phenol as the template. X-ray diffraction analysis indicated that the phenol molecules were located within the framework cavities, and that they were disordered such that the space average of the orientation mimic catechol. However when catechol is used as the templating agent, a different hybrid network is obtained.

Our hybrid network series **II** contains different transition metal ions with BIB ligand. The BIB ligand has a long molecular axis (the distance of N…N is approximately 14.1Å). It is relatively rigid with only rotational flexibility is about the molecular axis. We hoped to synthesize hybrid network with rigid molecular size pores. The hybrid networks we have synthesized do not contain large cavities. We have found that BIB ligand tends to form 1D chains, or interpenetrated networks instead of open 3D frameworks. In the future, the use of templates to fill the pores should be used in construction of networks with BIB. Template molecules are expected to direct the network formation, maintain the large porosity, and avoid interpenetration.

We also investigated the possibility of preparing chiral hybrid networks. The most efficient way of synthesis chiral networks is to use enantiomerically pure ligands. One of the simplest and most readily available difunctional chiral ligands is tartaric acid, consequently this became our ligand of choice. We tried to make Mn tartrate networks, however Mn^{2+} ion didn't coordinate to tartrate ion in the hydrothermal synthesis. We were able to coordinate tartrate to Na^{+} ions to form a network (**Chapter 4**). At the reaction with a temperature of 130 °C, the tartrate formed a racemic mixture and the hybrid material produced is not chiral. As it has been shown that chiral hybrid networks are potential candidates for chiral synthesis and enantiomeric separation we would like to direct our future research towards the synthesis of chiral materials.

To synthesize chiral hybrid networks, typically two approaches can be used: (I) Chiral

templates can be used to direct the chirality of the network during its formation. (II) Chiral ligands can be used in the synthesis to force the formation of a chiral network. Of these two approaches, the use of chiral ligands is the most promising method for the construction of chiral hybrid networks. Therefore, future work may include the use of relatively rigid ligands with chiral functional groups for the synthesis of chiral materials. Examples of such ligands are chiral derivatives of 4, 4'-bipyridine[162] (Scheme 6.1).

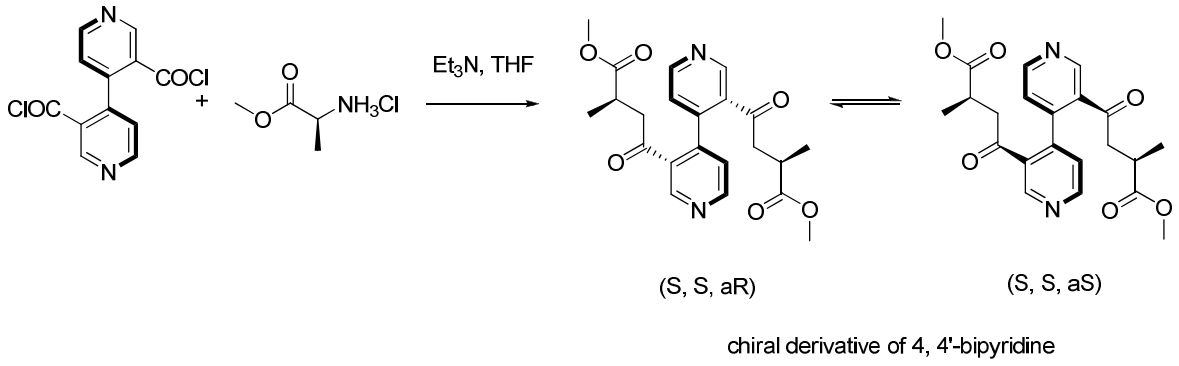

Scheme 6.1: Chiral derivatives of 4, 4'-bipyridine.[162] (Rang, A.; Nieger, M.; Engeser, M.; Luetzen, A.; Schalley, C. A.: Self-assembling squares with amino acid-decorated bipyridines: heterochiral self-sorting of dynamically interconverting diastereomers. *Chem. Commun. (Cambridge, U. K.)* **2008,** (39), 4789-4791. Copyright Wiley-VCH Verlag GmbH & Co. KGaA. Reproduced with permission.) (Permission is in Appendix E)

The results from our research are significant with regards to furthering our basic understanding of the structural topologies of hybrid materials, as well as providing design methods to enable a systematic approach to be used during hybrid network synthesis. This is desirable for the continued development of these materials. While the research in inorganic-organic hybrid materials is still growing rapidly, we believe that the development of these functional materials for use in catalysis, separation, and gas storage is a realistic goal.

References

1. Scifinder, **2007**.
2. Uemura, K.; Matsuda, R.; Kitagawa, S., Flexible microporous coordination polymers. *J. Solid State Chem.* **2005,** *178* (8), 2420-2429.
3. Rowsell, J. L. C.; Yaghi, O. M., Metal-organic frameworks: a new class of porous materials. *Microporous Mesoporous Mater.* **2004,** *73* (1-2), 3-14.
4. Werner,A., *http://nobelprize.org/nobel_prizes/chemistry/laureates/1913/werner-lecture.html* **1913**.
5. Bailar, J. C. J., *Prep. Inorg. React.* **1964,** *1* (1).
6. Abrahams, B. F.; Hoskins, B. F.; Robson, R., A honeycomb form of cadmium cyanide. A new type of 3D arrangement of interconnected rods generating infinite linear channels of large hexagonal cross-section. *J. Chem. Soc., Chem. Commun.* **1990,** (1), 60-1.
7. Gable, R. W.; Hoskins, B. F.; Robson, R., A new type of interpenetration involving enmeshed independent square grid sheets. The structure of diaquabis(4,4'-bipyridine)zinc hexafluorosilicate. *J. Chem. Soc., Chem. Commun.* **1990,** (23), 1677-8.
8. Gable, R. W.; Hoskins, B. F.; Robson, R., Synthesis and structure of $[Me_4N][CuPt(CN)_4]$: an infinite three-dimensional framework related to PtS which generates intersecting hexagonal channels of large cross section. *J. Chem. Soc., Chem. Commun.* **1990,** (10), 762-3.
9. Grannas, M. J.; Hoskins, B. F.; Robson, R., A new tetranucleating tetraamino tetraphenolic macrocyclic ligand and the crystal structure of a Zn4 derivative. *J. Chem. Soc., Chem. Commun.* **1990,** (22), 1644-6.
10. Hoskins, B. F.; McKenzie, C. J.; Robson, R.; Zhenrong, L., Positively charged dipalladium complexes of a new thiophenoxide-hinged binucleating ligand. The crystal and molecular structure of micro -{4-methyl-2,6-bis[2-(2-pyridyl-.vkappa.N)ethylimino-.vkappa.N-methyl]thiophenolato-1.vkappa.S:2.vkappa.S}-bis[dichloropalladium(II)] chloride-water-methanol (1/1/0.5). *J. Chem. Soc., Dalton Trans.* **1990,** (9), 2637-41.
11. Hoskins, B. F.; Robson, R.; Smith, P., Synthesis and crystal structure of a complex in which a single macrocyclic ligand binds six copper(II) centers in a cyclohexane boat arrangement. *J. Chem. Soc., Chem. Commun.* **1990,** (6), 488-9.
12. Hoskins, B. F.; Robson, R., Infinite polymeric frameworks consisting of three dimensionally linked rod-like segments. *J. Am. Chem. Soc.* **1989,** *111* (15), 5962-4.
13. Yaghi, O. M., Construction of microporous materials from molecular building blocks. *Access Nanoporous Mater., [Proc. Symp.]* **1995**, 111-121.
14. Yaghi, O. M., Conversion of molecules and clusters to extended 3-D cage and channel networks. *Met.-Containing Polym. Mater., [Proc. Int. Symp.]* **1996**, 219-228.
15. Yaghi, O. M.; Li, H., T-Shaped Molecular Building Units in the Porous Structure of $Ag(4,4'\text{-bpy}).NO_3$. *J. Am. Chem. Soc.* **1996,** *118* (1), 295-6.
16. Yaghi, O. M.; Li, H.; Davis, C.; Richardson, D.; Groy, T. L., Synthetic Strategies, Structure Patterns, and Emerging Properties in the Chemistry of Modular Porous Solids. *Acc. Chem. Res.* **1998,** *31* (8), 474-484.

17. Ferey, G., Metal-organic frameworks. The young child of the porous solids family. *Stud. Surf. Sci. Catal.* **2007,** *170A* (From Zeolites to Porous MOF Materials), 66-86.
18. Lin, W., Homochiral porous metal-organic frameworks: why and how? *J. Solid State Chem.* **2005,** *178* (8), 2486-2490.
19. Rosi, N. L.; Eddaoudi, M.; Kim, J.; O'Keeffe, M.; Yaghi, O. M., Advances in the chemistry of metal-organic frameworks. *CrystEngComm* **2002,** *4*, 401-404.
20. Yaghi, O. M., Metal-organic Frameworks: A tale of two entanglements. *Nat. Mater.* **2007,** *6* (2), 92-93.
21. Yaghi, O. M.; O'Keeffe, M.; Ockwig, N. W.; Chae, H. K.; Eddaoudi, M.; Kim, J., Reticular synthesis and the design of new materials. *Nature (London, U. K.)* **2003,** *423* (6941), 705-714.
22. Yang, P.-P.; Li, B.; Wang, Y.-H.; Cu, W.; Liu, X., Synthesis, structure, and luminescence properties of zinc(II) and cadmium(II) complexes containing the flexible ligand of 3,3'-thiodipropionic acid. *Z. Anorg. Allg. Chem.* **2008,** *634* (6-7), 1221-1224.
23. Li, H.; Eddaoudi, M.; O'Keeffe, M.; Yaghi, M., Design and synthesis of an exceptionally stable and highly porous metal-organic framework. *Nature (London)* **1999,** *402* (6759), 276-279.
24. Maji, T. K.; Mukherjee, P. S.; Chaudhuri, N. R.; Mostafa, G.; Zangrando, E., 1D porous framework of copper(II) showing a novel coordination mode of Ni(CN)42. *Chem. Commun. (Cambridge, U. K.)* **2001,** (15), 1368-1369.
25. Chen, Z.; Fang, M.; Ren, P.; Li, X.-H.; Zhao, B.; Wei, S.; Cheng, P., Synthesis, structure and luminescent property of two new 2D metal-organic frameworks containing lanthanide ions. *Z. Anorg. Allg. Chem.* **2008,** *634* (2), 382-386.
26. Chen, Z.-F.; Zhang, Z.-L.; Tan, Y.-H.; Tang, Y.-Z.; Fun, H.-K.; Zhou, Z.-Y.; Abrahams, B. F.; Liang, H., Coordination polymers constructed by linking metal ions with azodibenzoate anions. *CrystEngComm* **2008,** *10*, 217-231.
27. Energy, U. S. D. o., http://www1.eere.energy.gov/hydrogenandfuelcells/storage/metal_hydrides.html. **2006**.
28. Rowsell, J. L. C.; Millward, A. R.; Park, K. S.; Yaghi, O. M., Hydrogen Sorption in Functionalized Metal-Organic Frameworks. *J. Am. Chem. Soc.* **2004,** *126* (18), 5666-5667.
29. Latroche, M.; Suble, S.; Serre, C.; Mellot-Draznieks, C.; Llewellyn, P. L.; Lee, J.-H.; Chang, J.-S.; Jhung, S. H.; Ferey, G., Hydrogen storage in the giant-pore metal-organic frameworks MIL-100 and MIL-101. *Angew. Chem., Int. Ed.* **2006,** *45* (48), 8227-8231.
30. Wong-Foy, A. G.; Matzger, A. J.; Yaghi, O. M., Exceptional H_2 Saturation Uptake in Microporous Metal-Organic Frameworks. *J. Am. Chem. Soc.* **2006,** *128*, 3494-3495.
31. Rowsell, J. L. C.; Yaghi, M., Effects of Functionalization, Caternation, and Variation of the Metal Oxide and Organic Linking Units on the Low-Pressure Hydrogen Adsorption Properties of Metal-Organic Frameworks. *J. Am. Chem. Soc.* **2006,** *128*, 1304-1315.
32. Chun, H.; Dybtsev, D. N.; Kim, H.; Kim, K., Synthesis, X-ray crystal structures, and gas sorption properties of pillared square grid nets based on paddle-wheel motifs: Implications for hydrogen storage in porous materials. *Chem.--Eur. J.* **2005,** *11* (12), 3521-3529.
33. Kesanli, B.; Cui, Y.; Smith, M. R.; Bittner, E. W.; Brockrath, B. C.; Lin, W., Highly interpenetrated metal-organic frameworks for hydrogen storage. *Angew. Chem., Int. Ed.* **2005,** *44* (1), 72-75.

34. Chen, B.; Ockwig, N. W.; Millward, A. R.; Contreras, D. S.; Yaghi, O. M., High H2 adsorption in a microporous metal-organic framework with open metal sites. *Angew. Chem., Int. Ed.* **2005,** *44* (30), 4745-4749.
35. Ezuhara, T.; Endo, K.; Aoyama, Y., Helical Coordination Polymers from Achiral Components in Crystals. Homochiral Crystallization, Homochiral Helix Winding in the Solid State, and Chirality Control by Seeding. *J. Am. Chem. Soc.* **1999,** *121* (14), 3279-3283.
36. Bradshaw, D.; Prior, T. J.; Cussen, E. J.; Claridge, J. B.; Rosseinsky, M. J., Permanent Microporosity and Enantioselective Sorption in a Chiral Open Framework. *J. Am. Chem. Soc.* **2004,** *126* (19), 6106-6114.
37. Seo, J. S.; Whang, D.; Lee, H.; Jun, S. I.; Oh, J.; Jeon, Y. J.; Kim, K., A homochiral metal-organic porous material for enantioselective separation and catalysis. *Nature (London)* **2000,** *404* (6781), 982-986.
38. Brandys, M.-C.; Puddephatt, R. J., Strongly Luminescent Three-Coordinate Gold(I) Polymers: 1D Chain-Link Fence and 2D Chickenwire Structures. *J. Am. Chem. Soc.* **2001,** *123* (20), 4839-4840.
39. Evans, O. R.; Xiong, R.-G.; Wang, Z.; Wong, G. K.; Lin, W., Crystal engineering of acentric diamondoid metal-organic coordination networks. *Angew. Chem., Int. Ed.* **1999,** *38* (4), 536-538.
40. Gavezzotti, A.; Flack, H., Crystal Packing. *International Union of Crystallography, http://ww1.iucr.org/comm/cteach/pamphlets/21/index.html* **2005**.
41. www.vwr.com.
42. Boyle, P. D., Growing Crystals That Will Make Your Crystallographer Happy. *Department of Chemistry, North Carolina State University* **2007**.
43. Mukherjee, R., Coordination Chemistry with Pyrazole-based Chelating Ligands: Molecular Structural Aspects. *Coordination Chemistry Reviews* **2000,** *203*, 151-218.
44. Liu, H.-K.; Huang, X.; Lu, T.; Wang, X.; Sun, W.-Y.; Kang, B.-S., Discrete and infinite 1D, 2D/3D cage frameworks with inclusion of anionic species and anion-exchange reactions of Ag_3L_2 type receptor with tetrahedral and octahedral anions. *Dalton Trans.* **2008,** (24), 3178-3188.
45. Choi, H. J.; Dinca, M.; Long, J. R., Broadly Hysteretic H2 Adsorption in the Microporous Metal-Organic Framework Co(1,4-benzenedipyrazolate). *J. Am. Chem. Soc.* **2008,** *130* (25), 7848-7850.
46. Castillo, I.; Fernandez-Gonzalez, J. M.; Garate-Morales, J. L., Synthesis and Solid State Structures of Copper(II) Complexes of Schiff Bases Derived From Cyclopropyl and Cyclobutylamine. *Journal of Molecular Structures* **2003,** *657*, 25-35.
47. Angulo-Cornejo, J.; Lino-Pacheco, M.; Richter, R.; Hennig, L.; Hallmeier, K.-H.; Beyer, L., Metal Chelates of N-benzothiazol-2-yl-, N-benzoxazol-2-yl- and N-(1H-benzimidazol-2-yl)-benzamide. *Inorganica Chimica Acta* **2000,** *305*, 38-45.
48. Dong, Y.-B.; Simith, M. D.; Loye, H.-C. z., Metal-Containing Ligands for Mixed-Metal Polymers: Novel Cu(II)-Ag(I) Mixed Metal Coordination Polymers Generated form [Cu(2-methylpyrazine-5-carboxylate)$_2$(H_2O)]. $3H_2O$ and Silver(I) Salts. *Inorg. Chem. (Washington, DC, U. S.)* **2000,** *39*, 1943-1949.
49. Clausen, H. F.; Overgaard, J.; Chen, Y. S.; Iversen, B. B., Synchrotron X-ray Charge Density Study of Coordination Polymer $Co_3(C_8H_4O_4)_4(C_4H_{12}N)_2(C_5H_{11}NO)_3$ at 16 K. *J. Am.*

Chem. Soc. **2008,** *130* (25), 7988-7996.
50. Yao, Y.; Che, Y.; Zheng, J., The Coordination Chemistry of Benzimidazole-5,6-dicarboxylic Acid with Mn(II), Ni(II), and Ln(III) Complexes (Ln = Tb, Ho, Er, Lu). *Cryst. Growth Des.*, ACS ASAP.
51. Liu, Q.-X.; Zhao, X.-J.; Wu, X.-M.; Liu, S.-W.; Zang, Y.; Ge, S.-S.; Wang, X.-G.; Guo, J.-H., Novel Cd(II) and Co(II) 2-D frameworks based on terephthalate and 1-substitutedimidazole mixed-ligands. *Inorg. Chem. Commun.* **2008,** *11* (7), 809-813.
52. Jolly, W. L., Modern Inorganic Chemistry. *McGraw-Hill, Inc* **1984**.
53. Gomez-Hortigueela, L.; Marquez-Alvarez, C.; Sastre, E.; Cora, F.; Perez-Pariente, J., Effect of fluorine-containing chiral templates on Mg distribution in the structure of MgAPO-5 and its influence on catalytic activity. *Catal. Today* **2006,** *114* (2-3), 174-182.
54. Chen, S.; Zhang, J.; Bu, X., Ionothermal Synthesis of Homochiral Framework with Acetate-Pillared Cobalt-Camphorate Architecture. *Inorg. Chem. (Washington, DC, U. S.)* **2008**, ACS ASAP.
55. Li, Y.-W.; Wang, Y.-H.; Li, Y.-G.; Wang, E.-B., New anion-templated 3D heterobimetallic open frameworks based on lanthanide-carboxylate layers and copper pillars. *J. Solid State Chem.* **2008,** *181* (6), 1485-1491.
56. Drago, R. S., Physical Methods for Chemist. *Saunders College Publishing* **1992**.
57. Willard, H. H.; Merritt, L. L., Jr.; Dean, J. A.; Settle, F. A., Jr., Instrumental Methods of Analysis. *WADSWORTH PUBLISHING COMPANY* **1988**.
58. Harrison, W. T. A., $(NC_5H_{12})_2.Zn_3(HPO_3)_4$: A Low-Density Framework Built Up from a Fully Connected (3,4) Net of ZnO4 Tetrahedra and HPO3 Pseudo Pyramids. *J. Solid State Chem.* **2001,** *160* (1), 4-7.
59. Dong, W.; Li, G.; Shi, Z.; Fu, W.; Zhang, D.; Chen, X.; Dai, Z.; Wang, L.; Feng, S., Hydrothermal synthesis and structural characterization of an organically-templated zincophosphite: $[C_4N_2H_{12}]_{0.5}.[Zn_3(HPO_3)_4].H_3O$. *Inorg. Chem. Commun.* **2003,** *6* (6), 776-780.
60. Liang, J.; Wang, Y.; Yu, J.; Li, Y.; Xu, R., Synthesis and structure of a new layered zinc phosphite $(C_5H_6N_2)Zn(HPO_3)$ containing helical chains. *Chem. Commun. (Cambridge, U. K.)* **2003,** (7), 882-883.
61. Chen, X.; Wang, Y.; Yu, J.; Zou, Y.; Xu, R., $(C_6H_{17}N_3)[Zn_4(PO_4)_2(HPO_3)_2]$: a new layered zinc phosphate-phosphite templated by 1-(2-aminoethyl)piperazine. *J. Solid State Chem.* **2004,** *177* (7), 2518-2522.
62. Fu, W.; Shi, Z.; Li, G.; Zhang, D.; Dong, W.; Chen, X.; Feng, S., Synthesis and characterization of an organically-templated zincophosphite: $[C_6H_{16}N_2].Zn_3(HPO_3)_4$. *Solid State Sci.* **2004,** *6* (2), 225-228.
63. Johnstone, J. A.; Harrison, W. T. A., Triethanolamine Zinc Phosphite, $(C_6H_{13}NO_3)Zn_2(HPO_3)$: A Templated Network or a Network of Clusters? *Inorg. Chem.* **2004,** *43* (15), 4567-4569.
64. Pan, J.-X.; Zheng, S.-T.; Yang, G.-Y., Hydrothermal Synthesis and Structure of a New Two-dimensionalZincophosphite: $Zn_2(HPO_3)_3{\times}H_2$DACH (DACH = 1,2-Diaminocyclohexane). *Chin. J. Struct. Chem.* **2004,** *23* (8), 850-854.
65. Wang, L.; Shi, Z.; Fu, W.; Li, G.; Zhang, D.; Dong, W.; Dai, Z.; Chen, X.; Feng, S., Hydrothermal synthesis and structural characterization of two organically templated

zincophosphites with three-dimensional frameworks, $(C_6H_{14}N_2).[Zn_3(HPO_3)_4]$ and $(C_4H_{12}N_2).[Zn_3(HPO_3)_4]$. *J. Solid State Chem.* **2004,** *177* (1), 80-88.
66. Zhang, D.; Shi, Z.; Dong, W.; Fu, W.; Wang, L.; Li, G.; Feng, S., Hydrothermal synthesis and structural characterization of novel organically templated zincophosphites: $[C_6H_4(CH_2NH_3)_2].[Zn_3(HPO_3)_4]$ and $[CH_3CH_2CH_2NH_3]_2.[Zn_3(HPO_3)_4]$. *J. Solid State Chem.* **2004,** *177* (1), 343-349.
67. Armstrong, A. F.; Chivers, T.; Krahn, M.; Parvez, M., Synthesis and structural characterization of zinc complexes of the imido-amido phosphate anions OP[(NHR)$_3$-x(NR)]x- (R = Me, t-Bu; x = 1-3) and EP[(NH-t-Bu)$_2$(N-t-Bu)]-(E = S, NSiMe3). *Can. J. Chem.* **2005,** *83* (10), 1768-1778.
68. Groves, J. A.; Wright, P. A.; Lightfoot, P., The pH-controlled hydrothermal synthesis and crystal structures of two zinc N,N'-piperazinebis(methylenephosphonate) frameworks. *Dalton Trans.* **2005,** (11), 2007-2010.
69. Wang, L.; Yang, M.; Li, G.; Shi, Z.; Feng, S., Hydrothermal synthesis and characterization of a new three-dimensional hybrid zinc phosphate $[Zn_2(HPO_4)_2(4,4'\text{-bipy})].3H_2O$ with neutral porous framework. *J. Solid State Chem.* **2006,** *179* (1), 156-160.
70. Phillips, M. L. F.; Nenoff, T. M.; Thompson, C. T.; Harrison, W. T. A., Variations on the (3,4)-Net Motif in Organo-Zincophosphite Chemistry: Syntheses and Structures of $(CN_3H_6)_2.Zn_3(HPO_3)_4.H_2O$ and $H_3N(CH_2)_3NH_3.Zn_3(HPO_3)_4.H_2O$. *J. Solid State Chem.* **2002,** *167* (2), 337-343.
71. Liu, W.; Yang, X.-X.; Chen, H.-H.; Zhao, J.-T., Synthesis, characterizations and spectral properties of a new one-dimensional organically templated zincophosphite. *J. Alloys Compd.* **2005,** *392* (1-2), 100-104.
72. Kitagawa, S.; Kitaura, R.; Noro, S.-i., Functional porous coordination polymers. *Angew. Chem., Int. Ed.* **2004,** *43* (18), 2334-2375.
73. Hsu, Y.-F.; Lin, C.-H.; Chen, J.-D.; Wang, J.-C., A novel interpenetrating diamondoid network from self-assembly of N,N'-di(4-pyridyl)adipoamide and copper sulfate: an unusual 12-fold, [6 + 6] mode. *Cryst. Growth Des.* **2008,** *8* (4), 1094-1096.
74. Shi, W.-J.; Ruan, C.-X.; Li, Z.; Li, M.; Li, D., Tuning framework formation by flexible ligand elongation and second ligating spacer variation: increasing dimensionality and macrocycle size. *CrystEngComm* **2008,** *10* (6), 778-783.
75. Ferguson, G.; Glidewell, C.; McManus, G. D.; Meehan, P. R., A perforated molecular tape in the 1:1 salt of 4,4'-trimethylenedipyridine and 1,3,5-benzenetricarboxylic acid. *Acta Crystallogr., Sect. C: Cryst. Struct. Commun.* **1998,** *C54* (3), 418-421.
76. Ferguson, G.; Glidewell, C.; Gregson, R. M.; Lavender, E. S., Crystal engineering using bisphenols: interwoven ladders, sheet and framework structures in the binary adducts of 4,4'-sulfonyldiphenol with pyrazine (2/1), 4,4'-bipyridyl (1/1), trans-1,2-bis(4-pyridyl)ethene (1/1), 1,2-bis(4-pyridyl)ethane (1/1) and 4,4'-trimethylenedipyridine (1/1), and in 4,4'-sulfonyldiphenol-4,4'-trimethylenedipiperidine-water (2/2/1). *Acta Crystallogr., Sect. B: Struct. Sci.* **1999,** *B55* (4), 573-590.
77. Wheatley, P. S.; Lough, A. J.; Ferguson, G.; Glidewell, C., Four interpenetrating three-dimensional frameworks in the hydrogen-bonded structure of 5-hydroxyisophthalic acid-4,4'-trimethylenedipyridine (1/1). *Acta Crystallogr., Sect. C: Cryst. Struct. Commun.*

1999, *C55* (9), 1486-1489.
78. Bowes, K. F.; Ferguson, G.; Lough, A. J.; Glidewell, C., 4,4'-Trimethylenedipyridinium bis[carboxymethylphosphonate(1-)]: a three-dimensional framework structure built from O-H...O, N-H...O and C-H...O hydrogen bonds. *Acta Crystallogr., Sect. C: Cryst. Struct. Commun.* **2003,** *C59* (8), o464-o466.
79. Lee, T. W.; Lau, J. P.; Szeto, L., 4,4'-Trimethylenedipyridinium dinitrate. *Acta Crystallogr., Sect. E: Struct. Rep. Online* **2003,** *E59* (6), o792-o793.
80. Aakeroey, C. B.; Desper, J.; Urbina, J. F., Is conformational flexibility in a supramolecular reagent advantageous for high-yielding co-crystallization reactions? *CrystEngComm* **2005,** *7*, 193-201.
81. Bhogala, B. R.; Basavoju, S.; Nangia, A., Three-Component Carboxylic Acid-Bipyridine Lattice Inclusion Host. Supramolecular Synthesis of Ternary Cocrystals. *Cryst. Growth Des.* **2005,** *5* (5), 1683-1686.
82. Ma, Z. C., Crystal structure of (R)-1,1'-bi-2-naphthol 1,3-bis(pyrid-4-yl)propane, C20H14O2.C13H14N2. *Z. Kristallogr. - New Cryst. Struct.* **2006,** *221* (1), 65-67.
83. Ranjbar, Z. R.; Morsali, A.; Zhu, L.-G., Spectroscopic, thermal and structural studies of cocrystal of 2,2'-diamino-4,4'-bis(1,3-thiazole) with 4,4'-bipyridine, 1,2-bis(4-pyridyl)ethylene and 1,3-bis(4-pyridyl)propane. *J. Mol. Struct.* **2007,** *826* (1), 29-35.
84. Lin, Z.-E.; Fan, W.; Gao, F.; Chino, N.; Yokoi, T.; Okubo, T., A New Organically Templated Zinc Phosphite Synthesized in Phosphorous Acid Flux and Its Hydrothermal Analogue. *Cryst. Growth Des.* **2006,** *6* (11), 2435-2437.
85. Hu, L.; Fan, J.; Slebodnick, C.; Hanson, B. E., Structural Diversity in 4,4'-Trimethylenedipyridine-zinc phosphite Hybrids: Incorporation of Neutral Guest Molecules in Hybrid Materials. *Inorganic Chemistry* **2006,** *45* (19), 7681-7688.
86. Niu, Y.; Song, Y.; Zhang, N.; Hou, H.; Che, D.; Fan, Y.; Zhu, Y.; Duan, C., Reactivity of polyiodides towards 1,3-bis(4-pyridyl)propane (bpp): a new CuI cluster polycatenane framework and a novel 2D AgI cluster motif. *Eur. J. Inorg. Chem.* **2006,** (11), 2259-2267.
87. Dai, Y. M.; Shen, H. Y.; Huang, J. F., Terephthalic acid-1,3-di-4-pyridylpropane (1/1). *Acta Crystallogr., Sect. E: Struct. Rep. Online* **2005,** *E61* (10), o3410-o3411.
88. Kao, Y.-C.; Chen, J.-D., Transition Metal Halide Salts of 1,3-bis(4-Pyridyl)propane: Synthesis and Structural Characterization. *Struct. Chem.* **2004,** *15* (4), 269-276.
89. Liao, Y.-C.; Liao, F.-L.; Chang, W.-K.; Wang, S.-L., A Zeolitic Organo-Metallophosphate Hybrid Material with Bimodal Porosity. *J. Am. Chem. Soc.* **2004,** *126* (5), 1320-1321.
90. Kong, D.; McBee, J. L.; Clearfield, A., Crystal Engineered Acid-Base Complexes with 2D and 3D Hydrogen Bonding Systems Using a Bisphosphonic Acid as the Building Block. *Cryst. Growth Des.* **2005,** *5* (2), 643-649.
91. Han, L.; Valle, H.; Bu, X., Homochiral Coordination Polymer with Infinite Double-Stranded Helices. *Inorg. Chem.* **2007,** *46* (5), 1511-1513.
92. Zamora, M. A.; Santagata, L. N.; Masman, M. F.; Bombasaro, J. A.; Freile, M. L.; Enriz, R. D., Conformational study of internally retrograde and quasi-retrograde molecules - An ab initio and DFT study. *Can. J. Chem.* **2005,** *83* (2), 122-137.
93. Stewart James, J. P., Comparison of the accuracy of semiempirical and some DFT methods for predicting heats of formation. *Journal of molecular modeling* **2004,** *10* (1), 6-12.

94. Margraf, G.; Lerner, H.-W.; Bolte, M.; Wagner, M., Kristallstruktur des Zinkamids $Zn[N(SiMe_3)_2]_2$. *Z. Anorg. Allg. Chem.* **2004,** *630*, 217-218.
95. Hannant, M. D.; Schormann, M.; Bochmann, M., Synthesis and catalytic activity of three-coordinate zinc cations. *J. Chem. Soc., Dalton Trans.* **2002,** (22), 4071-4073.
96. Evans, O. R.; Lin, W., Rational Design of Nonlinear Optical Materials Based on 2D Coordination Networks. *Chem. Mater.* **2001,** *13* (9), 3009-3017.
97. Fox Derek, C.; Fiedler Adam, T.; Halfen Heather, L.; Brunold Thomas, C.; Halfen Jason, A., Electronic structure control of the nucleophilicity of transition metal-thiolate complexes: an experimental and theoretical study. *J Am Chem Soc* **2004,** *126* (24), 7627-38.
98. Fan, J.; Sui, B.; Okamura, T.-a.; Sun, W.-Y.; Tang, W.-X.; Ueyama, N., Synthesis, structures and properties of two-dimensional honeycomb and stepwise networks from self-assembly of tripodal ligand 1,3,5-tris(imidazol-1-ylmethyl)-2,4,6-trimethylbenzene with metal salts. *J. Chem. Soc., Dalton Trans.* **2002,** (20), 3868-3873.
99. Conzi, P.; Pinto, A.; Roda, G.; Tamborini, L.; Arosio, D.; De Micheli, C., Stereoselective synthesis of 4-amino-3-hydroxy-4,5,6,6a-tetrahydro-3aH-cyclopenta[d]isoxazole-4-carboxylic acid, a conformationally constrained analogue of aspartic acid. *Synthesis* **2007,** (14), 2145-2148.
100. Zhang, X.-J.; Xing, Y.-H.; Sun, Z.; Han, J.; Zhang, Y.-H.; Ge, M.-F.; Niu, S.-Y., A Series of Two-Dimensional Metal-Organic Frameworks Based on the Assembly of Rigid and Flexible Carboxylate-Containing Mixed Ligands with Lanthanide Metal Salts. *Cryst. Growth Des.* **2007,** *7* (10), 2041-2046.
101. Wang, H.-Y.; Gao, S.; Huo, L.-H.; Ng, S. W.; Zhao, J.-G., Three interpenetrated frameworks assembly from a long multicarboxylate ligand and transition metal. *Cryst. Growth Des.* **2008,** *8* (2), 665-670.
102. Zhao, H.; Ye, Q.; Qu, Z.-r.; Fu, D.-W.; Xiong, R.-G.; Huang, S. D.; Chan, P. W. H., Huge deuterated effect on permittivity in a metal-organic framework. *Chem.--Eur. J.* **2008,** *14* (4), 1164-1168.
103. Fluck, E.; Binder, H., Preparation of compounds with phosphorus-phosphorus and phosphorus-phosphorus-phosphorus frameworks. *Inorg. Nucl. Chem. Lett.* **1967,** *3* (8), 307-13.
104. Shieh, M.; Martin, K. J.; Squattrito, P. J.; Clearfield, A., New low-dimensional zinc compounds containing zinc-oxygen-phosphorus frameworks: two-layered inorganic phosphites and a polymeric organic phosphinate. *Inorg. Chem.* **1990,** *29* (5), 958-63.
105. Burford, N.; Dyker, C. A.; Lumsden, M.; Decken, A., Small cyclopolyphosphinophosphonium cations: Systematic development of fundamental catena-phosphorus frameworks. *Angew. Chem., Int. Ed.* **2005,** *44* (38), 6196-6199.
106. Li, M.-X.; Miao, Z.-X.; Shao, M.; Liang, S.-W.; Zhu, S.-R., Metal-Organic Frameworks Constructed from 2,4,6-Tris(4-pyridyl)-1,3,5-triazine. *Inorg. Chem. (Washington, DC, U. S.)* **2008,** *47* (11), 4481-4489.
107. Murugavel, R.; Walawalkar, M. G.; Dan, M.; Roesky, H. W.; Rao, C. N. R., Transformations of molecules and secondary building units to materials: a bottom-up approach. *Acc Chem Res* **2004,** *37* (10), 763-74.
108. O'Keeffe, M.; Eddaoudi, M.; Li, H.; Reineke, T.; Yaghi, O. M., Frameworks for extended solids: geometrical design principles. *J. Solid State Chem.* **2000,** *152* (1), 3-20.

109. Fan, J.; Slebodnick, C.; Troya, D.; Angel, R.; Hanson, B. E., Five New Zinc Phosphite Structures: Tertiary Building Blocks in the Construction of Hybrid Materials. *Inorg. Chem.* **2005,** *44* (8), 2719-2727.
110. Fan, J.; Slebodnick, C.; Angel, R.; Hanson, B. E., New Zinc Phosphates Decorated by Imidazole-Containing Ligands. *Inorg. Chem.* **2005,** *44* (3), 552-558.
111. Fan, J.; Hanson, B. E., Novel Zinc Phosphate Topologies Defined by Organic Ligands. *Inorg. Chem.* **2005,** *44* (20), 6998-7008.
112. Fan, J.; Slebodnick, C.; Hanson, B. E., A tetranuclear zinc cluster, $(bipy)_4Zn_4(HPO_3)_4$, that stabilizes a hydrogen bonded chain of water molecules: Transformation of a zinc phosphite 4-ring to a cluster. *Inorg. Chem. Commun.* **2006,** *9* (1), 103-106.
113. Lin, Z.-E.; Zhang, J.; Zheng, S.-T.; Yang, G.-Y., A new inorganic-organic hybrid with zinc phosphate layers pillared by the 4,4'-bipyridine units. *Z. Anorg. Allg. Chem.* **2005,** *631* (1), 155-159.
114. Lin, Z.-E.; Zhang, J.; Zheng, S.-T.; Yang, G.-Y., Synthesis and characterization of a new hybrid zinc phosphite $(4,4'\text{-bipy})[Zn(HPO_3)]_2$ with a pillared layer structure. *Microporous Mesoporous Mater.* **2004,** *68* (1-3), 65-70.
115.Paz, F. A. A.; Klinowski, J., Two- and Three-Dimensional Cadmium-Organic Frameworks with Trimesic Acid and 4,4'-Trimethylenedipyridine. *Inorg. Chem.* **2004,** *43* (13), 3882-3893.
116. Kong, D.; Zon, J.; McBee, J.; Clearfield, A., Rational Design and Synthesis of Porous Organic-Inorganic Hybrid Frameworks Constructed by 1,3,5-Benzenetriphosphonic Acid and Pyridine Synthons. *Inorg. Chem.* **2006,** *45* (3), 977-986.
117. Farrugia, L. J., WinGX Suite for Small-Molecule Single-Crystal Crystallography. *J. Appl.Cryst.* **1999,** *32*, -838.
118. Oxford Diffraction (2004), CrysAlisPro and RED (version 171.32), Oxford Diffraction Ltd., Abingdon, England. **2004**.
119. Sheldrick, G. M., A short history of SHELX. *Acta Crystallogr., Sect. A: Found. Crystallogr.* **2008,** *A64* (1), 112-122.
120. Cox, S. D.; Gier, T. E.; Stucky, G. D.; Bierlein, J., Inclusion Tuning of Nonlinear Optical Materials: Switching the SHG of p-nitroaniline and 2-methyl-p-nitroaniline with Molecular Sieve Hosts. *J. Am. Chem. Soc.* **1988,** *110* (9), 2986-2987.
121. Cox, S. D.; Gier, T. E.; Stucky, G. D., Second Harmonic Generation by the self-Aggregation of Organic Guests in Molecular Sieve Hosts. *Chem. Mater.* **1990,** *2* (5), 609-619.
122. Poutasse, C. A.; Day, R. O.; Holmes, R., Hydrogen Bonded Phosphate Esters. Synthesis and Structure of Catechol-containing Salts of 2-Hydroxyphenyl Phenylphosphonic Acid. *J. Am. Chem. Soc.* **1984,** *106* (13), 3814-3820.
123. Bosshard, C.; Pan, F.; Wong, M. S.; Manetta, S.; Spreiter, R.; Cai, C.; Gunter, P.; Gramlich, V., Nonlinear optical organic co-crystals of merocyanine dyes and phenolic derivatives with short hydrogen bonds. *Chem. Phys.* **1999,** *245* (1-3), 377-393.
124. Etter, M. C.; Baures, P. W., Triphenylphoaphine Oxide as a Crystallization Aid. *J. Am. Chem. Soc.* **1988,** *110*, 639-640.
125. Etter, M. C.; Reutzel, S. M., Hydrogen Bond Directed Cocrystallization and Molecular Recognition Properties of Acyclic Imides. *J. Am. Chem. Soc.* **1991,** *113*, 2586-2598.

126. Coupar, P. I.; Glidewell, C.; Ferguson, G., Crystal engineering using bisphenols and trisphenols. Complexes with hexamethylenetetramine (HMTA): strings, multiple helixes and chains-of-rings in the crystal structures of the adducts of HMTA with 4,4'-thiodiphenol (1/1), 4,4'-sulfonyldiphenol (1/1), 4,4'-isopropylidenediphenol (1/1), 1,1,1-tris(4-hydroxyphenyl)ethane (1/2) and 1,3,5-trihydroxybenzene (2/3). *Acta Crystallogr., Sect. B: Struct. Sci.* **1997,** *B53* (3), 521-533.
127. Carlucci, L.; Ciani, G.; Proserpio, D. M., A new type of entanglement involving one-dimensional ribbons of rings catenated to a three-dimensional network in the nanoporous structure of $[Co(bix)_2(H_2O)_2](SO_4).7H_2O$ [bix = 1,4-bis(imidazol-1-ylmethyl)benzene]. *Chem. Commun. (Cambridge, U. K.)* **2004,** (4), 380-381.
128. Fei, B.-L.; Sun, W.-Y.; Zhang, Y.-A.; Yu, K.-B.; Tang, W.-X., Synthesis and crystal structure of an infinite one-dimensional chain containing a poly-metallocage of MnII with 4,4'-bis(imidazol-1-ylmethyl)biphenyl. *Dalton* **2000,** (14), 2345-2348.
129. Kondo, M.; Yoshitomi, T.; Seki, K.; Matsuzaka, H.; Kitagawa, S., Three-dimensional framework with channeling cavities for small molecules: $\{[M_2(4,4'\text{-bpy})_3(NO_3)_4].xH_2O\}n$ (M = Co, Ni, Zn). *Angew. Chem., Int. Ed. Engl.* **1997,** *36* (16), 1725-1727.
130. Kepert, C. J.; Rosseinsky, M. J., Zeolite-like crystal structure of an empty microporous molecular framework. *Chem. Commun. (Cambridge)* **1999,** (4), 375-376.
131. Darensbourg, D. J.; Lee, W.-Z.; Yarbrough, J. C., Synthesis and Characterization of a Monocyanide-Bridged Bimetallic Iron(II) and Copper(I) Complex. *Inorg. Chem. (Washington, DC, U. S.)* **2001,** *40*, 6533-6536.
132. Walfort, B.; Auth, T.; Degel, B.; Helten, H.; Stalke, D., Copper and Silver Trimidosulfites: $S(N^tBu)_3^{2-}$-Bicapped M_3-Triangles Connected via Lithium Halide Ladders or Fragments Thereof. *Organometallics* **2002,** *21*, 2208-2214.
133. Gabelica, Z.; Fernandes, A.; Ribeiro, M. F.; Lourenco, J. P.; Valange, S.; Louati, A.; Murphy, D. M., Unusual framework stabilization of Cu(II) and Cu(I) ions in a novel copper-substituted aluminophosphate with AEN topology prepared by one pot synthesis. *Stud. Surf. Sci. Catal.* **2007,** *170A* (From Zeolites to Porous MOF Materials), 185-192.
134. Barrier, N.; Hervieu, M.; Nguyen, N.; Raveau, B., Example of unusual tetrahedral coordination of Cu(I) in oxides. Cu3VO4. *Solid State Sci.* **2008,** *10* (2), 137-140.
135. Kirillov, A. M.; Smolenski, P.; Guedes da Silva, M. F. C.; Kopylovich, M. N.; Pombeiro, A. J. L., Three-dimensional hydrogen-bonded supramolecular assembly in tetrakis(1,3,5-triaza-7-phosphaadamantane)copper(I) chloride hexahydrate. *Acta Crystallogr., Sect. E: Struct. Rep. Online* **2008,** *E64* (5), m603-m604.
136. Comba, P.; Jurisic, P.; Lampeka, Y. D.; Peters, A., Axial Bonds in Copper(II) Compounds. *Inorganica Chimica Acta* **2001,** *324*, 99-107.
137. Noro, S.-i.; Kitaura, R.; Kondo, M.; Kitagawa, S.; Ishii, T.; Matsuzaka, H.; Yamashita, M., Framework Engineering by Anions and Porous Functionalities of Cu(II)/4,4'-bpy Coordination Polymers. *J. Am. Chem. Soc.* **2002,** *124* (11), 2568-2584.
138. Cai, Y.-P.; Su, C.-Y.; Xu, A.-w.; Kang, B.-S.; Tong, Y.-X.; Liu, H.-Q.; Jie, S., Synthesis and Characterization of Copper(II) Complexes of Bis(acatylacetone)trimethylenediimine. *Polyhedron* **2001,** *20*, 657-662.
139. Zhang, P.; Niu, Y.-Y.; Wu, B.-L.; Zhang, H.-Y.; Niu, C.-Y.; Hou, H.-W., 2D frameworks of Cu(II) and Zn(II) organo-metallic polymers self-assembled with

N,N'-(1,2-phenylene)diisonicotinamide: Syntheses, structures, photoluminescence, and thermal properties. *Inorg. Chim. Acta* **2008,** *361* (9-10), 2609-2615.
140. Puiu, S. C.; Warren, T. H., Three-Coordinate beta -Diketiminato Nickel Nitrosyl Complexes from Nickel(I)-Lutidine and Nickel(II)-Alkyl Precursors. *Organometallics* **2003,** *22* (20), 3974-3976.
141. Zhu, Y.-Z.; Liu, J.-Y.; Li, Y.-S.; Tong, Y.-J., Synthesis, Structure and Norbornene Polymerization Behavior of Nickel Complexes Bearing Two beta-Ketoiminato Chelate Ligands. *Journal of Organometallic Chemistry* **2004,** *689*, 1295-1303.
142. Morale, F.; Data, R. W.; Duillon, D.; Bruce, D.; Finn, R. L.; Wilson, C.; Blake, A. J.; Schroder, M.; Donnio, B., Columnar Mesomorphism form Hemi-Disklike Metallomesogens Derived from 2,6-Bis[3',4',5'-tri(alkoxy)phenyliminomethyl]pyridines (L): Crystal and Molecular Structures of $[M(L)Cl_2]$ (M = Mn, Ni, Zn). *Chem. Eur. J.* **2003,** *9*, 2484-2501.
143. Goher, M. A. S.; Escuer, A.; Mautner, F. A.; Al-Salem, N. A., A new series of 1D polymeric nickel(II) complex cations of pyridine derivative ligands with a single micro -1,3 azide bridge and x-ray crystal structure and magnetic properties of polymeric {[Ni(4-ethylpyridine)4(N3)]n(PF6)n}. *Polyhedron* **2002,** *21* (19), 1871-1876.
144. Oxford Diffraction (2008), CrysAlisPro and RED (version 171.32), Oxford Diffraction Ltd., Abingdon, England.
145. Fan, J.; Hanson, B. E., A Two-Dimensional Cationic Lattice Built from $[Zn_6(HPO_4)_2(PO_4)]^{2+}$ Clusters *J. C. S. Chem. Commun.* **2005**, 2327-2329.
146. Tian, G.; Zhu, G.; Yang, X.; Fang, Q.; Xue, M.; Sun, J.; Wei, Y.; Qiu, S., A Chiral Layered Co(II) Coordination Polymer with Helical Chains from Achiral Materials. *Chem. Commun. (Cambridge)* **2005**, 1396-1398.
147. Hirano, T.; Kuroda, M.; Takeda, N.; Hayashi, M.; Mukaida, M.; Oi, T.; Nagao, H., Cis-trans Isomerization of $\{RuNO\}^6$-type Nitrosylruthenium Complexes Containing 2-pyridinecarboxylate and Structural Characterization of a u-H_3O_2 Bridged Dinuclear Nitrosylruenium Complex. *J. Chem. Soc., Dalton Trans.* **2002**, 2158-2162.
148. March, R.; Clegg, W.; Coxall, R. A.; Cucurull-Sanchez, L., Synthesis, Characterization and Magnetic Properties of Cobalt(II) Complexes with Picolinic Acid Derivatives: the Crystal and Molecular Structures of $[Co(MeC_5H_3NCOO)_2(H_2O)]$ and $[CoCl_2(C_5H_4NCOOPr^i)_2]$. *Inorganica Chimica Acta* **2003,** *353*, 129-138.
149. Huang, D.; Wang, W.; Zhang, X.; Chen, C.; Chen, F.; Liu, Q.; Liao, D.; Li, L.; Sun, L., Synthesis, Structural Characterizations and Magnetic Properties of a Series of Mono-, Di- and Polynuclear Manganese Pyridinecarboxylate Compounds. *Eur. J. Inorg. Chem.* **2004**, 1454-1464.
150. Ouellette, W.; Hudson, B. S.; Zubieta, J., Hydrothermal and Structural Chemistry of the Zinc(II)- and Cadmium(II)-1,2,4-Triazolate Systems. *Inorg. Chem. (Washington, DC, U. S.)* **2007,** *46*, 4887-4904.
151. Houlihan, W. J. 2- Or 4-Substituted-[2-(1H-imidazol-1-yl)ethyl]piperidines as neoplasm inhibitors. 89-355956
4925851, 19890523., 1990.
152. Missavage, R. J.; Belford, R. L.; Paul, I. C., The Crystal and Molecular Structure of Tetrasodium Copper(II)-dI-Tartrate Decahydrate. *J. Coord. Chem.* **1972,** *2*, 145-157.
153. Sircar, J. K.; Yadava, K. L., Ionophoretic Studies in Copper(II)-, Nickel(II)-, Cobalt(II)-,

Uranyl(II)-, and Thorium(IV)-Tartaric Acid Systems. *J. Chem. Eng. Data* **1982,** *27*, 231-233.
154. Gregory, D. D.; Wan, Z.; Jenks, W. S., Photodeoxygenation of Dibenzothiophene Sulfoxide: Evidence for a Unimolecular S-O Cleavage Mechanism. *J. Am. Chem. Soc.* **1997,** *119* (1), 94-102.
155. Fowler, F. W.; Lauher, J. W., A rational design of molecular materials. *J. Phys. Org. Chem.* **2000,** *13* (12), 850-857.
156. Beatty, A. M., Open-framework coordination complexes from hydrogen-bonded networks: toward host/guest complexes. *Coord. Chem. Rev.* **2003,** *246* (1-2), 131-143.
157. Kampschulte, L.; Lackinger, M.; Maier, A.-K.; Kishore, R. S. K.; Griessl, S.; Schmittel, M.; Heckl, W. M., Solvent Induced Polymorphism in Supramolecular 1,3,5-Benzenetribenzoic Acid Monolayers. *J. Phys. Chem. B* **2006,** *110* (22), 10829-10836.
158. Bernstein, J.; Davis, R. E.; Shimoni, L.; Chang, N.-L., Patterns in Hydrogen Bonding: Functionality and Graph Set Analysis in Crystals. *Angew. Chem. Int. Ed.* **1995,** *34*, 1555-1573.
159. Desiraju, G. R., The C-H...O hydrogen bond in crystals: what is it? *Acc. Chem. Res.* **1991,** *24* (10), 290-6.
160. Etter, M. C., Encoding and Decoding Hydrogen-Bond Patterns of Organic Compounds. *Acc. Chem. Res.* **1990,** *23*, 120-126.
161. Hunter, C. A.; Lawson, K. R.; Perkins, J.; Urch, C. J., Aromatic Interactions. *J. Chem. Soc., Perkin Trans.* **2001,** *2*, 651-669.
162. Rang, A.; Nieger, M.; Engeser, M.; Luetzen, A.; Schalley, C. A., Self-assembling squares with amino acid-decorated bipyridines: heterochiral self-sorting of dynamically interconverting diastereomers. *Chem. Commun. (Cambridge, U. K.)* **2008,** (39), 4789-4791.

Appendix A: Thermal Gravimetric Analysis (TGA)

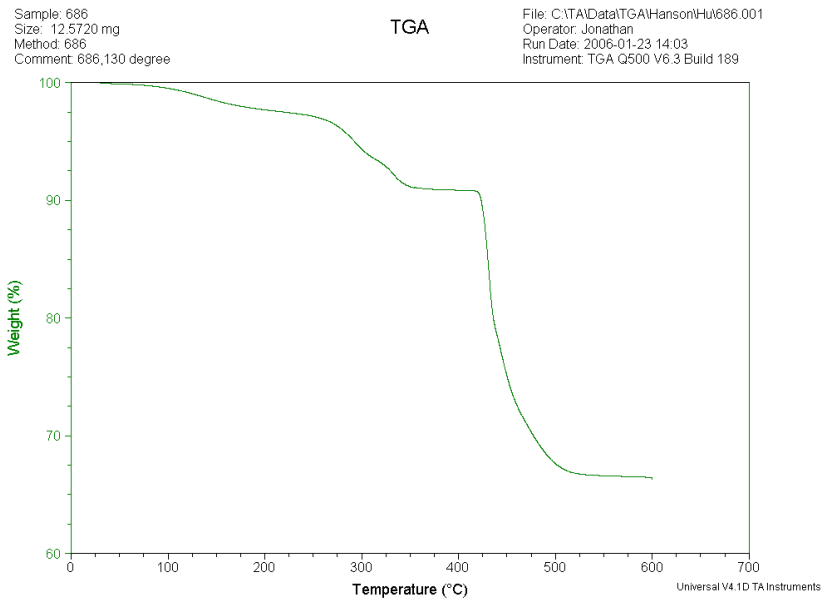

TGA for **1**

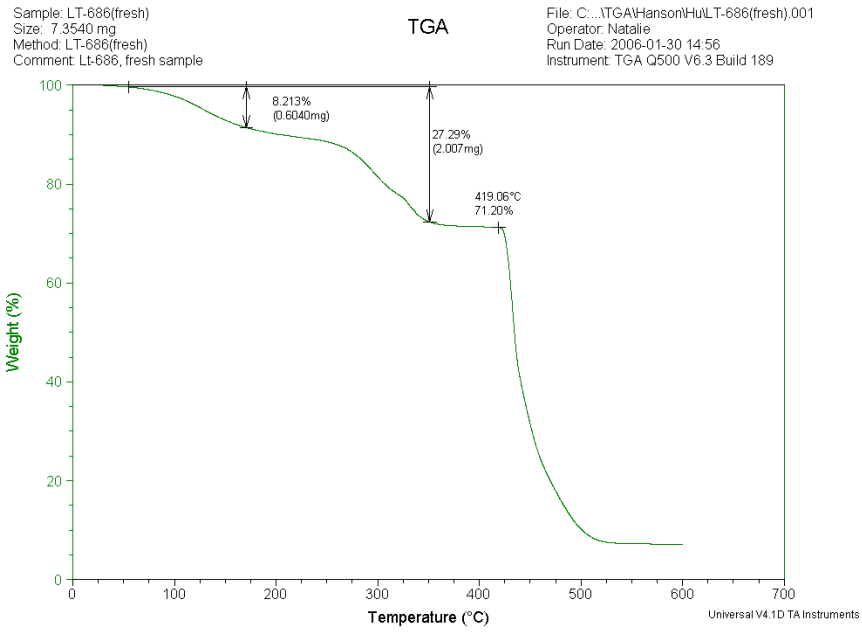

TGA for **2**

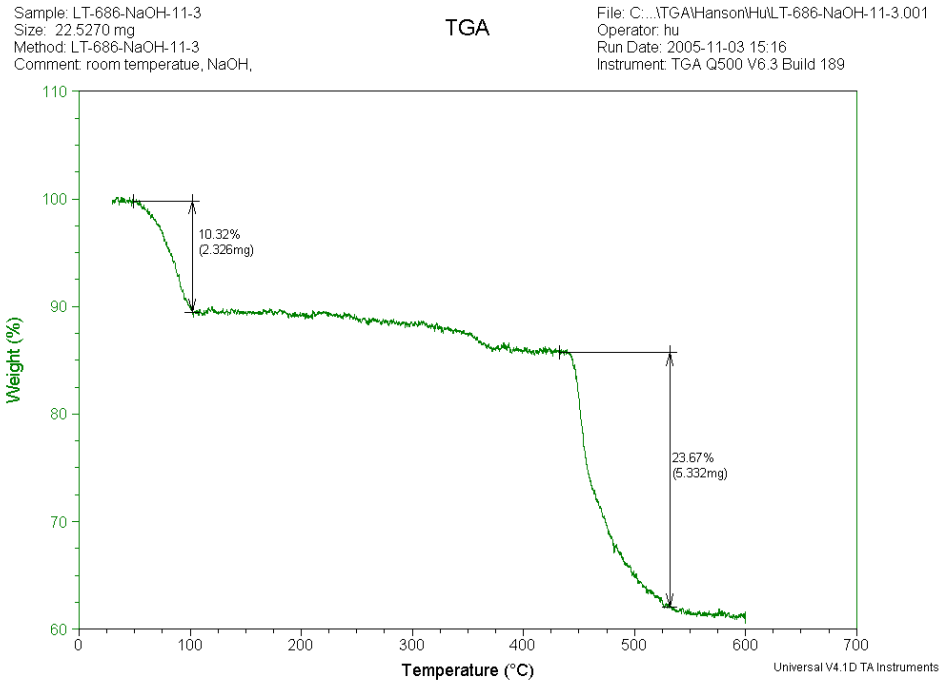

TGA for **3**

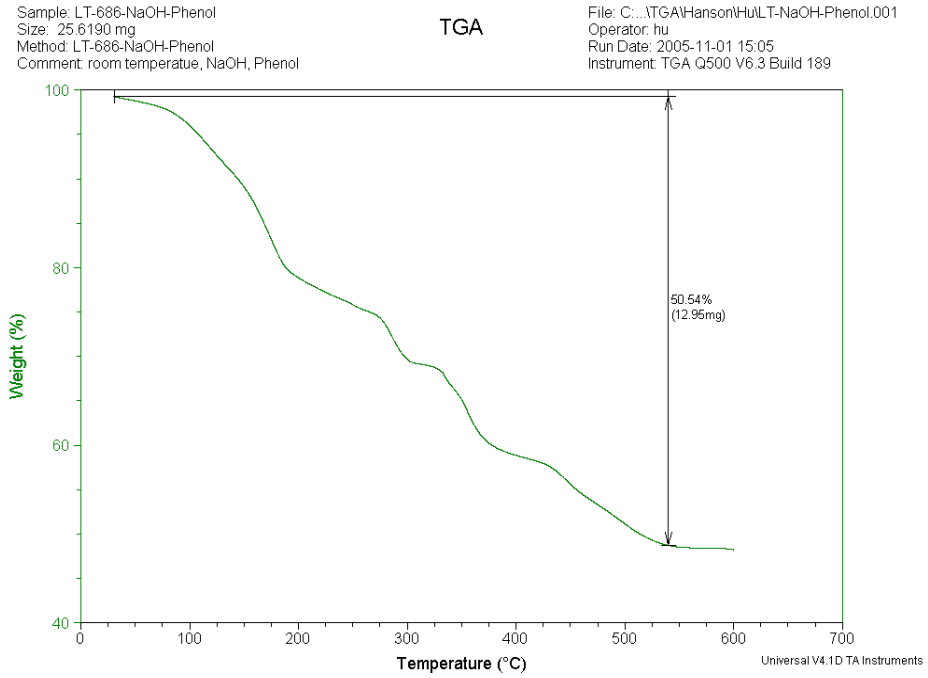

TGA for **4**

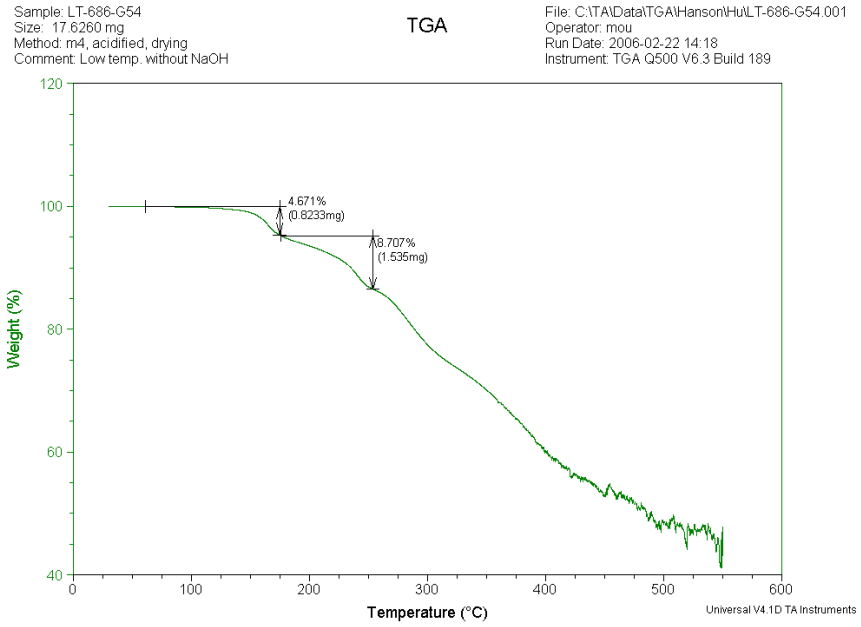

TGA for **5**

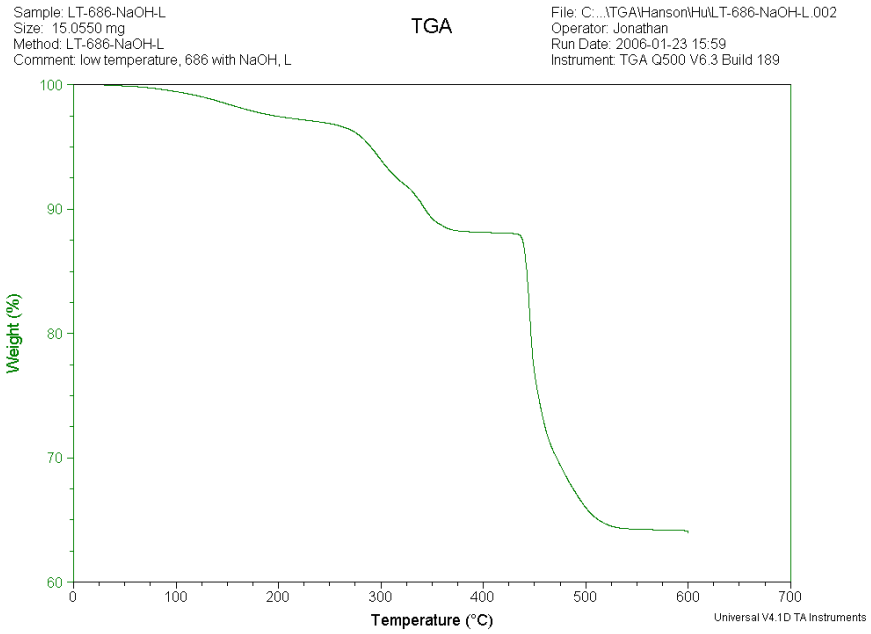

TGA for **6**

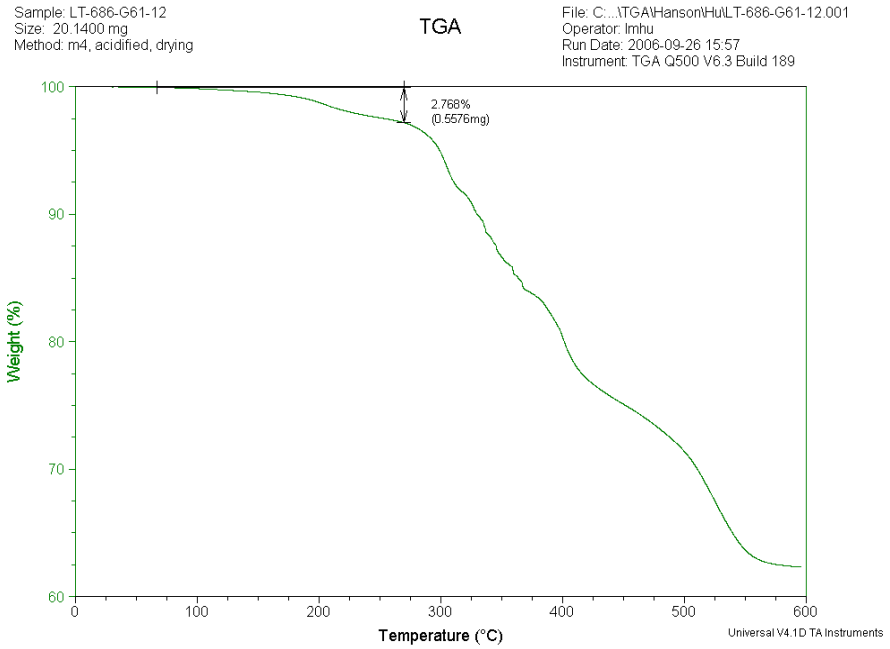

TGA for **7**

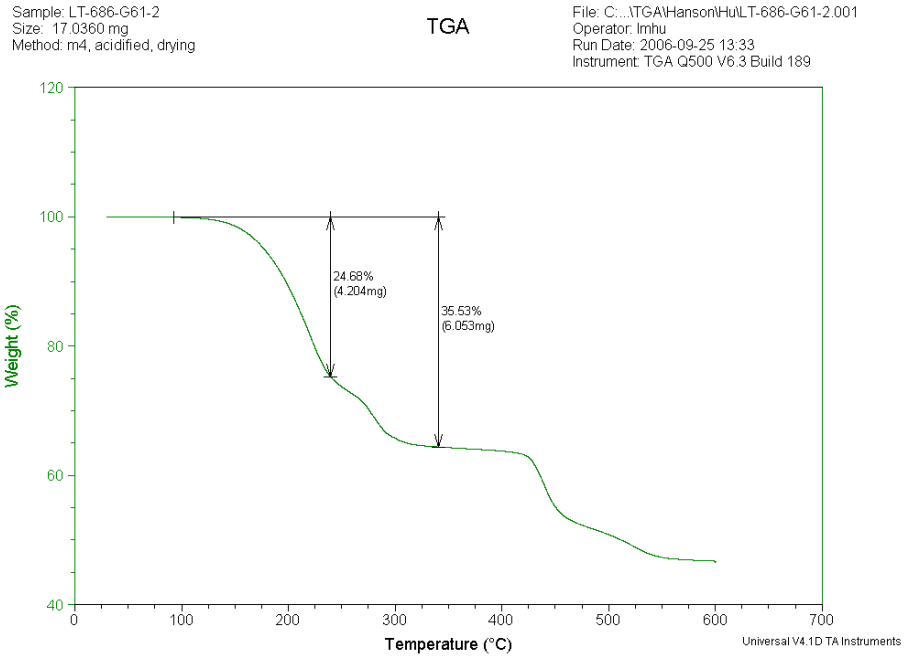

TGA for **8**

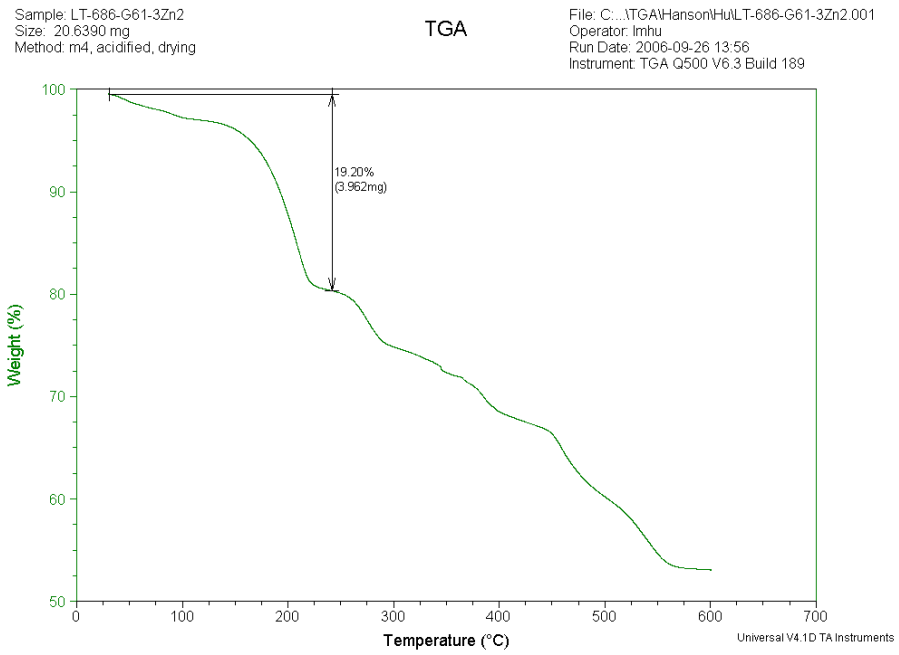

TGA for **9**

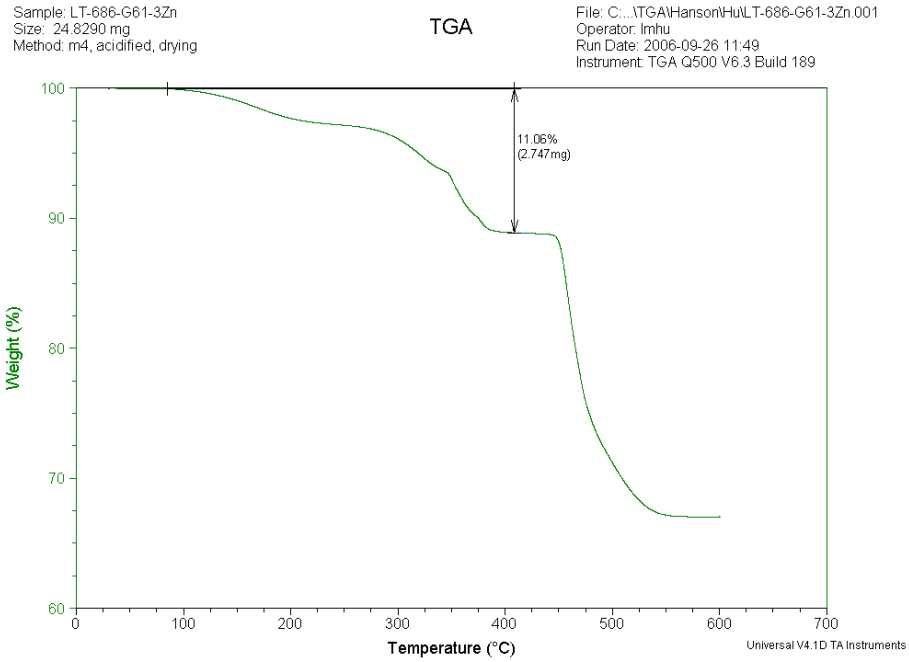

TGA for **10**

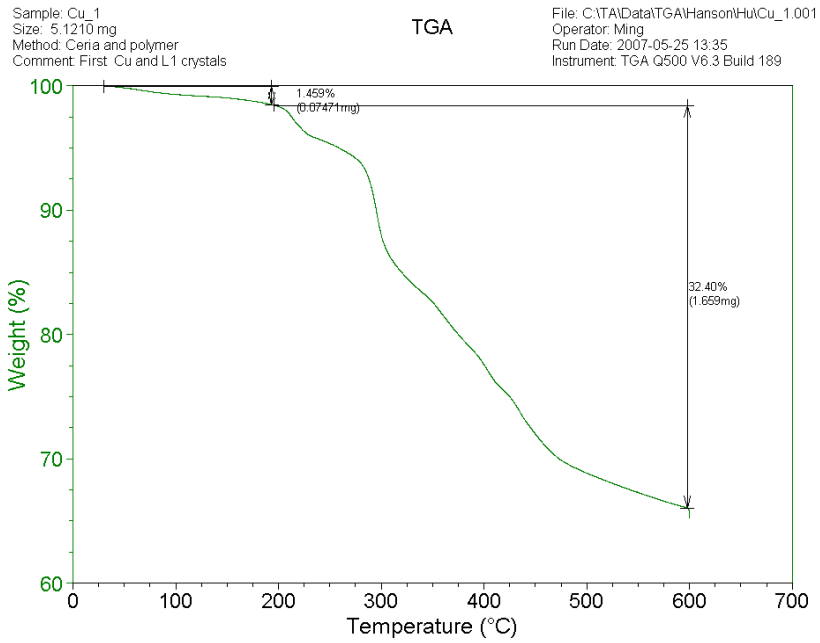

TGA for **11**

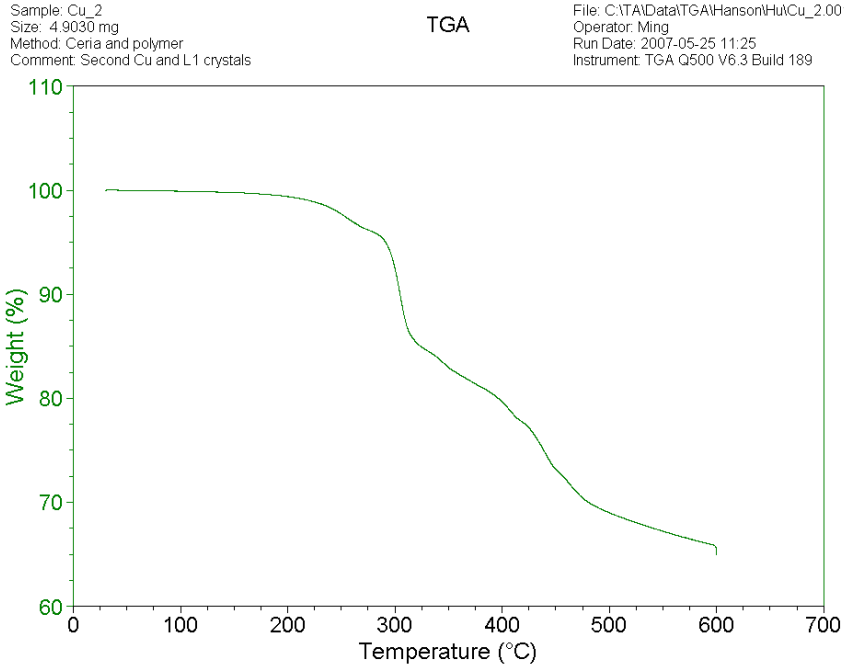

TGA for **12**

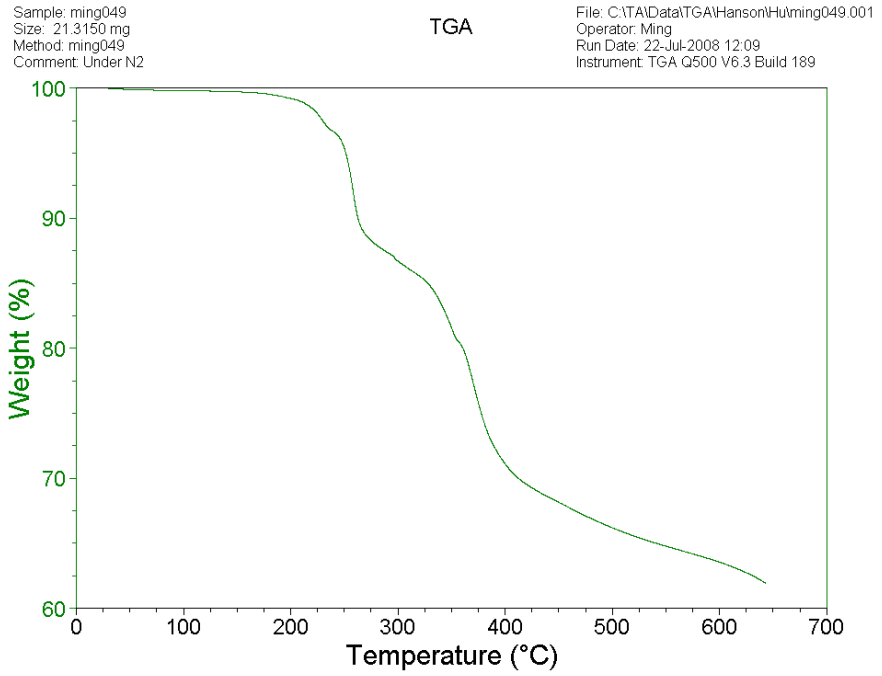

TGA for **13**

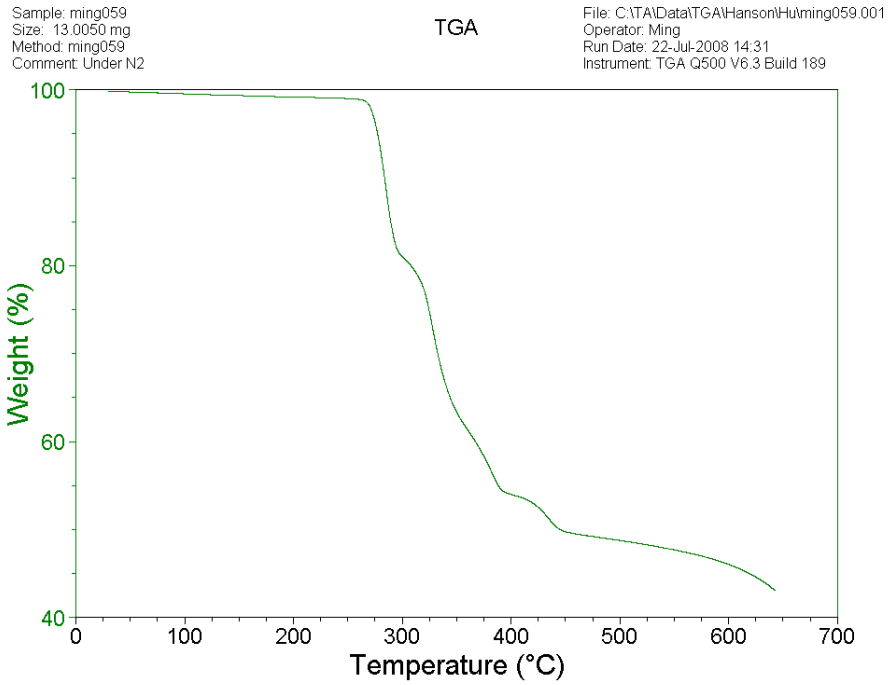

TGA for **14**

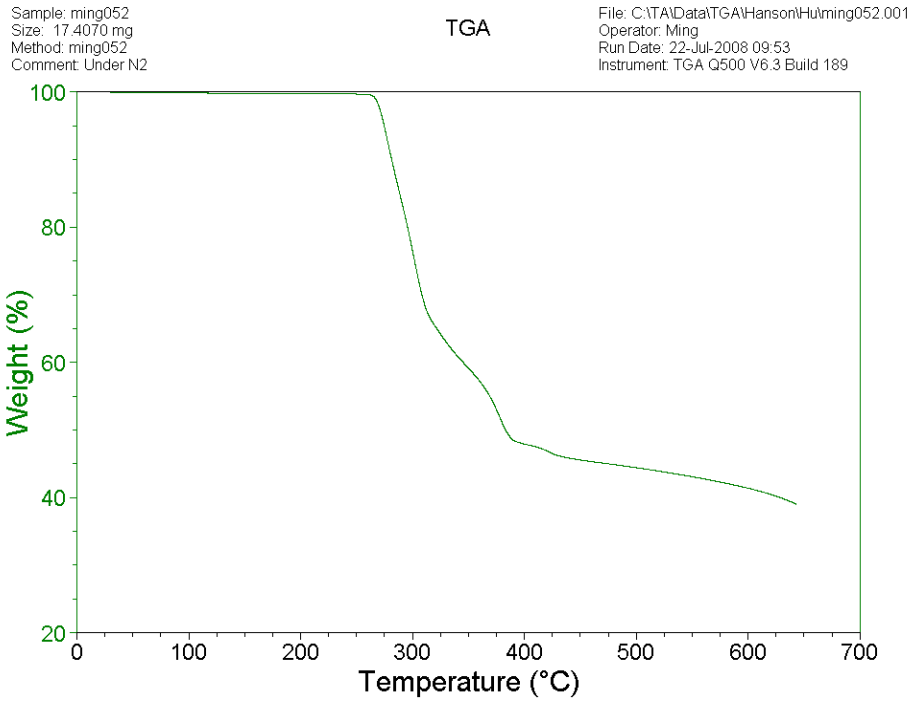
Sample: ming052
Size: 17.4070 mg
Method: ming052
Comment: Under N2
TGA
File: C:\TA\Data\TGA\Hanson\Hu\ming052.001
Operator: Ming
Run Date: 22-Jul-2008 09:53
Instrument: TGA Q500 V6.3 Build 189
Weight (%)
100
80
60
40
20
0
100
200
300
400
500
600
700
Temperature (°C)

TGA for **15**

Appendix B: X-ray powder diffraction pattern

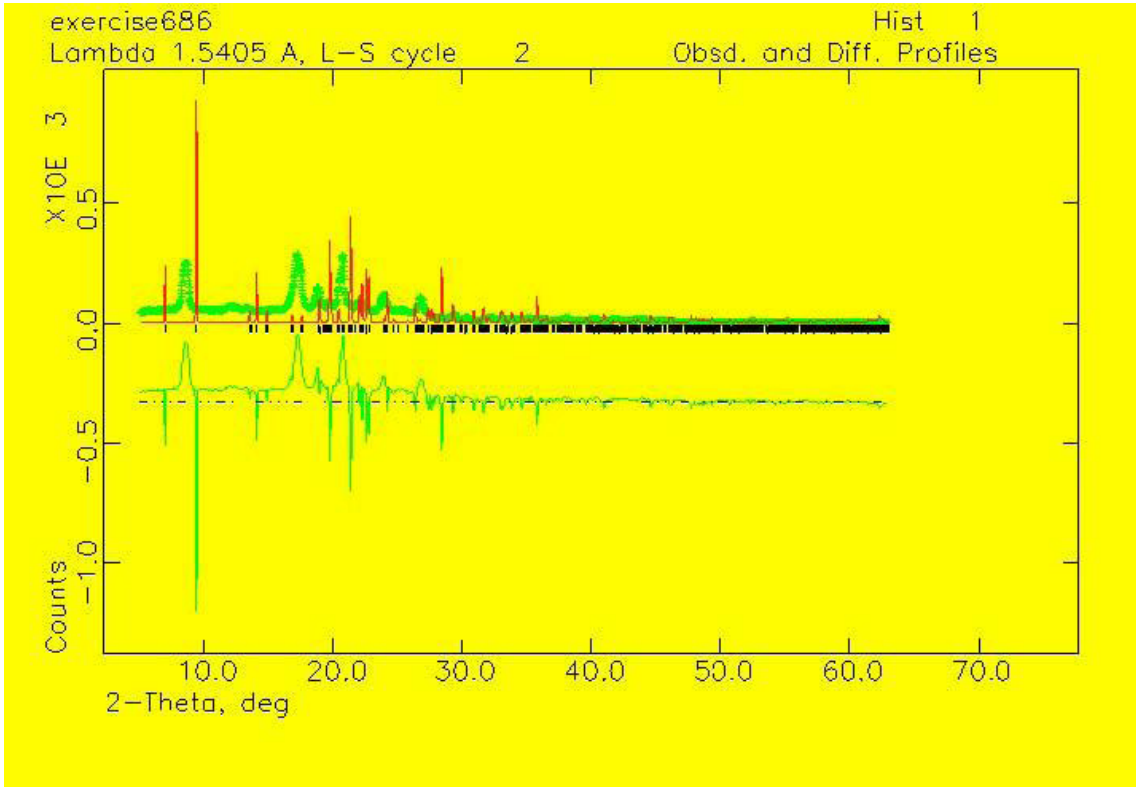

Experimental (green top trace) and calculated (red top trace) powder diffraction patterns for **1**. The bottom trace is the difference pattern and shows that the bulk sample contains very little of **1**.

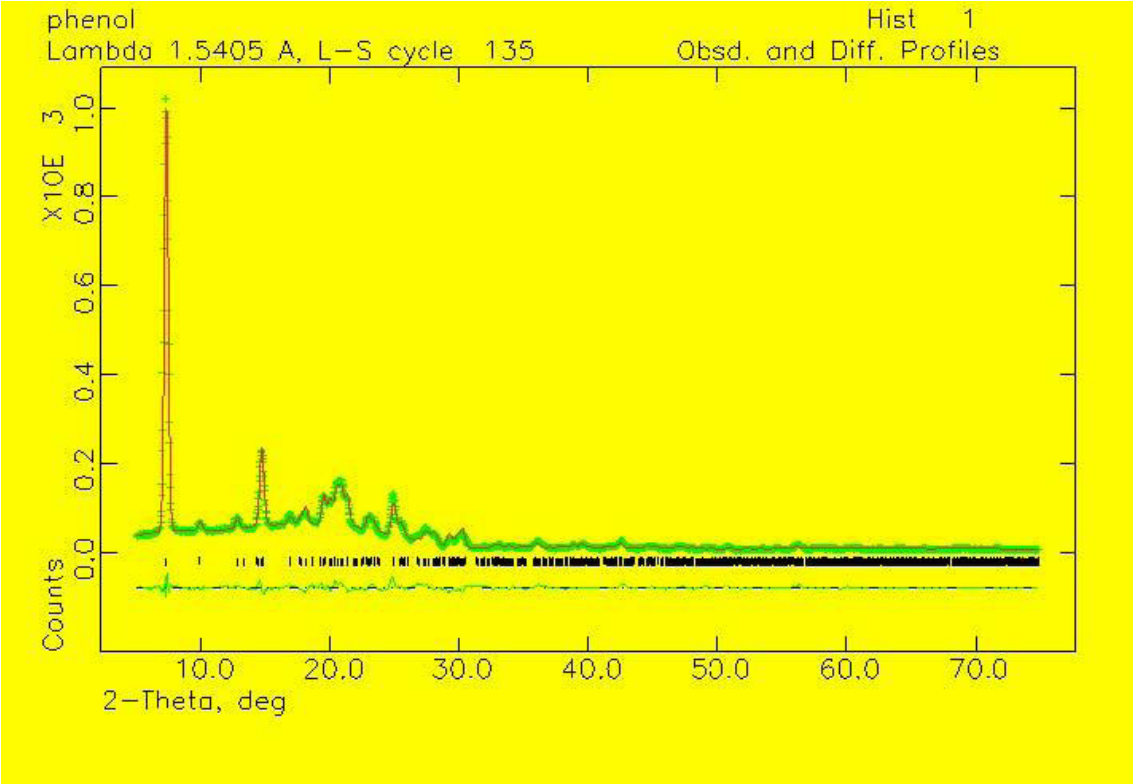

Experimental (green top trace) and calculated (red top trace) powder diffraction patterns for **4**. The bottom trace is the difference pattern and shows that the bulk sample consists mostly of **4.**

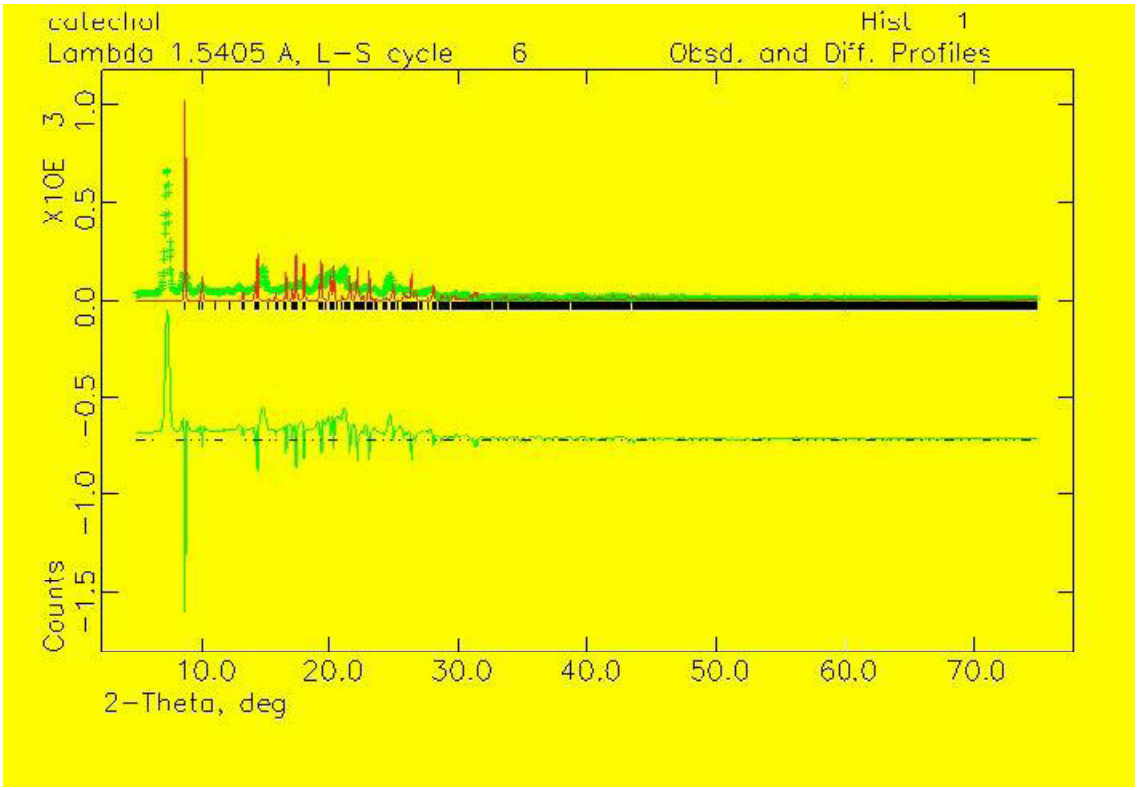

Experimental (green top trace) and calculated (red top trace) powder diffraction patterns for **5**. The bottom trace is the difference pattern and shows that the bulk sample contains very little of **5**.

Appendix C: NMR Spectra

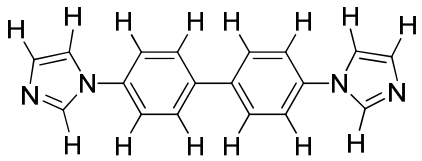

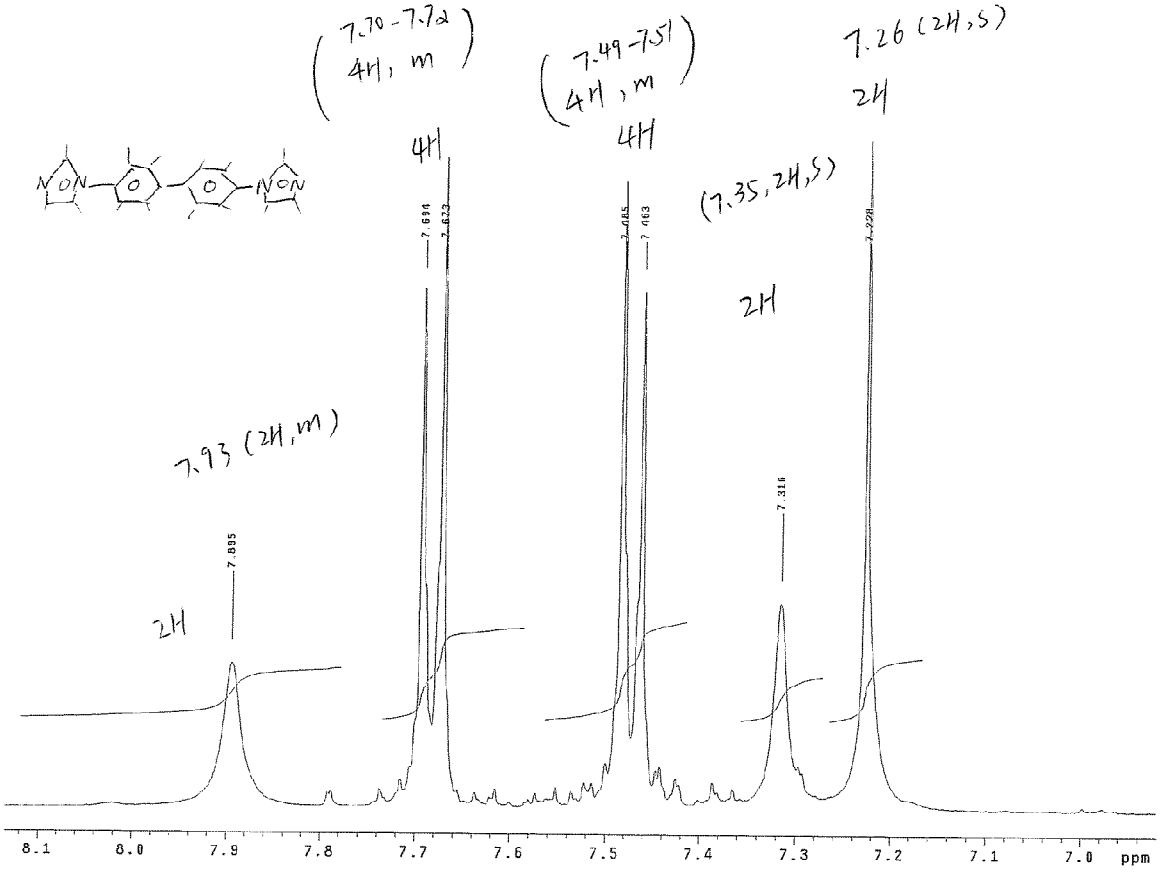

NMR spectroscopy for 4, 4'-bisimidazolylpiphenyl (BIB)

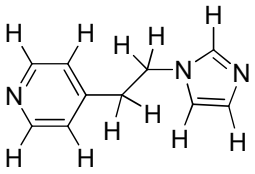

```
hu_L2_2

Pulse Sequence: s2pul
 Solvent: CDCl3
 Ambient temperature
UNITY-400  "unityultra"

 Relax. delay 1.000 sec
 Pulse 21.1 degrees
 Acq. time 3.744 sec
 Width 6000.6 Hz
 28 repetitions
OBSERVE   H1, 399.9486787 MHz
DATA PROCESSING
 Line broadening 0.2 Hz
FT size 65536
Total time 2 min, 32 sec
Sep 11 2007
VA Tech Chemistry NMR Lab
```

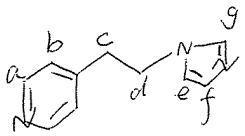

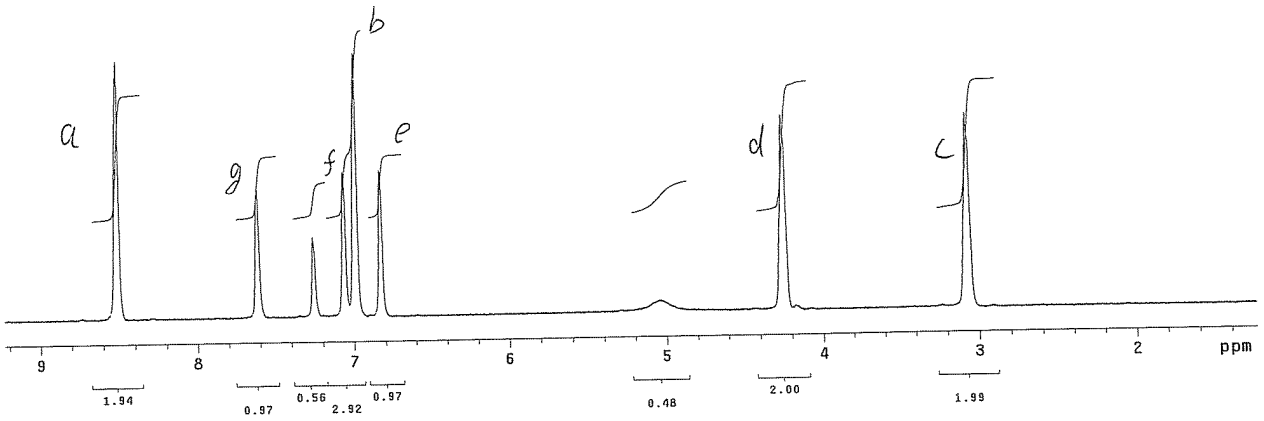

NMR spectroscopy for 4-(2-(1H-imidazol-1-yl)ethyl)pyridine

Appendix D: Mass Spectra

Chemputer

Isotope pattern	Element percentages	Yields	Oxidation state	Electron count	VSEPR	MLXZ

Sheffield ChemPuter

Result of isotope pattern calculation

Formula: $C_{18}H_{14}N_4$

mass	%
286	100.0
287	21.1
288	2.1
289	0.1

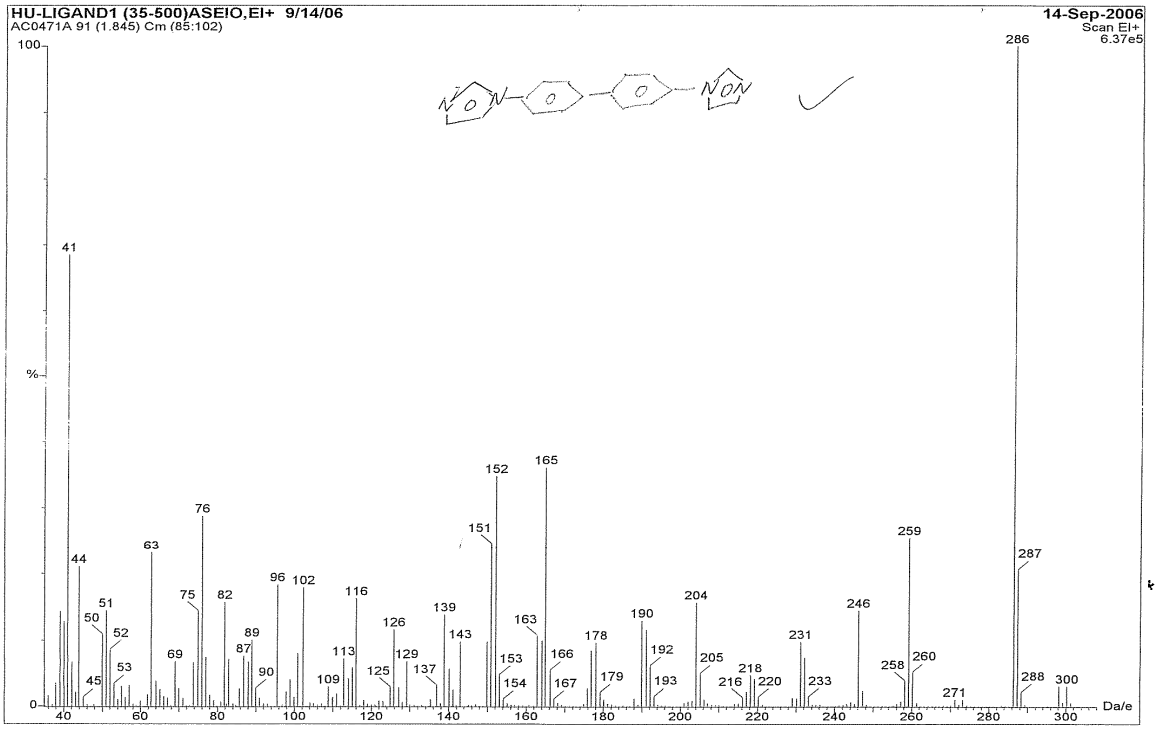

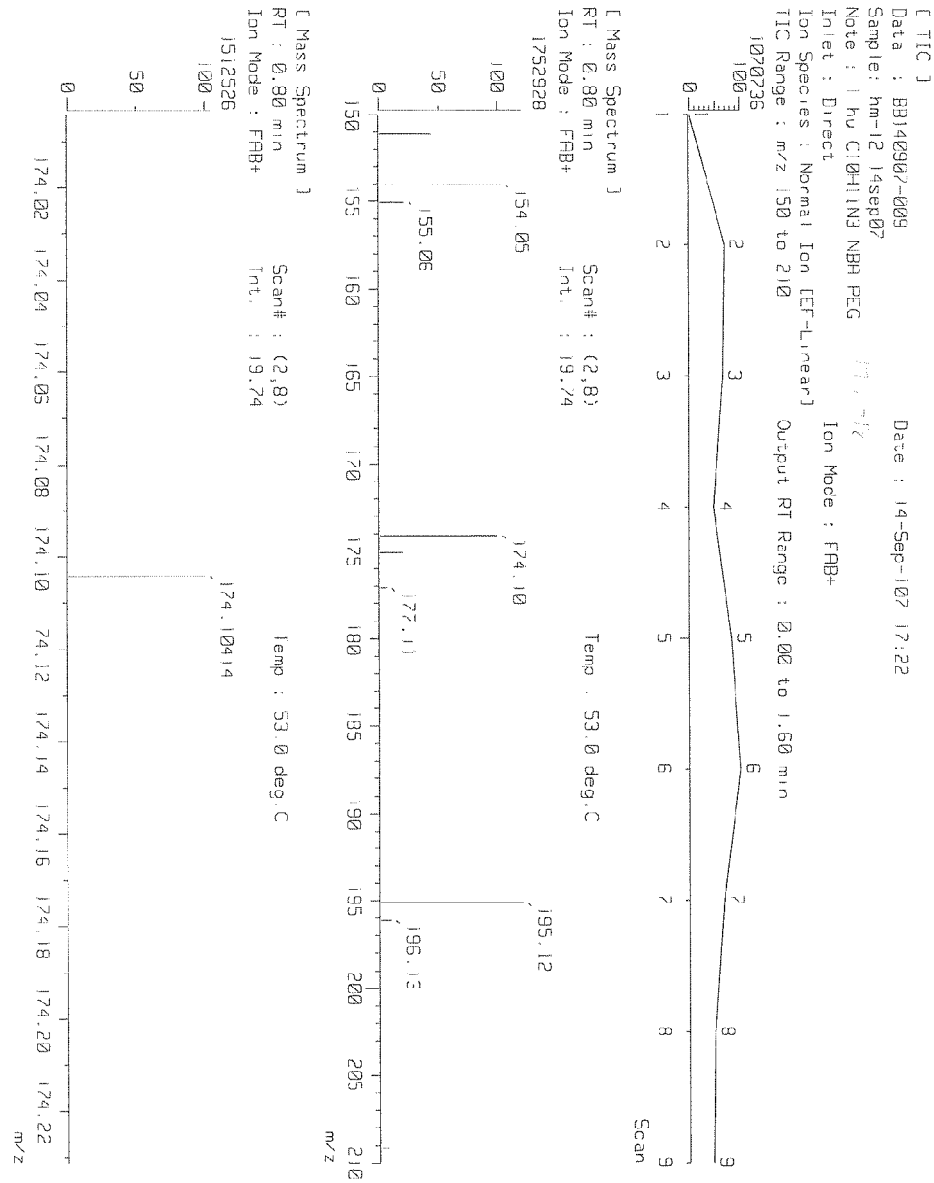

Mass spectroscopy for 4-(2-(1H-imidazol-1-yl)ethyl)pyridine

Appendix E: Copyrights

Date: Thu, 02 Apr 2009 06:59:28 +0100
From: Rights DE <RIGHTS-and-LICENCES@wiley-vch.de>
To: "lmhu@vt.edu" <lmhu@vt.edu>
Subject: **AW: Form: Permission request**

Dear Customer,

Thank you for your email.

We hereby grant permission for the requested use expected that due credit is given to the original source.
For material published before 2007 additionally: Please note that the author's permission is also required.

If material appears within our work with credit to another source, authorisation from that source must be obtained.

Credit must include the following components:
- Books: Author(s)/ Editor(s) Name(s): Title of the Book. Page(s). Publication year. Copyright Wiley-VCH Verlag GmbH & Co. KGaA. Reproduced with permission.

- Journals: Author(s) Name(s): Title of the Article. Name of the Journal. Publication year. Volume. Page(s). Copyright Wiley-VCH Verlag GmbH & Co. KGaA. Reproduced with permission.

With kind regards

Bettina Loycke
****
Bettina Loycke
Copyright & Licensing Manager
Wiley-VCH Verlag GmbH & Co. KGaA
Boschstr. 12
69469 Weinheim
Germany

Phone: +49 (0) 62 01- 606 - 280
Fax: +49 (0) 62 01 - 606 - 332
Email: rights@wiley-vch.de
_____

-----Ursprüngliche Nachricht-----
Von: lmhu@vt.edu [mailto:lmhu@vt.edu]
Gesendet: Mittwoch, 1. April 2009 23:05

An: Rights DE
Betreff: Form: Permission request

Form: Permission request
Path: Service Permission Request
Language: en

Adress
First Name: Liangming
Surname: Hu
Street: 804 Ascot Lane
Zip code: 24060
City: Blacksburg
Country: United States
Fax:
E-mail: lmhu@vt.edu
Media Type: journal
Author or Editor:
ISBN:
Journal Title: Angewandte Chemie International Edition
Journal Month:
Journal Year: 1995
Journal Volume: 34
Media Type: journal
Page No: Page 1557, Table 1.
Website or Intranet: yes
University/Institute: Virginia Polytechnic Institute and State University
Instructor:
Course:
Wiley Author: no

Delete Reply Reply All Forward Redirect View Source Move to: This message to Message **1** of **2**

Date: Wed, 01 Apr 2009 07:34:12 +0100
From: "CONTRACTS-COPYRIGHT (shared)" <Contracts-Copyright@rsc.org>
To: "'lmhu@vt.edu'" <lmhu@vt.edu>
Subject: **RE: Permission Request Form: Liangming Hu**

Dear Dr Hu

The Royal Society of Chemistry hereby grants permission for the use of the material specified below in the work described and in all subsequent editions of the work for distribution throughout the world, in all media including electronic and microfilm. You may use the material in conjunction with computer-based electronic and information retrieval systems, grant permissions for photocopying, reproductions and reprints, translate the material and to publish the translation, and authorize document delivery and abstracting and indexing services. The Royal Society of Chemistry is a signatory to the STM Guidelines on Permissions (available on request).

Please note that if the material specified below or any part of it appears with credit or acknowledgement to a third party then you must also secure permission from that third party before reproducing that material.

Please ensure that the published article carries a credit to The Royal Society of Chemistry in the following format:

[Original citation] - Reproduced by permission of The Royal Society of Chemistry

and that any electronic version of the work includes a hyperlink to the article on the Royal Society of Chemistry website. The recommended form for the hyperlink is http://dx.doi.org/10.1039/DOI suffix, for example in the link http://dx.doi.org/10.1039/b110420a the DOI suffix is 'b110420a'. To find the relevant DOI suffix for the RSC paper in question, go to the Journals section of the website and locate your paper in the list of papers for the volume and issue of your specific journal. You will find the DOI suffix quoted there.

Regards

Gill Cockhead
Contracts & Copyright Executive

Gill Cockhead (Mrs), Contracts & Copyright Executive
Royal Society of Chemistry, Thomas Graham House
Science Park, Milton Road, Cambridge CB4 0WF, UK
Tel +44 (0) 1223 432134, Fax +44 (0) 1223 423623
http://www.rsc.org<http://www.rsc.org/>

-----Original Message-----
From: lmhu@vt.edu [mailto:lmhu@vt.edu]
Sent: 31 March 2009 21:30
To: CONTRACTS-COPYRIGHT (shared)
Subject: Permission Request Form: Liangming Hu

Name : Liangming Hu

Address :

804 Ascot Lane

Blacksburg, VA 24060

United States

Tel : 540-250-3866

Fax : 540-231-3255

Email : lmhu@vt.edu

I am preparing the following work for publication:

Article/Chapter Title : Thesis

Journal/Book Title : Thesis

Editor/Author(s) : Liangming Hu

Publisher : Virginia Tech

I would very much appreciate your permission to use the following material:

Journal/Book Title : Chemical Communications

Editor/Author(s) : Rang, Alexander; Nieger, Martin; Engeser, Marianne; Luetzen, Arne; Schalley, Christoph A.

Volume Number : 39

Year of Publication : 2008

Description of Material : Scheme 1

Page(s) : 4789

Any Additional Comments :

I am writing my thesis. I would appreciate your permission to use this scheme in my thesis.

DISCLAIMER:

This communication (including any attachments) is intended for the use of the addressee only and may contain confidential, privileged or copyright material. It may not be relied upon or disclosed to any other person without the consent of the RSC. If you have received it in error, please contact us immediately. Any advice given by the RSC has been carefully formulated but is necessarily based on the information available, and the RSC cannot be held responsible for accuracy or completeness. In this respect, the RSC owes no duty of care and shall not be liable for any resulting damage or loss. The RSC acknowledges that a disclaimer cannot restrict liability at law for personal injury or death arising through a finding of negligence. The RSC does not warrant that its emails or attachments are Virus-free: Please rely on your own screening.

Delete Reply Reply All Forward Redirect View Source Move to: This message to Message **2** of **2**